INVESTIGATION OF THE ELECTRICAL AND MAGNETIC PROPERTIES OF CONDUCTOR-INSULATOR (WC/Co) COMPOSITES

A THESIS SUBMITTED
IN PARTIAL FULFILMENT OF THE REQUIREMENTS
FOR THE DEGREE OF MASTER OF PHILOSOPHY (M. Phil)

BY
MOST. ASMA AKTER BALLY
EXAMINATION ROLL NO. 03
REGISTRATION NO. 198
SESSION 1999-2000

TO
THE DEPARTMENT OF PHYSICS
UNIVERSITY OF DHAKA

APRIL, 2008.

Candidate's Declaration

It is hereby declared that this thesis or any part of it has not been submitted elsewhere for the award of any degree or diploma.

Date: April, 2008.
Dhaka University, Dhaka.

Most. Asma Akter Bally
Roll: 03
Registration No. 198
Session:1999-2000.

INVESTIGATION OF THE ELECTRICAL AND MAGNETIC PROPERTIES OF CONDUCTOR-INSULATOR (WC/Co) COMPOSITES

A THESIS SUBMITTED

BY

MOST. ASMA AKTER BALLY

EXAMINATION ROLL NO. 03

REGISTRATION NO. 198

SESSION 1999-2000

Accepted as satisfactory in partial fulfillment of the requirement for the degree of Master of Philosophy (M. Phil) in Physics on April, 2008.

4.5.2008

(Dr. Sabina Hussain)

Supervisor

(Dr. Dilip Kumar Saha)

Joint Supervisor

DEDICATED

TO

MY BELOVED PARENTS AND MY HUSBAND

ACHNOWLEDGEMENT

Great pleasure and gratitude coming out from the core of my heart, I would like to recognize a number of people, each of whom have contributed to the preparation of my thesis paper.

At first I thank Allah, then with due respect and deepest gratitude, I acknowledge the invaluable guidance of my thesis supervisor, Associate Professor Dr. Sabina Hossain, Department of Physics, University of Dhaka and Joint Supervisor, Dr. Dilip Kumar Saha, Principal Scientific Officer, Material science division, Atomic Energy Center, Dhaka. I must thank Dr. Feroz Alam Khan, Associate Professor, Department of Physics, BUET, Dhaka, for his continuous interest in my work, for constant and unflinching support, for being so optimistic as well as helping me with fruitful discussion and ideas. My special thanks to the Department of Physics, BUET, Dhaka, for permitting me to work in material science laboratory, Department of Physics, BUET, Dhaka. I also thank to the Authority of AEC, Dhaka, for allowing me to use X-ray diffractometer.

I am obliged to my parents, husband, sisters and brothers for their love and support. I wish also to thank all of my colleagues, Department of Physics, Carmichael college, Rangpur, specially Mohammed Ali and Professor Abeda Khatun for their continuous support and inspiration during my research work.

Lastly not the least I am grateful to Shantanu Sinha, M. S. student and Shipon, M. Phil student, for their help through out the work.

Date: April, 2008

Most. Asma Akter Bally

ABSTRACT

In the present study attention has been focused on a polycrystalline WC dispersed with increasing fraction of Co inclusions (6 to 14 volume %). Co has been chosen as filler due to its significant properties. X-ray diffraction analysis was carried out on the samples to determine weight percentage of WC & Co and some structural parameters of WC. WC and Co showed two different phases. Co was found to be in the range of (5 – 20) weight percent, the rest was found as WC. The lattice parameter (a, b, c) of the sample crystal was determined plotting the lattice parameter value versus Nelson-Riley (N. R.) function and the values were found to be a=b=2.9047 and c=2.8275. The volume of the unit cell of a hexagonal sample is 23.87. An experimental setup was established for the measurement of DC electrical and magnetic field dependent resistance and magnetoresistance. The electrical conductivity and magneto resistance were measured as a function temperature starting from RT to 210°C keeping magnetic field constant. Also same measurements were carried out as a function of magnetic field at constant temperature. The measurement was performed using standard four-probe method to examine how the volume fraction of Co particles affects the electrical properties of WC-Co composite. It was observed that for all these temperatures, the current-voltage curves show linear behavior for all percentages of Co. With increasing temperature, the conductivity of the samples was found to be decreased. The electrical conductivity as a function of Co concentration in a WC matrix shows that above 8.5 volume percentage of Co the composite shows higher conductivity due to the percolation effect. Bellow 8.5 volume percentage of Co, the electrical conductivity rises, but the behavior is still similar to that of pure WC. The MR as a function of magnetic field for all the samples was obtained at RT (300K) and at high temperature. Also the MR as a function of temperature for all the samples were obtained at H = 0, 1, 2, 3, 4 KG. At room temperature (300K) observed MR was negative and almost constant with the field. With increase in temperature the value of negative MR started decreasing and above 423K positive MR was observed but the values of Magneto Resistances were very close to zero.

CONTENTS

List of Figures

List of Symbols, Abbreviations and Nomenclature

XRD	X-ray diffraction
d	distance between crystal planes
θ	incident angle
λ	the wave length of X-ray
n	a positive integer and represents the order of reflection
MR	Magnetoresistance
FWHM	full width at half maximum of the peak
I_A	the integrated intensity of a particular peak
I_P	the peak intensity of that particular peak and
ρ	resistivity
σ	conductivity
C_A	the concentration of a particular material in the sample in weight percent.
K	Kelvin
°C	Degree centigrade
AC	Alternating current
DC	Direct current
R	Resistance
eV	Electron volt $\approx 1.609\times10^{-19}$ J
AMR	Anisotropic magnetoresistance
GMR	Giant magnetoresistance
PMR	Powder magnetoresistance
BMR	Ballistic magnetoresistance
CMR	Colossal magnetoresistance
IMR	Itergrain magnetoresistance
TMR	Tunneling magnetoresistance
EMR	Extraordinary magnetoresistance
VLMR	Very Large magnetoresistance

CHAPTER ONE

INTRODUCTION

When two or more materials combine exhibiting properties distinctly different from those of the individual component make the composite. The different materials work together to give the composite unique properties, but within the composite the different materials remain apart – they don't dissolve or blend into each other. Most commonly, composite materials have a bulk phase, which is continuous, called the matrix and one dispersed, non-continuous phase is called the reinforcement (also called filler), which is usually harder and stronger. The bulk phase accepts the load over a large surface area and transfers it to the reinforcement, which being stiffer, increases the strength of the composite. The significance here lies in that there are numerous matrix materials and many fiber types, which can be combined in countless ways to produce the desired properties [1].

This present work deals with the study of structural, electrical and magnetoresistive properties of WC/Co composite. It consists of 6 to 14 volume percentage of Co, the rest being tungsten carbide (WC). Composite materials are of interest because by simply changing the concentration of their constituent phases results in a wide range of properties. In many areas of scientific research and engineering a key problem is the prediction of the effective physical properties of composite media from the properties and microstructure of the constituents. For example, when two powders with different electrical conductivity are mixed, the resulting composite often has an electrical conductivity that is unpredictable in practice. The properties of composites (mechanical, thermal, electrical, or optical) are difficult to predict and highly dependent on the composite microstructure. The size, shape, concentration and conductivity of the components are all important in determining the mechanical, thermal, electrical and optical properties of a material [1].

Cemented tungsten carbides are commercially one of the oldest and most successful powder metallurgy products. These composites are essentially aggregates of particles of tungsten carbide bonded with cobalt metal via liquid-phase sintering. The properties of these materials are derived from those of constituents – namely, the hard and brittle carbide and the softer, more ductile binder. The wide applications of cemented carbides for cutting tools and wear parts arise because of their unique combination of mechanical, physical and chemical properties [2].

Interest in cemented tungsten carbides is increasing rapidly but not because of their use as cutting tools. They are used as mining drills. They are potential armor or ballistic potential materials. But, above all, they are useful for high-temperature aerospace applications: for thermal protection shrouds, leading edge, rocket nozzles, and to protect space capsules against micro-meteorite bombardment. They are also used in die and wear parts, and rock cutting tools.

A lot of research work on WC/Co composite has been carried out and still going on. Work performed previously on WC/Co are-

Effect of Cobalt Particle Size on the Processing and Properties of Fine-Grained WC/Co Materials. Liquid Phase Sintering Aids for Nanograin and Micrograin WC/Co. Aspect of Ultrafine Hardmetal Sintering. Macrocrystalline Thermit Derived WC: Process, Properties and Applications . The Influence of Binder Constitution on the Shape of WC Grains. Microstructural Development During Microwave Sintering of Cemented Tungsten Carbide. Solid State Sintering of Cemented Carbides Under Field Application. A Comparison of Electrical and Magnetic Measurements on WC/Co Hardmetals. Monitoring the Delubing and Sintering of Hard Metals by Means of Mass Spectrometry. Development of a Dual composite of Cemented Tungsten Carbide. A typical Microstructure in WC-Co Technical Cemented Carbides.

In our work WC/Co cemented carbide composites with different volume percentages of Co have been prepared to observe the electrical and magnetic properties using four-probe method as well as structural properties by X-ray diffraction (XRD) method.

The electrical measurement have been taken into consideration because they can have a variety of technological applications such as heater, ignites, heat exchangers, resistors, sensors, transducers, electromagnetic shielding of electronic components, electrical stress relief in high voltage devices, electrodes for fuel cells and as crucibles for vacuum induction furnaces [2-4]. Moreover if the electrical conductivity of these composites is found to be high enough it is feasible to use electrical discharge method (EDM), an economical way to prepare complex shapes of very hard materials. Recently, composites with controlled electrical conductivity have been used for replacing metal parts in electrical and electronic devices, improving not only the performance of the components but also the temperature of their applications [5, 6] .

As regards composites the main interest is the improvement of both electrical and mechanical properties. In this respect the design of a composite and specially metal matrix composites is usually a compromise between the desire to raise conductivity as much as possible and retain refractoriness, hardness and stiffness that will be depleted by the imbedded metal particles. Metal particles are also used in ceramic matrices to increase their toughness. However, often the amount of metal in these cermets, in order to have enough electrical conductivity for technological applications, is above 20-30 vol%. Therefore, in order to design composites for specific applications it is useful to be able to model the properties theoretically based on knowledge of the constituent phases and their relative distribution [2].

Usually at a certain threshold value of volume fraction of metal particles, they are sufficiently close-packed to form an unbroken conducting pathway through

the composites and the conductivity of the material increases sharply. This threshold is known as the percolation limit. A way of maximizing composite conductivity while retaining the good properties typical of ceramic materials would be to control not only the amount but also the shape and size of the embedded particle in order to reach the percolation limit at relatively low volume fractions [7].

So far, not many composites have been tested for their electrical properties: Al_2O_3/TiN [8], Si_3N_4/TiN [9],Si_3N_4/TiN-TiC, Si_3N_4/$MoSi_2$, Si_3N_4/TaN, SiC/TiB, SiC/ZrB_2 and even less metal toughened ceramics ZrO_2/(Ti or Ni) [3], SiO_2/Mo, BaTiO/Ag, $BaBi_8O_{13}$/Ag [10].

For these reasons, WC/Co composites can be ideal for applications where two distinct properties, toughness and electrical conductivity, need to be combined in the same material. Therefore this system was chosen, in this study, as a convenient model to begin a systematic investigation of electrical properties.

Co is a brittle, hard, transition metal that is quite unreactive. It has magnetic properties similar to those of iron. Bulk cobalt metal is one of the pure elements that is ferromagnetic at room temperature. However, the magnetic properties will vary as the bulk metal is broken into finer and finer pieces [9]. In WC/Co composite Co is used as a bonding matrix because its wetting or capillary action during liquid phase sintering allows the achievement of high densities. Again Co is a magnetic material. So it may have a significant magnetic influence on the composite. That is why magnetic properties were also investigated.

It is mentioned before that volume fraction of constituent phases is very important in composite materials because by changing it a wide rang of properties can be changed. To know the fraction of Co and WC in WC/Co composite XRD were performed. Also some structural parameters were calculated from that XRD data.

The present study has been planned to achieve the following objectives:

1) Concentration study of WC/Co composite using X-ray diffraction method
2) Lattice parameter determination using Nelson-Really method
3) The voltage-current characteristics of all the samples.
4) Effect of high temperature on Conductivity of WC/Co composite.
5) Effect of Co particles on Conductivity of WC/Co composite.
6) Study of Magnetoresistance as a function of applied field.
7) Study of Magnetoresistance as a function of temperature.

References

1. Shantanu Sinha, 'Study of electrical and structural properties of WC/Co composites', M.S. thesis, p6, 2000-2001.
2. Martinelli,J.R. and Sene,F.F. Electrical resistivity of ceramic metal composite materials: application in crucibles for induction furnaces. Ceram. Intl., 2000, 26(3), 325-335
3. Martin,C., Mathieu,P. and Cales,B., Electrical discharge machinable ceramic composites, Mater. Sci. Eng., 1989, A109, 351-356.
4. Tressler, J. F., Alkoy,S. and Dogan, A., Functional composites for sensors, actuators and tranducers. Compos. Part-A.S.,1999, 30(4),477-482.
5. Onitsuka,K., Dogan,A., and tressler,J.F. Metal-ceramic composite transducer, the Moonie.J.Intel Mat. Syst. Str., 1995,6(4), 447-455.
6. Jimou,R., Takahashi,K. Matsushita,Y. and T., SiC-ZrB_2 Electroconductive ceramic composites. Adv. Ceram. Mater., 1986, 1, 341-345.
7. Sabina Hussain, 'Analysis of electrical and microstructural properties of Al_2O_3/Mo composites', Ph D thesis, p2, 2000-2001.
8. Mukerji,J., and Biswas,S.K., Synthesis, properties and oxidation of Alumina titanium nitride composite. J. Am. Cerm. Soc., 1990,73(1), 142-145.
9. Bellosi,A., Gucciardini,S. and tampeiri,A., Development and characterization of electroconductive Si_3N_4/TiN composites. J. Eur. Ceram. Soc., 1992, 8, 83-93.
10. lee,T.H., Yang,Y.L. and Jacobson,A.J., Electrical conductivity and Oxygen permeation of Ag/$BaBi_8O_{13}$ coposites. Splid state Ionics, 2000, 134(3-4), 331-339.

CHAPTER TWO

CHAPTER 2: THEORY

2.1 Introduction:

In this chapter, a brief description on composite material, two-point and four-point resistivity measurement technique, mechanism of different type of MR observed in magnetic materials have been given. The X-ray diffraction technique is also discussed in this chapter.

2.2 A brief description on composite material:

2.2.1Composite material

A composite material can be defined as a combination of two or more materials exhibiting properties distinctly different from those of the individual components. The different materials work together to give the composite unique properties, but within the composite the different materials remain apart – they don't dissolve or blend into each other. Most commonly, composite materials have a bulk phase, which is continuous, called the matrix and one dispersed, non-continuous phase is called the reinforcement (also called filler), which is usually harder and stronger. The bulk phase accepts the load over a large surface area and transfers it to the reinforcement, which being stiffer, increases the strength of the composite. The significance here lies in that there are numerous matrix materials and many fiber types, which can be combined in countless ways to produce the desired properties [1].

The components usually also perform different functions. For instance, in fiber composites a fiber carries load. In cermets we have mechanical strengthening of the original phase due to dislocation impediment produced by a second phase.

Since a composite material consists of a mixture and reinforcement it can be classified according to both the aspects. Because of the very nature of composite

materials, there is an infinite variety of them. It might be useful, as suggested by Hilling[1], to distinguish between structural and functional composites. The former are used mainly for their mechanical properties while the latter rather for their special electrical, chemical or other characteristics. Some important classes of composites are cermets, concrete and asphalt, fiber composites, laminates and surface coating, wood and cellulosic materials.

2.2.2 Components of Composite Materials :

- Bulk phase: matrix materials
  Polymers
  Metals
  Ceramics
- Reinforcement or filler: fibers and particulate
  Glass
  Carbon
  Organic
  Boron
  Ceramic
  Metallic
- Interface

2.2.3 Classification of Composite Materials:

Since a composite material consists of a matrix and a reinforcement it can be classified according to both the aspects [1].

Classification according to reinforcement:

The reinforcement system in a composite material strongly determines the strengthening mechanism in a composite. It is thus convenient to classify composites according to the characteristics of the reinforcement, such as length, orientation etc.

Reinforcements are not necessarily in the form of long fibers. They can be particles, whiskers, discontinuous fibers, sheets etc. A great majority of materials is stronger and stiffer in the fibrous form than in any other form. This explains the emphasis on using fibers in composite materials design.

There are many naturally occurring fibers: cotton, flax, jute, hemp, ramie, wood, straw, hair, wool, silk etc., but these have varying properties, and present many processing challenges.

Fibers used in advanced composites have very high strength and stiffness but low density. They also should be very flexible (to allow a variety of methods for processing) and have high aspect ratio (length/diameter), that allows a large fraction of the applied to be transferred via the matrix to the fiber.

Fibers are added to a ductile matrix (like polymers and metals) usually to make it stiffer, while fibers are added to a brittle matrix (like ceramics) to increase toughness [1].

i) Glass fibers

1) The most common and inexpensive fiber used is glass fiber, usually for the reinforcement of polymer matrices.
2) Typical composition is 50-60% SiO_2, and other oxides of Al, Ca. Mg, Na. etc.

3) "Sizing" is a treatment applied to glass fibers to protect the strands from surface defects, bind the filaments into a strand, and reinforce the interface bond to the matrix. It is usually based on PVAc and silane coupling agents.

4) Glass fibers are available as:

a) Chopped strands

b) Continuous yarn

c) Roving ' d) Fabric sheets

5) Moisture decreases glass fiber strength.

6) Glass fibers are susceptible to static fatigue, i.e. they cannot withstand static loads for long periods of time.

7) Properties:

a) Density is quite low (-2.55 g/cc)

b) Tensile strength is quite high (-1.8 GPa)

c) Stiffness is, however, low (70 GPa) (i.e., strains more easily)

d) Therefore, whereas strength/density is high, stiffness/density is low.

e) Good dimensional stability, resistant to heat, cold and corrosion.

ii) Carbon fibers

1) Carbon is a very light element, with density about 2.3 g/cc

2) The graphitic structure is preferred over the diamond-like crystalline forms for making fibers.

3) Fibers are made by carbonization of precursor fibers, followed By graphitization at high temperature. The precursors are usually PAN (polyacrylonotrile) and Rayon, which are both textile polymers.

4) Since the graphitic structure is made of densely packed hexagonal layers, stacked in a lamellar style, the mechanical and thermal properties are highly anisotropic. Controlling the orientation of the crystalline layers is a crucial issue.

a) Young's modulus in the layer plane can be 1000 GPa.

while that along the c-axis is equal to about 35 GPa.

Carbon has excellent compression properties.

b) Transverse CTE is 5.5 to 8.4 E-6/K, while parallel CTE is -0.5 to-1.3 E-6/K

5) Carbon fiber composites find wide applications in the aerospace and sporting goods industries. The ability to tailor the required stiffness and strength properties of internal bone plates gives them a definite advantage over metallic parts. Most biomedical applications are in the orthopedic market.

6) Carbon fiber adds electrical conductive properties to composites. While this may be preferred where static charges need to be dissipated, it can cause corrosion problems, especially in proximity to metallic parts.

iii) Polymer fibers

1) Strong covalent bonds in polymers, if aligned long the fiber axis of high molecular weight chains, can lead to impressive properties.

2) Two examples are UHMPE (ultra high molecular weight polethylene) called Spectra, made by Allied Corp., and Kevlar made by DuPont.

4) Spectra is a very light fiber (denisty -0.97 g/cc) made from gels and solution. It has a stiffness of about 200 GPa. Its primary disadvantage is its low melting point (around 150 Celsius), but this may not be an issue in biomedical applications.

5) Kevlar is an aramid (aromatic polyamide) composed of oriented aromatic chains, which makes them rigid rod-like polymers. It has a very high Tg and poor solubility. Since very concentrated acids are used in its processing, this can be an issue in biomedical applications if all acid residues are not extracted. Although very strong in tension, Kevlar has very poor compression properties. Its stiffness can be as high as 125 GPa. The fibers are mostly used to increase toughness in otherwise brittle matrices.

6) Adsorbable fibers such as PLA and PGA are used in composites for their biodegradation propeties, and not for mechanical strengthening.

iv) Other fibers

1) Ceramic fibers, such as Alumina and SiC (Silicon carbide) are advantageous in very high temperature applications, and also where environmental attack is an issue. Since ceramics have poor properties in tension and shear, most applications as reinforcement are in the particulate form (e.g. zinc and calcium phosphates).

2) Metallic fibers, such as steel and tungsten, have high strengths and show very consistent properties, unlike ceramic fibers. Since density is very high for these fibers, they are rarely used to reduce weight in a composite. Drawing very thin metallic fibers (less than 100 micron) is also very expensive.

Composites are classified according to their matrix phase:

* Polymer Matrix Composites (PMCs) - These are the most common and also known as FRP - Fibre Reinforced Polymers (or Plastics) - these materials use a polymer-based resin as the matrix, and a variety of fibres such as glass, carbon and aramid as the reinforcement.

* Metal Matrix Composites (MMCs) - Increasingly found in the automotive industry, these materials use a metal such as aluminium as the matrix, and reinforce it with fibres such as silicon carbide.

* Ceramic Matrix Composites (CMCs) - Used in very high temperature environments, these materials use a ceramic as the matrix and reinforce it with short fibres, or whiskers such as those made from silicon carbide and boron nitride.

2.2.4 Interface :

1) The interface is a bounding surface or zone where a discontinuity occurs, whether physical, mechanical, chemical etc.

2) More often than not, the interface between fiber and matrix is rather rough, instead of ideal planar.

3) The matrix material must 'wet" the fiber. Coupling agents are frequently used to improve wettability. Well 'wetted" fibers increase the interface surface area.

4) To obtain desirable properties in a composite, the applied load should be effectively transferred from the matrix to the fibers via the interface. This means that the interface must be large and exhibit strong adhesion between fibers and matrix. Failure at the interface (called debonding) may or may not be desirable. This will be explained later in fracture propagation modes.

5) Bonding with the matrix can be either weak van der Walls forces or strong covalent bonds.

6) The internal surface area of the interface can go as high as 3000 cm^2 /cm^3.

7) Interfacial strength is measured by simple tests that induce adhesive failure between the fibers and the matrix. The most common is the Three-point bend test or ILSS (interlaminar shear stress test).

2.2.5 Types of bonding at the interface:

The following are the important types of interfacial bonding.

1) Mechanical bonding

2) Chemical bonding.

a) Dissolution and wettability

b) Reaction bonding.

1. Mechanical bonding:

Mechanical key can lead to bonding. Figure - (2.1.a) shows an ideal, smooth interface while figure - (2.1.b) shows a real interface which is rough.

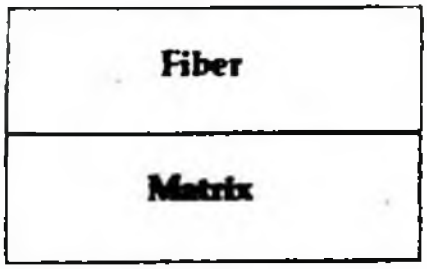

Figure - (2.1a): an ideal smooth interface

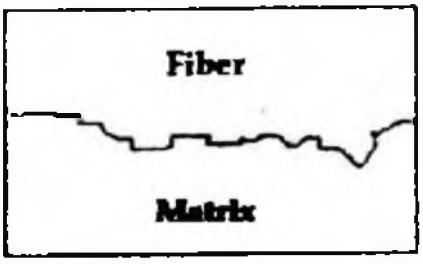

Figure - (2.1b): a real rough interface

Imagine for example, a situation where the matrix is a composite radially shrinks more than the fiber on cooling from a high surface, by liquid or viscous flow or high temperature diffusion, can lead to temperature. This would lead to a gripping of the fiber by the matrix even in the absence of any chemical bonding (figure-2). The matrix penetrating the crevices on the fiber some mechanical bonding. In figure-2 we have radial gripping stress, σ_r this is related to the interfacial stress, τ_i, as:

$$\tau_i = \mu\sigma_r$$

where is the coefficient of friction, generally between 0.1 and 0.6. In general, mechanical bonding is a low-energy bond.

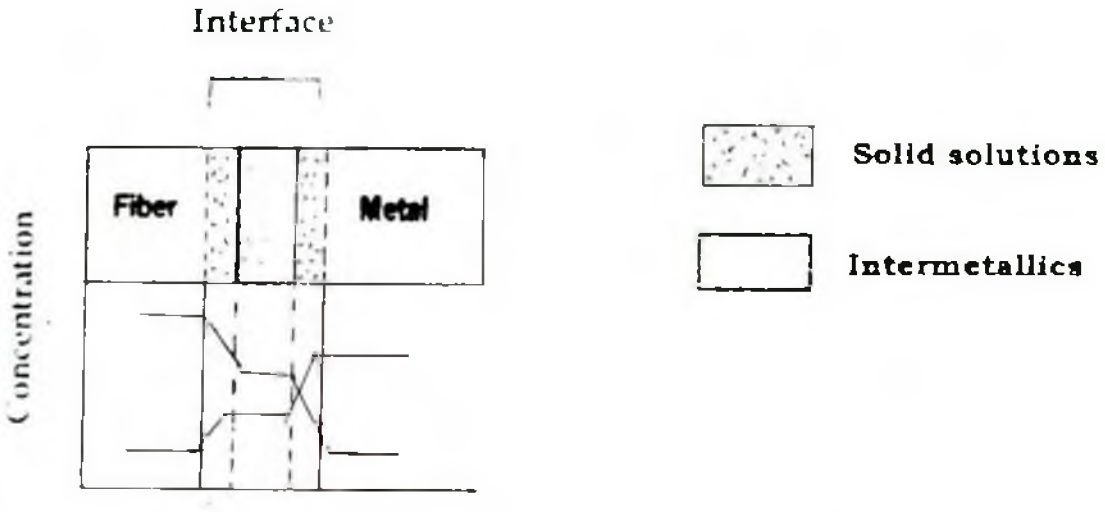

Figure – 2.3: Interface zone in a metal matrix composite showing solid solution and intermetallic compound formation.

The plateau region, which has a constant proportion of the two atomic species, is the region of the intermetallic compound formation. Generally, one tries to fit such data to expressions of the form:

$$x^2 = Dt$$

$$A = Aexp(-Q/kT)$$

Where x is the interface reaction zone thickness (i.e. the diffusion distance), D is the diffusivity, t is the time, Q is the activation energy, k is the Boltzmann constant, T is the temperature in Kelvin, and the pre-exponential constant A depends on the matrix alloy composition, fiber, and the atmosphere. For a composite containing cylindrical fibers of small diameter, the diffusion distance is E very small. In this case we can write,

$$x^2 = Kt$$

where K is a pseudo-diffusivity and has the dimensions of diffusivity (m^2s^{-1}). This relation is valid only when the reaction thickness is small compared with the interfiber spacing under these conditions, one can use an Arhenius-type relationship,

K = A exp (-Q/kT), where A is a pre-exponential constant. A plot of lnK versus 1/T can then be used to obtain the activation energy, Q, for a fiber/matrix reaction in a given temperature range.

2.2.6. Fabrication of Composites:

i) PMC (Polymer Matrix Composites) ,

1) Filament winding

2) Pultrusion

3) Compression molding

4) Laminate stacking/Vacuum Bagging/ Autoclaving

5) Wet flow methods

a) Injection molding

b) Resin transfer molding

ii) CMC (Ceramic Matrix Composites)

1) Usually a two-step process

a) Incorporation of a reinforcing phase into an unconsolidated matrix.

b) Matrix consolidation

2) Several methods are common:

c) Melt infiltration

d) Chemical vapor deposition/infiltration (CVD)

iii) MMC(Metal Matrix Composite)

Metal-matrix composites are either in use or prototyping for the Space Shuttle, commercial airliners, electronic substrates, bicycles, automobiles, golf clubs, and a variety of other applications. While the vast majority are aluminum matrix

composites, a growing number of applications require the matrix properties of super alloys, titanium, copper, magnesium, or iron.

Compared to monolithic metals. MMCs have:

- Higher strength-to-density ratios
- Higher stiffness-to-density ratios
- Better fatigue resistance
- Better elevated temperature properties c -- Higher strength - -- *Lower* creep rate
- Lower coefficients of thermal expansion
- Better wear resistance

The advantages of MMCs over polymer matrix composites are:

- Higher temperature capability
- Fire resistance
- Higher transverse stiffness and strength

-No moisture absorption

-Higher electrical and thermal conductivities

-Better radiation resistance

-No out gassing

-Fabricability of whisker and particulate-reinforced MMCs with conventional metalworking equipment.

Some of the disadvantages of MMCs compared to monolithic metals and polymer matrix composites are:

- Higher cost of some material systems
- Relatively immature technology
- Complex fabrication methods for fiber-reinforced systems (except for casting)
- Limited service experience

Numerous combinations of matrices and reinforcements have been tried since work on MMC began in the late 1950s. However, MMC technology is still in the early stages of development, and other important systems undoubtedly will emerge.

The most important MMC systems are:

- Aluminum matrix

  Continuous fibers: boron, silicon carbide, alumina, graphite

  Discontinuous fibers: alumina, alumina-silica *c* Whiskers: silicon carbide

  Particulates: silicon carbide, boron carbide

- Magnesium matrix
- o Continuous fibers: graphite, alumina
- o Whiskers: silicon carbide
- o Particulates: silicon carbide, boron carbide

- Titanium matrix
- o Continuous fibers: silicon carbide, coated boron
- c Particulates: titanium carbide

- Copper matrix
- *o* Continuous fibers: graphite, silicon carbide
- c Wires: niobium-titanium, niobium-tin
- *o* Particulates: silicon carbide, boron carbide, titanium carbide.

- Super alloy matrices c Wires: tungsten

2.2.7 Cermets:

A group of essentially structural composites made of ceramics and metals are known as cermets; they are also called cemented carbides or hard metals. Cermets were first developed in the 1920 s as materials for cutting tools. Until then tool materials were mainly of plain carbon steels; these steels are still used in less demanding application. The disadvantage of carbon steel tools is that their hardness decreases rapidly with temperature above 500 K. Alloy tool steels, containing, for instance, Mn and W, has sustain temperatures of the order of 1000 K, but this is still not enough with high cutting speeds, exceeding 30 m/min. By contrast, cermets tools have better wear resistance and toughness, and can sustain cutting speeds of the order of 300 m/min.

The most often used cermets consist of between 6 and 20 vol% co, the rest being tungsten carbide (WC). In more recent cermets of this category, the tungsten carbide is either partially or wholly replaced by other carbides, such as TaC, TiC or MoC. We also have cermets such as ZrC + Fe, Cr_3C+Ni, MgO+Ni, Mo_2B+Ni and Al_2O_3+Cr.

Interest in cermets is increasing rapidly but not because of their use as cutting tools. They are used as mining drills. They are potential armor or ballistic potential materials. But, above all, they are useful for high-temperature aerospace applications: for thermal protection shrouds, leading edge, rocket nozzles, and to protect space capsules against micro-meteorite bombardment. They are also used in die and wear parts, and rock cutting tools.

There are several theories explaining strengthening of a given phase by incorporation of a fine dispersion of second phase particles, as it is done in cermets. Donald & Mc Millan reviewed such theories. Usually strengthening is attributed to a

dislocation impediment mechanism; and various theories are based on different mechanism.

Chemical composition and microstructure are varied in each application to produce the desired properties. It is important that both the manufacturers and users of these various grades of cemented carbides be familiar with their microstructures and the related physical properties. A good working knowledge of structures will greatly assist the engineer in selecting the grade of carbide required in a particular application [1].

2.3 Tungsten Carbide (WC) - the matrix under consideration:

Cutting tools must be able to resist high temperature and serve temperature gradients, thermal shock, abrasion, attrition, and chemical induced wear [2,3]. Thus materials for cutting tools and dies must have high hardness to combat wear, hot strength to overcome the heat involved and sufficient toughness to withstand interrupted cuts or vibrations occurring during the machining process. Cutting tools are a two billion-dollar industry worldwide and from the backbone of manufacturing operations for metals, polymers and advanced materials such as intermetallics and composites of all types [2,3].

Tungsten carbide (WC) has been well known for its exceptional hardness and wear/ erosion resistance. Matrices of ductile metals, such as cobalt, greatly improve its toughness so that brittle fracture can be avoided. Tungsten carbides are commercially one of the oldest and most successful powder metallurgy products [4].These composites are essentially aggregates of particles of Tungsten carbide bonded with cobalt metal via liquid-phase sintering. The properties of these materials are derived from those of the constituents - namely, the hard and brittle carbide and

the softer, more ductile binder. The cutting tool and wear part applications arise because of their unique combination of mechanical, physical and chemical properties.

Although other metal carbides, such as TiC, are also used in cutting tools, around 95% of all cemented-carbide cutting tools are Tungsten carbide-based [4]. In 1992, 60% of metallic tungsten produced went into WC for cutting tools, dies, etc., only 25% went into lamp filaments, heating elements and mill products, with most of the remainder was used in steels and supper- alloys [5]. Annual production of Tungsten for use in Tungsten carbide worldwide was about 25,000 metric tons in 1991/92 [6].

2.3.1 The Discovery of Tungsten carbide:

Henri Moissan (1852-1907), a Nobel Laureate (1906), is best known as the inventor of the electric furnace and for his successful attempts to prepare artificial diamonds. It was his laboratory at the school of Pharmacy at the University of Paris, that the two carbides of Tungsten were discovered, namely W2C (1896) by H. Moissan and WC (1898) by P. Williams [7].

The first commercial Tungsten carbide products were melt cast wire-drawing dies. Unfortunately, the cast pure WC is quite impractical because the stoichiometric compound WC, with 6.13 weight percent carbon, does not melt congruently; it decomposes to a fragile mixture of W2C, WC and graphite upon cooling. However, at lower carbon contents, mixtures of WC and W2C are formed on cooling, which melt at a relatively moderate temperature, around 2750°C and result in a cast product which is very hard, although by nature quite brittle, but nevertheless for some applications, such as dies [7].

The first sintered Tungsten carbide was produced in 1914 for use in drawing dies and rock drills. It was developed in an attempt to avoid the casting defects common to the molten products, and consisted of powdered Tungsten carbides or molybdenum carbide or mixtures of both, which were pressed and then sintered just below the melting temperature of the pure WC. However, the sintered product was very brittle and unsuccessful in industrial use [7].

2.3.2 The Development of Cemented Carbides:

Cemented tungsten carbide originated in the electric incandescent lamp industry in the US and in Germany. Since the invention of tungsten filaments for use in incandescent lamps at the beginning of the 20^{th} century, the lamp manufacturers had been searching for a replacement for the expensive diamond dies used in the wire-drawing of fine tungsten filaments. Promoted by a strategic shortage of industrial diamonds at the begining of World War I, the German lamp industry turned to the tungsten carbides as potential substitute materials. Because of their extreme hardness, the carbides of tungsten initiated a substantial research and development effort on the part of the incandescent lamp industry and their suppliers, for more than two decades.

A major breakthrough took place with the advent of cemented tungsten carbide in the 1920's. The successful development of the cemented carbides was generally attributed to the work of Karl Schriter who was a chemist [7]. At the beginning of World War I, he began searching for substitute materials for diamond in tungsten-wire-drawing equipment, starting with cast and sintered tungsten carbides. But neither the sintering process nor the casting process for making tungsten carbide wire-drawing dies was deemed successful and the work was abandoned. It was resumed about 1920 at Osram.

Systematic experiments to bind powdered tungsten carbide with iron, nickel or cobalt were carried out from 1918 to 1923 [8]. The first sintered cemented carbide dies were prepared in 1922. The wire-drawing tests showed cobalt to be the best additive. The invention of the cemented carbide tool materials was first disclosed in 1923 in Karl Schriter's patent application [9]. The two inventions claimed by the patent were:

- A unique hard metal alloy composition, namely the combination of the very hard tungsten carbide, WC, with small amount of a metal of the iron group; Fe, Ni, Co.
- The manufacture of the hard metal alloys by the application of the process of powder metallurgy, namely the pressing and sintering of mixed powders of tungsten carbide and binder metal.

The manufacturing process, then and now, is one of powder metallurgy, with liquid phase sintering. Karl Schr'ter's "decisive step" consisted of sintering a mixture of 90 wt% tungsten carbide and 10wt% of binder metal namely iron, nickel or cobalt, but preferably cobalt, at temperatures at which the binder is liquid and complete consolidation of the compact occurs. The resulting microstructure consists of an aggregate of fine (1-2 micrometers) WC particles embedded in the cobalt rich binder. The properties are controlled by composition and microstructure: the hardness increases with decreasing Co content and small particle size of WC, but, in general, at some cost of rupture strength and fracture toughness. The result was what we now know as "cemented carbides", a class of materials having distinctive microstructure and superior physical properties. The importance of the invention is confirmed by noting that today, seventy years later, the same compositions, made by essentially the same process, are still a very significant product of the tool materials industry.

In tungsten-wire plants, the cemented carbides drawing dies quickly replaced diamond dies for reducing heated tungsten wire in the coarse rang, after the swaging operation, i. e. from about 0.7 mm down to 0.3 mm in diameter. Significant as it was for wire drawing dies, the new material represented a truly revolutionary cutting tool

material for machining. The addition of cobalt to tungsten carbide not only allows the sintering of dense compacts at reasonable temperatures, but also results in materials with adequate toughness at very high hardness levels. When the new tools, made from sintered WC-Co, were placed on the market in 1927, they caused a sensation in the machine tool industry, by allowing cutting speeds 3 to 5 times faster than the best high speed steel tools in use at that time.

Modification of Schriter's compositions by replacing either a portion or all of the tungsten carbide with other carbides (in particular those of titanium, tantalum, and molybdenum) led to the major discovery that such additions were essential for cutting steel at speeds that provide economic advantages. The discovery by Schwarzkopf that solid solutions of carbides are superior to individual carbide was the starting point of the development of multi-carbide cutting tools for high speed machining of steel [10].

The most important advance in cutting tool technology since the development of WC-Co was the development of coated tools in late the 60's and early 70's [11]. Coatings are diffusion barriers, and they prevent the interaction between the chip formed during machining and the cutting material. Typical coatings are Titanium Carbide (TiC), Titanium Nitride (TiN), Titanium Carbonitride (TiCN), and Alumina (A1203), which are extremely hard, thus very abrasion resistant. TiN has the added advantage of a significantly lower coefficient of friction against steels compared to WC/Co. Thus it reduces the energy needed during the cutting operation. All these compounds have extremely low solubility in iron and they enable inserts to cut at much higher speeds than is possible with uncoated cemented carbides. It was estimated that 80% of carbide tools sold today are coated [12]

2.3.3 Properties of Tungsten carbide:

The properties of sintered WC-Co composites are critically dependent on their final composition and structure [4].Slight deviations from the ideal carbon contents bring about the occurrence of either graphite or a ternary compound. Both of these phases are usually undesirable and result in degradation of mechanical properties and cutting performance. Therefore, the carbon content must be maintained within narrow limits to obtain the desired composite with optimum properties. It is now well established that two types of h phase can be obtained - M12C (Co6W6C) of substantially constant composition and an M6C in which the composition can vary within the range of Co3.2W2.8C and Co2W4C. TheM6C type of h phase is in equilibrium with the liquid phase and can nucleate and grow during the sintering process. This not only embrittles the structure by replacing the binder with a brittle phase, but also reduces the effective contribution of WC to the strength of composite. The M12C type is formed in the solid state (during cooling) with small grains distributed throughout the matrix and is therefore effectively less embrittling. Table 1 shows the list of properties of representative grades of cemented WC [13]

Table2.1: Properties of representative grades of WC-Co composite.

cemented carbide	Room temperature hardness HV	Modulus of elasticity. GPa	Transverse rupture strength MPa	Co-fficient of thermal expansion. 10^{-6}/K	Thermal conductivity. W/m.K	Density. g/cm^3
WC-20 wt% Co	1050	490	2850	6.4	100	13.55
WC-10 wt% Co	1625	580	2280	5.5	110	14.50
WC-3 wt% Co	1900	673	1600	5.0	110	15.25
WC-10 wt% Co-22 wt%(Ti,Ta,Nb) C	1500	510	2000	6.1	40	11.40

Compared to other refractory carbides, the thermodynamic stability of tungsten carbide is relatively low, as is its room-temperature hardness. At high temperatures, most cubic carbides rapidly lose their hardness, whereas the hardness of the WC is quite stable. Coupled with this fact, the unique deformation characteristics of WC are the basis for its predominance as the hard refractory phase in cemented carbides. Other noteworthy properties of WC are its extremely high modulus of elasticity, second only to that of diamond, and its high thermal conductivity. The other refractory carbides have been used effectively as grain growth inhibitors in liquid phase sintering of WC-Co. It has been found that the effectiveness of a

transition metal carbide as a grain growth inhibitor is related to its thermodynamic stability, and they may be ranked as follows:

VC>Mo2C>Cr3C2>NbC>TaC>TiC>Zr/HfC

It was found that there is a maximum level above which no further grain growth inhibition occurs. This level is believed to correspond to the maximum solubility of the carbide phase in liquid cobalt. A liquid phase that is saturated with inhibitor carbide would reduce the solubility of WC, and thereby reduce its coarsening rate. Table2 shows the lists of properties of refractory carbides and binder metals [14].

Table2.2: Properties of refractory metal carbides and binder metals.

Material	Hardness HV (50 kg)	Crystal structure	Melting temperature (°C)	Theoretical density. g/cm^3	Modulus of elasticity. GPa	Thermal expansion. µm/m.K
WC	2200	Hexagonal	2800	15.63	696	5.2
W_2C	3000	Hexagonal	2777	17.30	.....	.....
Co	<100	Cubic/ Hexagonal	1495	8.90	207	16.0

2.3.4 The role of Co as a binder:

The role of cobalt in cemented carbides is to provide a ductile bonding matrix for tungsten carbide particles. Cobalt is used as a bonding matrix because its wetting or capillary action during liquid phase sintering allows the achievement of high densities. Because of the high cost of cobalt, attempts have been made to design

alternate materials, with iron and nickel as the predominant cobalt substitutes. However, sliding wear tests show that cobalt content is very important for cemented carbides to have good wear resistance.

Fracture in WC/Co systems with high Co contents has been found to occur mainly by the ductile rupture of Co through void nucleation and coalescence [15]. Other fracture modes such as fracture along WC/Co interface and WC/WC grain boundary decohesion as well as cleavage across WC grains were also noted. These mechanisms occur especially at low volume fractions of Co binder in the composite at which the contiguity of WC grains begin to increase. The effect of the contiguity of WC skeleton on fracture toughness has also been demonstrated. In a fracture toughness experiment , in a given crack plane , the crack propagation is easy along the relatively weak WC/Co and WC/WC boundaries and final fracture is primarily controlled by the area fraction of Co regions intact across the crack plane ahead of the tip .Since the WC/WC decohesion WC/Co interface fracture energies are likely to be lower than the fracture energy absorbed in ductile fracture of the binder, ductile failure of Co can be considered as a primary mechanism manifesting the fracture resistance

Several investigations attempted to correlate the micro structural parameters and mechanical properties of constituent phases to experimentally measured fracture toughness values. In particular, it has been universally found that the fracture toughness increases with volume fraction, the mean free path length of the binder and the size of WC grains .In addition higher toughness has been suggested to result from the increased contiguity of Co binder, which minimizes the fracture along weak WC/WC boundaries. For a given volume fraction, geometrical arrangement of the ductile binder as a continuous thin matrix phase is beneficial for high toughness while retaining high strength. This arrangement could be most desirable of several possible arrangements in which the deformation ductile Co phase is highly constraint in the microstructure [15].

References:

1. Shantanu Sinha, 'Study of electrical and structural properties of WC/Co composites', M.S. thesis, 2000-2001.

2. R. Edwards, "Cutting Tools", The Institute of Materials, London, 1993

3. E. M. Trent, " Metal Cutting", Buttetworths, Boston, 2nd Ed.,1984.

4. V. K. Sarin, "Cemented CarbideCutting Tools", Advances in Powder Technology, Ed. D. Y. Chin. ASM, pp. 253-287, 1981.

5. "Tungsten", Mac Graw-Hill, Ency6clopedia of Science and technology, 7th Ed.1992.

6. H. Kolaska, "The Dawn of the Hardmetal Age", Powder Metallurgical International, v24, no.5, p 311-314,1992.

7. J. Gurland and J. D. Knox., "From Sintered Tungsten to Cemented Tungsten Carbide-A Historical Review of Two Related Technologies", Tungsten Refract. Met.3-1995, Proc. Int. Conf., 3rd 1995(Pub. 1996), 219-228.Edited by Bose, Animesh: Dowding, R. J. Metal Powder Industries Fedaration.

8. K.V. Krishna, Proc. Of the Int. School on powder Diffraction (ISPD'98). IACS. Calcutta, India, 7-10 Oct.1998, pp 109

9. K. Schrter, US Patent 1.549.615 (application Oct. 31. 1923: patented 1925).

10. P. Schwarzkopf. Deutsche Edelstahlwerke. AG German Patent 720.502 (patented v 1929. issued 1942).

11. P. Craii:. "Behind the Carbide Curtain". Cutting Tool Hnjiineering. August 1997.

12. K. Schr ter. "The Inception and Development of Hard Metal Carbides". The Iron Age. V. 135. Feb. 1, 1934. 27-29.

13. H J. Scussel. "Friction and Wear of'Cemented Carbides". ASM HandK>ok. Vol. 18. ASM Int.. pp. 795. 1992.

14. K. S Ravichandran. "Fracture Toughness of Two Phase WC-Co Cermets". Acta Metall. Mater.. 42. 143-J50. 1994

CHAPTER THREE

CHAPTER 3: SAMPLE PREPARATION AND EXPERIMENTAL THEORIES & MEASUREMENTS

3.1 Introduction:

In this chapter, various experimental methods of sample preparation and characterization technique employed in synthesis of the material are described briefly. A brief description of the apparatus, which is used for the magnetoresistance measurements, is also given.

3.2 Sample preparation and Sintering:

Preparation: Cobalt is a hard transition metal. Because of its unique set of physical and electrical properties, it was chosen as the dispersoid in the WC matrix. The main procedure for manufacturing this composite is based on sintering. Increasing amount (6 to 14 vol%) of Co powder (Japan New Metals Co, Japan)were mixed with high purity tungsten carbide (WC) powder (AKP-53, Sumotimo Chemicals LTD., Japan) and heated until a liquid phase appears. The liquid wets the solid WC particles and fills the empty space between them. The continuous matrix thus formed is maintained after cooling and solidification of the whole phase.

After drying, samples of each composite were hot-pressed in a graphite die with it inner walls coated with a BN slurry to avoid any interaction between specimens and graphite die. The hot press atmosphere was argon. For all the composites, the maximum hot pressing pressure was 30 MPa. The selected sintering temperature and time were 1640°C and 1 h, respectively. The samples were then cooled down (200° C / h) to room temperature. The hot-pressed samples were in the form of rectangular solid bars with length, width and thickness of 100 mm, 12 mm and 3 mm respectively. The samples were then cut into convenient sizes for the experimental purpose.

Proper sample preparation is an absolute necessity in carbide metallographic. As with other materials, improper preparation leads to inaccurate interpretation. Care must therefore be exercised in sectioning, grinding and polishing of all samples.

3.3 X-ray diffraction technique

X-ray diffraction is one of the most ancient and effective tools for the investigation of the fine structure of matter. This technique had its beginning in Von Laue's discovery in 1912 that crystals diffract X-ray, the manner of diffraction revealing the structure of the crystal. At first, X-ray diffraction was used only for the determination of crystal structure. Later on, however, other uses were developed and today the method is applied not only to structure determination, but also to such diverse problems as chemical analysis and stress measurement, to the study of phase equilibria and the measurement of particle size, to the determination of the orientation of one crystal or the ensemble of orientation in a polycrystalline aggregate. In 1912, Von Laue first proposed that if crystals are composed of regularly spaced atoms which may act as scattering centre for X-rays and if X-rays are electromagnetic waves of wavelength about equal to the inter-atomic distance (i. e. about 1A°) in crystals, then it should be possible to diffract X-rays by means of crystals. At the same year W.H. Bragg successfully analyzed the Laue experiment and was able to express the necessary conditions for diffraction in a considerably simpler mathematical form than that used by Laue. He suggested that whenever X-rays are incident on a crystal surface, they are reflected from it. The reflection abides by the celebrated Bragg's law as given bellow.

$$2d \sin \theta = n\lambda$$

Here d is the distance between crystal planes, θ is the incident angle, λ is the wave length of X-ray and n is a positive integer and represents the order of reflection. Bragg's law also suggests that the diffraction is only possible when $\lambda < 2$ d.

X-ray diffraction is a versatile non-destructive analytical technique for qualitative identification and quantitative estimation of the various crystalline forms present in powder or solid samples [1]. A given substance always produces a characteristic diffraction pattern, whether that substance is present in the pure state or as one constituent of a mixture of substances. This fact is the basis for the diffraction method of chemical analysis. Quality analysis for a particular substance is accomplished by identification of the pattern of that substance. Quantitative analysis is also possible, because the intensities of the diffraction lines due to one constituent of a mixture depend on the proportion of that constituent in the specimen [2].

The particular advantage of diffraction analysis is that it discloses the presence of a substance as that substance actually exists in the sample and not in terms of its constituent chemical elements. Diffraction analysis is therefore useful whether it is necessary to know the state of chemical combination of the elements involved or the particular phases in which they are present. As a result, the diffraction method has been widely applied for the analysis of such materials as mineral, ore, clay, soil, alloy, industrial dust etc. Compared with ordinary chemical analysis, the diffraction method has the advantages that it is usually much faster, requires only a very small sample and is nondestructive.

The main aim of the present study was to determine the actual concentration of Co in WC composite materials and some parameter of WC crystal.

3.4 X-ray diffractometer

Five samples of WC with percentage of Co (WC/Co) were prepared. Each of the samples had a dimension about (100/12/3) mm. The sample were then cut into convenient size which had a dimension about 17/13/3 mm. Then one by one the samples were hold with a sample holder so that its surface was at the same level of that of sample holder and preserved the sample for XRD experiment.

A Philip's PW3040 X'Pert PRO X-ray diffractometer was used to get X-ray data for the samples at the Material Science Division, Atomic Energy Centre, and Dhaka where powder diffraction technique was used with a primary beam powder of 40kV and 30 mA for Cu radiation. A Ni filter was used in front of the sample holder to get monochromatic X-ray. Ni filter reduces the Cu Kβ radiation [3] and finally Cu Kα radiation was only used. A (θ-2θ) scan was taken from 10° to 100° to get possible fundamental peaks of the samples with the sampling pitch of 0.02° and time for each step data collection was 0.06 second. The XRD machine was totally computer controlled and all the data were stored in the hard disk memory of the computer for further analysis.

To validate the present result, it was compared with the data of standard sample stored in computer memory.

3.5 Resistivity measurement:

The one of the simplest way of finding the resistivity ρ (ohm-centimeter) is to use a rectangular sample of known dimensions to measure the resistance R and use the relation

$$R = \rho L/A \qquad \text{..... (2.1)}$$

Where L is the sample length, A is the cross section. A disadvantage is that will also contain a contact-resistance term, which for semiconductors can be appreciable. The effect can be minimized by plotting measured resistivity versus applied voltage. The resistivity will ordinarily decrease as the voltage increases and finally become relatively constant. If injection from the contacts has not become excessive at the point, the resistivity is probably no more than a few percent high. Injection difficulties can arise only with long life time materials such as Si and Ge but should seldom be a problem.

3.5.1 Two-point probe:

The effect of contact resistance can eliminate by using two-point probe of fig. 2.1 if the specimen cross section is relatively uniform. Measurement restrictions are that the current must be kept low enough to prevent heating of the sample, the voltmeter must have a high input impedance and measurements must be made far enough away from the contacts that any minority carriers injected will have already recombined.

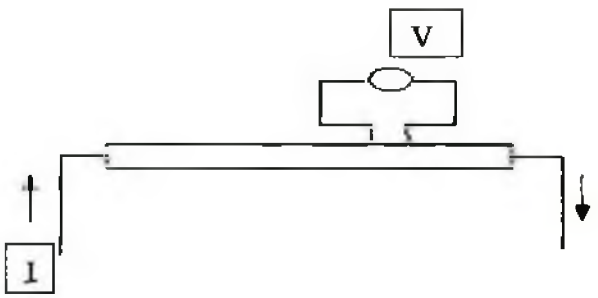

Fig.3.1: Two-point resistivity geometry. The voltage probes have fixed spacing and are moved in unison along the surface.

3.5.2 Four-point probe:

In the semiconductor technology the generally used technique for the measurement of resistivity is the four-point probe. The usual geometry is to place the probes in a line and use equal probe spacing. Current is passing through the outer two probes and potential developed across the inner two probes is measured. For probes resting on a semifinite medium the resistivity is

$$\rho = \frac{2\pi(V/I)}{[1/S_1 + 1/S_3 - 1/(S_1+S_2) - 1/(S_2+S_3)} \qquad \text{..... (2.2)}$$

where, S is the probe spacing in centimeters. When the probes are equally spaced, $S_1=S_2=S_3=S$ and Eq.2.2 reduces to

$$\rho = 2\pi S\frac{V}{I}$$

Since the four-point probes offer the most convenient mode of resistivity measurement, here the device has been used to perform four-point probes resistivity measurement.

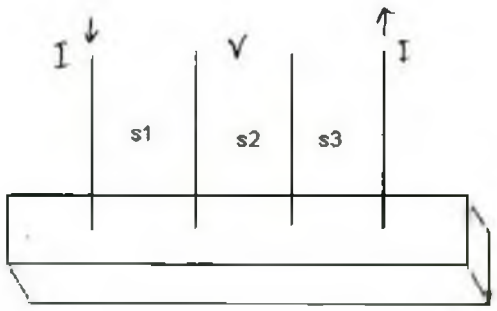

Fig.3.2: Linear four-point resistivity probe.

3.6 Electrical conductivity:

Electrical conductivity or specific conductivity is a measure of a material's ability to conduct an electric current. When an electrical potential difference is placed across a conductor, its movable charges flow, giving rise to an electric current. The conductivity σ is defined as the ratio of the current density J to the electric field strength E.

$$J = \sigma E$$

Conductivity is the reciprocal (inverse) of electrical resistivity and has the SI units of siemens per meter ($S \cdot m^{-1}$) i.e. if the electrical conductance between opposite faces of a 1-metre cube of material is 1 siemens then the material's electrical conductivity is 1 siemens per meter. Electrical conductivity is commonly represented by the Greek letter σ, but κ or γ are also occasionally used.

Temperature dependence of Electrical conductivity:

Electrical conductivity is strongly dependent on temperature. In metals, electrical conductivity decreases with increasing temperature, whereas in semiconductors, electrical conductivity increases with increasing temperature. Over a limited temperature range, the electrical conductivity can be approximated as being directly proportional to temperature. In order to compare electrical conductivity measurements at different temperatures, they need to be standardized to a common temperature. This dependence is often expressed as a slope in the conductivity-vs-temperature graph, and can be used:

$$\sigma_{T'} = \frac{\sigma_T}{1 + \alpha(T - T')}$$

where

$\sigma_{T'}$ is the electrical conductivity at a common temperature, T'

σ_T is the electrical conductivity at a measured temperature, T

α is the temperature compensation slope of the material,

T is the measured absolute temperature,

T' is the common temperature.

3.7 Magnetoresistance:

Magnetoresistance (MR) is the ability of a material to vary its electrical resistance depending on an applied magnetic field; is the key parameter for higher information storage densities in magnetic recording media. It is a property of magnetic materials which is crucial for a rapid development of new technologies. Magnetoresistance is defined as the change in the electrical resistance produced by the application of an external magnetic field. It is usually given as a percentage and expressed as

$$\mathrm{MR}\% = \frac{\rho(H) - \rho(H=0)}{\rho(H=0)} \times 100$$

Where $\rho(H)$ is the resistivity in an applied magnetic field and $\rho(0)$ is the resistivity in the absence of a magnetic field. With this definition, the magnetoresistance has a maximum value of 100%. Negative magnetoresistance means the application of a magnetic field causes a dramatic decrease of the resistivity.

3.8 Types of magnetoresistance and their mechanism

Magnetoresistance are divided on the basis of the mechanisms, spin orientations etc. Some classes of magnetoresistance are

-AMR (Anisotropic magnetoresistance)

-GMR (Giant magnetoresistance)

-PMR (Powder magnetoresistance)

-BMR (Ballistic magnetoresistance)

-CMR (Colossal magnetoresistance)

-IMR (Itergrain magnetoresistance)

-TMR (Tunneling magnetoresistance)

-EMR (Extraordinary magnetoresistance)

-VLMR (Very Large magnetoresistance)

3.8.1 Anisotropic magnetoresistance (AMR)

AMR is the change in resistance seen when the current flowing through a sample changes from being parallel to the internal magnetization to being perpendicular to it. The
dependence of the AMR effect is given by- [4]

$$R_{total} = R_{mim} + \nabla R_{amr} \cos^2(\varphi)$$

Where

R_{total} is the total electrical resistance,

R_{mim} is the minimum electrical resistance,

∇R_{amr} is the incremental AMR resistance,

and φ is the angle between the current flow direction and magnetization direction in the material.

Resistance is high when current is parallel (or antiparallel) to the field and low when field and current are orthogonal. Materials that exhibit AMR include Permalloy (Ni Fe) and iron filings. The AMR features are:

- appears in single crystal,
- depends on the relative orientation of current flow magnetization,
- slow read-access time of these materials is about 250 ns,
- critical dimension of the magnetic cell is larger than 1 μm,
- not competitive with general semiconductor memories in speed, density and cost.

3.8.2 Giant magnetoresistance (GMR)

The Giant Magnetoresistance was discovered in 1988 independently by Baibich *et al.* in Paris and Binasch *et al.* in Jülich. It is the phenomenon where the resistance of certain materials drops dramatically as a magnetic field is applied. It is described as Giant since it is a much larger effect than had ever been previously seen in metals. It has generated interest from both physicists & device engineers, as there is both new physics to be investigated and huge technological applications in magnetic recording and sensors.

Giant magnetoresistance has been the subject of a huge international research effort due to the numerous technological applications. The largest is in the data storage industry and IBM were first to market with hard disks based on GMR technology although today all disk drives make use of this technology. On-chip GMR sensors are available commercially from Non-Volatile Electronics who were the first

company to sell GMR products. Other applications are as diverse as solid-state compasses, automotive sensors, non-volatile magnetic memory and the detection of landmines.

GMR describes the behavior of materials that have alternating layers of ferromagnetic and nonmagnetic materials. The GMR effect is the change in resistance in the magnetic multilayer that occurs with a change in the relative directions of magnetization between layers. The spin up channel acts as a shunting current, lowering the resistivity of the complete stack of layers found considerable compared to when the moments are antiparallel. As a result, the conduction electrons with spin parallel to the material's magnetization move freely, while the motion of those electrons with antiparallel orientation is impeded via collisions with the atoms in the material. The dependence of the GMR effect is given by: [4]

$$R_{tot} = R_{min} + \Delta R_{gmr} \sin(\frac{\varphi}{2})$$

Where

R_{tot} is the total electrical resistance,

R_{min} is the minimum electrical resistance,

ΔR_{gmr} is the incremental GMR resistance,

and φ varies between π and $-\pi$ radians, is the angle between the magnetization directions in the storage and sensing layers.

The GMR features are

-requires two materials,

-depends on relative orientation of two magnetizations,

- magnetoresistance ratio of about 6%,
- read-access times of bellow 50ns were achieved for MRAM with GMR materials,
- low sense signal,

- magnetic cell would not work with sense lines narrower than about 1 μ m,
- there is a limit to how quickly the magnetization can change directions with distance.

3.8.3 Ballistic magnetoresistance (BMR)

The Ballistic magnetoresistance (BMR) is the resistance that the electric current manifests through a point contact when a magnetic field is applied. The BMR effect arises from non-adiabatic spin scattering across very narrow (atomic scale) magnetic domain walls (DW) assuming that the DW width formed at the contact is of the order of the contact size [5].

Garcio et al. [6] had reported a 400-700% BMR effect at room temperature in Ni contacts deposited on small gaps between Ni wires. These MR values clearly cannot be explained by DW scattering [5,7] since the contact size are of the order of 10 nm, while the DW scattering yields BMR values not larger than 10%. In bilk ferromagnets, Tatara and Fukuyama [8] have shown that the spin-dependent scattering by domain walls is negligible, owing to the adiabatic nature of electron transport across a wall, which is typically of the order of several tens of nanometers wide.

Recently much larger values (over 3000% at room temperature) of MR have also been reported [9] in Ni nanocontacts achieved at low switching fields (less than a few hundred Oersteds). This effect of large BMR values in 1 nm size contacts may be assigned to the formation of a very thin "dead layer" or non-stiochometric compound (oxide, sulfite etc.), at the nanocotact region that may reconfigure the spin density of states defining the electron transport. Unlike in bulk ferromagnets, (or thin films) Bruno has recently shown that atomically sharp domain walls can form in point contacts [10] giving rise to the nonadiabatic nature of spin scattering and a very

large BMR at room temperature. Thus, the large variation in BMR in different samples even with the same contact resistance is due to the fact that the BMR is not a function of the nanocontact diameter alone, also depends on the geometrical form of the nanocontact.

3.8.4 Itergrain magnetoresistance (IMR)

Itergrain magnetoresistance (IMR) is characterized by rapid resistance drop at low applied magnetic field, followed by a slow decrease at higher magnetic fields. These two regimes cross over at the magnetic field for which magnetic saturation is achieved. It has been shown that the IMR occurs at the grain boundaries, and the large degree of spin-polarization characteristic of half-metallic ferromagnets enhances these effects to a large extent [11].

3.8.5 Tunneling magnetoresistance (TMR)

A large change in the electrical resistance upon the application of a magnetic field of two magnetic layers separated by an insulating layer.

In physics, the tunnel magnetoresistance effect, commonly abbreviated as TMR, occurs when two ferromagnets are separated by a thin (about 1 nm) insulator. Then the resistance of the tunneling current changes with the relative orientation of the two magnetic layers. The resistance is normally higher in the anti-parallel case.
It was discovered in 1975 by Julliere, using iron as the ferromagnet and germanium as the insulator.

Room temperature TMR was discovered in 1995 by Moodera et. al. following renewed interest in this field fueled by the discovery of the giant

magnetoresistive effect. It is now the base for the magnetic random access memory (MRAM).

3.8.6 The Extraordinary magnetoresistance (EMR)

This effect shows an increase in MR as large as 100% has been seen in a non-magnetic semiconductor with an embedded metallic inhomogeneity. At room temperature and H=500 Gauss, which is the relevant magnetic field for high-density data storage applications using EMR materials.

3.9 Methodology

The resistivities of the samples were measured using a standard four-probe method within a temperature range of room temperature to 483K. The temperature dependence of conductivity at zero applied magnetic field for various samples and the corresponding behavior in presence of applied magnetic field (up to H=KG) have been investigated. The magnetoresistance measurements were carried out in a magnetic field of H=1KG to 4KG in the temperature range of room temperature(300K) to 483K.

3.10 Description of the apparatus used for the present investigation

3.10.1 Electromagnet

We have used an electromagnet to study magneto transport properties of our samples. In constructing the present electromagnet, commercial mild steel bar for the

body of the electromagnet and soft iron cylindrical rod for pole pieces, which were available in the local market was used.

The electromagnet used in the experiment is depicted in the schematic diagram of Fig.3.3. The pole pieces of the electromagnet were of 9.2 cm diameter and the pole gap was variable from 0 to 10 cm.

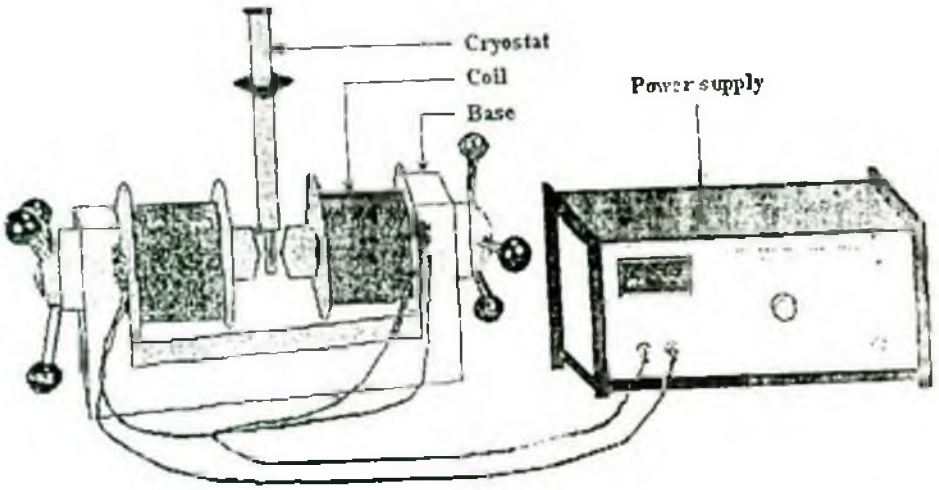

Fig. 3.3: Schematic diagram of an electromagnet with a power supply.

The maximum current applied to coils was 18 Amp. The current generated a dc magnetic field about 0.86 T in a pole gap of 3.8 cm. Magnetic field was measured by a Gauss meter. Fig. 3.4 shows variations of the magnetic field as a function of applied current with constant pole gap 3.8 cm. The electromagnet was used for the magnetoresistance measurement as a function of magnetic field.

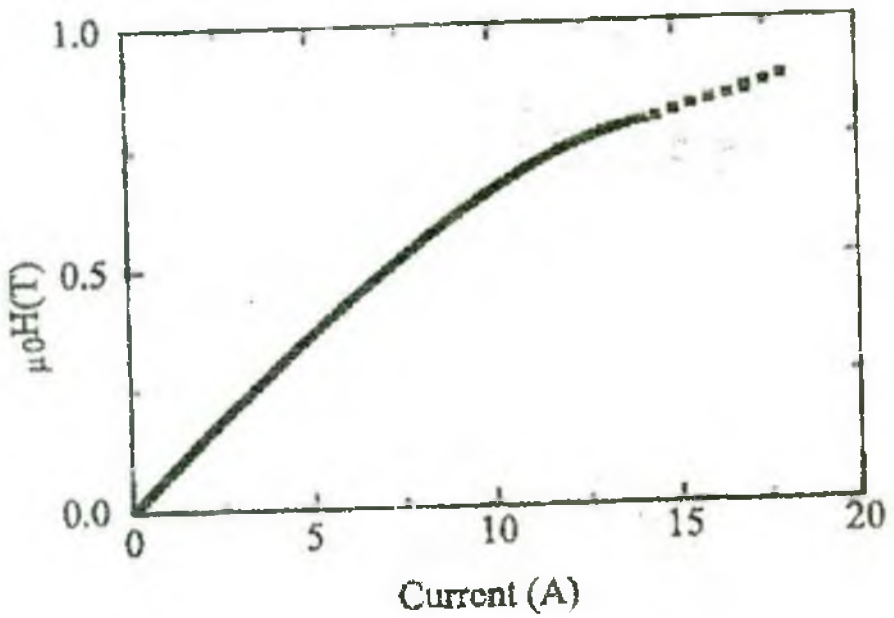

Fig. 3.4:Calibration of the homemade electromagnet (gap 3.8 cm)

3.10.2 Construction of sample holder rod

A sample holder rod is constructed for four-point resistance measurement. This is a hollow stainless tube. The upper part is connected with multi-pin connectors and lower part has a copper sample holder. A schematic diagram of the sample holder rod is shown in Fig.3.5.

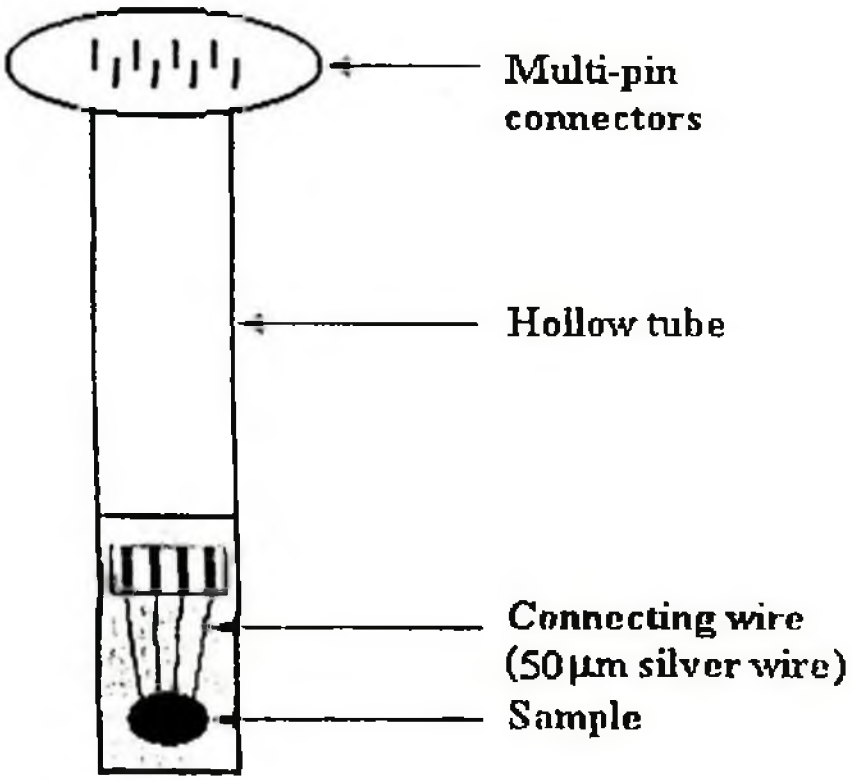

Fig.3.5: Schematic diagram of the sample holder rod

The sample probe is used for four-point resistance measurements. The temperature of the sample was measured using a thermocouple. For magnetoresistance measurement, we have to apply magnetic field in the sample space.

3.10.3 Magnetoresistance measurement set-up

Fig.3.6 shows the schematic diagram of the magnetoresistance measurement setup. The standard four-point technique was used for the resistance measurements. All samples for the test were mounted on a probe and inserted in the sample well of the cryostat. The temperature of the sample was measured using a thermocouple. The

thermocouple was powered by a constant current source and the resulting voltage as a function of temperature was measured with digital voltmeter.

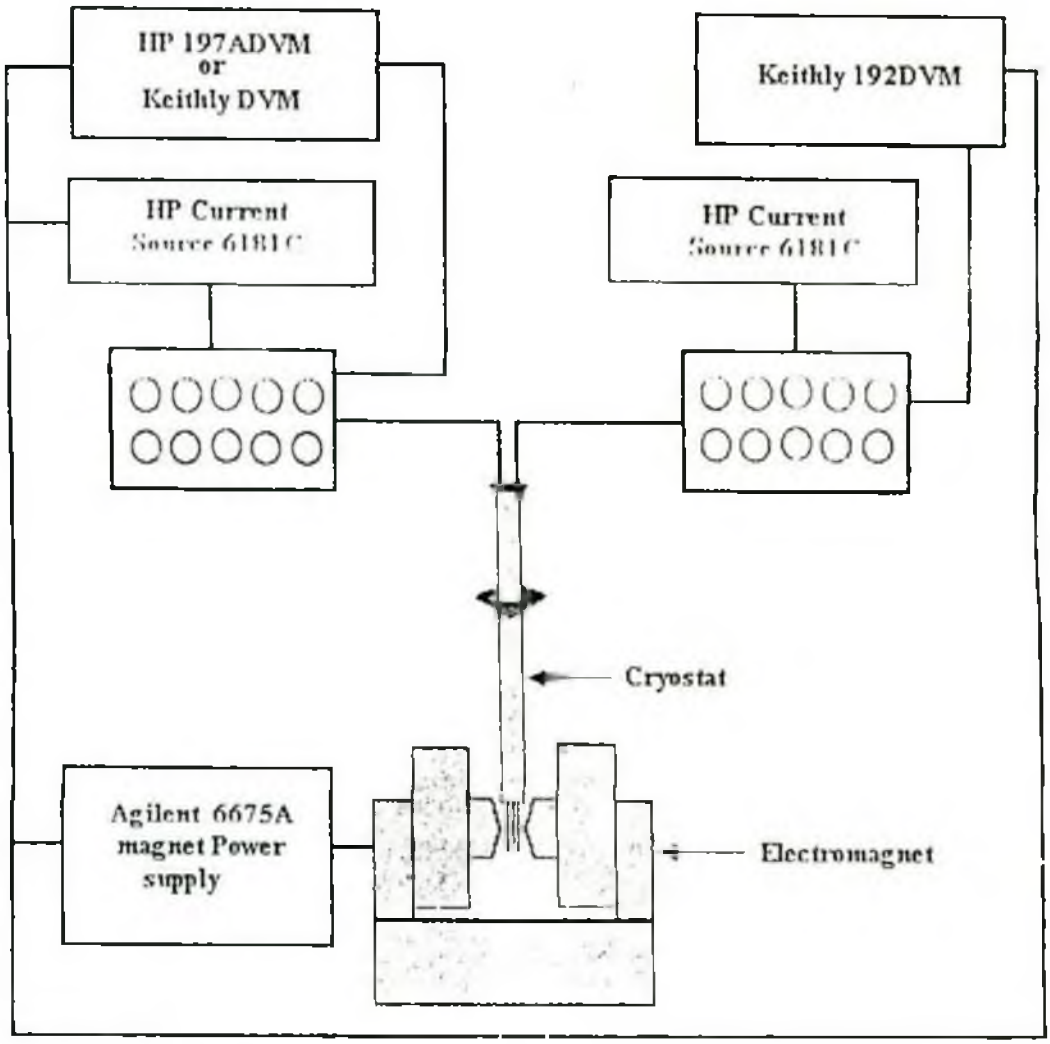

Figure 3.6 : Experimental setup for magnetoresistance measurements.

The current in the sample was supplied with another constant current source and the voltage drop was measured with a digital voltmeter. For magnetoresistance measurement, the electromagnet was powered with an Agilent 6675A power supply. The magnet was capable of creating a field of 0.86T for a current of 18 Amp.

References:

1. K.V. Krishna, Proc. of the Int. School on Powder Diffraction (ISPD), IACS, Calcutta, India, 7-10 October, 1998, pp 109.
2. D.K. Saha, Ph.D. Thesis, Inst. of Appl. Phys., Univ. of Tsukuba, Japan, 1994, pp35.
3. B.D. Cullty, Elements of X-ray Diffraction, Addison-Wesley Publication Company, Inc., USA, Second Edition, 1959, pp378.
4. Ananth Hegde and Ashwini Dwarkanath, Emerging memory technology. CSE597E, www.cse.psu.edu.typs.
5. G.Tatara, Y.W.Zhao, M.Munoz, and N. Garcia, Domain wall scattering explains 300% ballistic magnetoresistance of nanocotacts, Phys. Rev. Lett. 83, 2030(1999).
6. N. Garcia, M.Munoz, G. G. Qian, H. Rohrer, I. G. Saveliev,and Y.W.Zhao, ballistic magnetoresistance in a magnetic nanometer sized contact: An effective gate for spinotronics, Appl. Phys. Lett.79, 4550, (2001).
7. V.A.Molyneux, V.V. Osipov, and E.V.Ponizovskaya, "Stable two- and three- dimensional geometrically constrained magnetic structures: the action of magnetic fields," Phys. Rev. B85, 184425 (2002).
8. G.Tatara and H.Fukuyama, "Antiferromagnetic long range order in disordered spin-peierls systems," Phys. Rev. Lett. 78, 3773 (1997).
9. H.D. Chopra and S.Z. Hua, "ballistic magnetoresistance over 3000% in Ni nanocontacts at room temperature", Phys. Rev. B66, 0204403(R) (2002).
10. P.Bruno, "Geometrically constrained magnetic wall", Phys. Rev. Lett. 83, 2425 (1999).

11. I. Satoh, M.Oniduka, and T. Kobayashi, "magnetoresistance of (La, Sr)MnO_3 Tilted nano-column boundaries grown on step-edged (100) GaAs substrate", Graduate School of Engineering Science, Osaka University.

CHAPTER FOUR

CHAPTER 4: RESULTS

4.1 Introduction

The structural analysis and the transport properties of WC doped with various percentage of Co were studied. Here, the results of DC electrical measurements including resistively, conductivity and magneto resistance at temperature starting from RT to 210°C for 0-4 KG magnetic field are reported.

4.2 X-ray diffraction analysis

All the X-ray data of the samples were analyzed using computer to get d value of the fundamental peaks and their integrated intensity. The interplanar spacing d was calculated using the formula:

$$2\,d \sin\theta = n\lambda$$

Where λ is the incident radiation and for Cu (K_α), λ=1.54178 A° was used. The samples were then characterized using the d values of their main fundamental peaks (at least three for each) by comparing d values and their intensity ratios with the data available in the PDF File of Computer hard disk [1].

2.2.1 The concentration of WC and Co in different sample:

The concentration of WC and Co for each sample was estimated from their strongest peak of 100% I, where I is the intensity of the peak.

Both WC and CO were identified precisely and their concentration estimated within the error of maximum ± 2 % using XRD method. This has been done using the following method. The background of the system has been determined and

subtracted from the total intensity data. The total amount of WC and Co in a sample was considered as 100 percent. Then only one peak for a single material was selected, which has the maximum peak intensity (100% of I) among all the peaks of that particular material (i.e. WC or Co). Then the total integrated intensity for a particular peak was calculated by using the formula-

$$I_A = I_P \times FWHM$$

Where,

I_A is the integrated intensity of a particular peak,

I_P is the peak intensity of that particular peak and

FWHM is the full width at half maximum of the peak.

Again,

$$I_T = (I_1 + I_2 + \ldots\ldots\ldots I_n)$$

$$= \sum I_A$$

Where,

I_T is the total integrated intensity of the detected materials and

A = 1 , 2 , ...n.

The concentration of a particular material is calculated by

$$C_A = \frac{I_A}{I_T} \times 100$$

Where,

C_A is the concentration of a particular material in the sample in weight percent.

Table 4.1(a): Peak List for WC:

No.	h	k	l	d [A]	I[%]
1	0	0	1	2.84000	45.0
2	1	0	0	2.51800	100.0
3	1	0	1	1.8400	100.0
4	1	1	0	1.45400	20.0
5	0	0	2	1.42000	6.0
6	1	1	1	1.29400	25.0
7	2	0	0	1.25900	14.0
8	1	0	2	1.23600	30.
9	2	0	1	1.15100	20.0
10	1	1	2	1.01500	14.0
11	2	1	0	0.95100	10.0
12	0	0	3	0.94600	1.0
13	2	0	2	0.94200	10.0
14	2	1	1	0.90200	20.0

Table 4.1(b): Peak List for Co:

No.	d [Å]	I[%]
1	2.04000	100.0
2	1.77000	440.
3	1.25000	22.0
4	1.07000	22.0
5	1.02000	5.0
6	0.89000	3.0
7	0.81000	3.0
8	0.79000	3.0
9	0.72000	3.0
10	0.68000	3.0

Table 4.1(c): Peak List for WC/Co (6.5 vol. % Co) Composite.

Pos. [°2Th.]	Height[cts]	FWHM [°2Th.]	d-spacing[A]	Rel. Int.[%]
12.4779	1660.85	0.2362	7.09394	34.09
25.0512	182.31	0.2558	3.55473	3.74
29.6068	58.67	0.2165	3.01733	1.20
31.5061	4090.93	0.1574	2.83963	83.97
35.6281	4871.75	0.1771	2.51999	100.00
44.1724	66.23	0.2755	2.05036	1.36
48.2670	2697.90	0.1574	1.88556	55.38
51.3877	28.12	0.3542	1.77815	0.58
63.9877	609.51	0.1181	1.45507	12.51
65.7311	388.33	0.1440	1.41946	7.97
73.0855	563.56	0.1680	1.29370	11.57
75.4417	354.08	0.1440	1.25904	7.27
77.0926	567.43	0.1680	1.23614	11.65
77.3503	280.84	0.1440	1.23573	5.76
84.0562	425.68	0.1680	1.15057	8.74
84.3440	223.92	0.1440	1.15022	4.60
98.7664	235.31	0.2400	1.01478	4.83
108.1348	203.74	0.1920	0.95133	4.18
109.8671	187.71	0.2880	0.94113	3.85
117.2945	358.01	0.3600	0.90201	7.35
117.7975	215.10	0.2880	0.89961	4.42

Table 4.1(d): Peak List for WC/Co (7.5 vol. % Co) Composite.

Pos. [°2Th.]	Height[cts]	FWHM [°2Th.]	Spacing[A]	Rel. Int.[%]
31.5144	3215.94	0.1181	2.83890	75.23
35.6415	4275.02	0.0984	2.51907	100.00
44.1221	79.58	0.2755	2.05258	1.86
48.2949	2515.03	0.0960	1.88297	58.83
48.4370	1251.30	0.0720	1.88245	29.27
64.0240	562.05	0.1200	1.45313	13.15
64.1932	300.64	0.0960	1.45331	7.03
65.7680	412.14	0.0960	1.41876	9.64
65.9454	177.97	0.0720	1.41888	4.16
73.1074	459.20	0.1200	1.29337	10.74
73.3148	257.25	0.0960	1.29343	6.02
75.4876	326.31	0.0960	1.25839	7.63
77.1167	482.78	0.1200	1.23582	11.29
77.3493	217.68	0.1440	1.23574	5.09
84.0950	353.55	0.1440	1.15014	8.27
84.3463	201.29	0.0960	1.15020	4.71
98.7480	198.00	0.1200	1.01492	4.63
99.0613	109.59	0.1920	1.01506	2.56

Table 4.1(e): Peak List for WC/Co (8.5 vol. % Co) Composite.

Pos. [°2Th.]	Height[cts]	FWHM [°2Th.]	Spacing[A]	Rel. Int.[%]
31.7577	1419.11	0.1181	2.81771	67.21
35.8863	2111.59	0.1181	2.50245	100.00
44.4172	45.78	0.3149	2.03962	2.17
48.5232	1654.22	0.0960	1.87465	78.34
48.6590	877.89	0.0720	1.87438	41.57
64.2422	328.34	0.0960	1.44872	15.55
65.9772	137.97	0.1920	1.41476	6.53
73.3205	294.61	0.1920	1.29013	13.95
75.6816	160.32	0.1920	1.25564	7.59
77.3033	294.83	0.1680	1.23330	13.96
84.2680	214.15	0.1920	1.14821	10.14
98.9038	134.74	0.1920	1.01374	6.38

Table 4.1(f): Peak List for WC/Co (10 vol. % Co) Composite.

Pos. [°2Th.]	Height[cts]	FWHM [°2Th.]	Spacing[A]	Rel. Int.[%]
12.6865	50.71	0.3149	6.97779	2.27
23.0300	794.28	0.3936	3.86194	35.51
29.0597	82.16	0.3149	3.07288	3.67
32.0050	1470.51	0.1574	2.79650	65.74
36.1425	2236.76	0.1771	2.48530	100.00
44.5817	39.92	0.2362	2.03248	1.78
48.7787	1697.37	0.1574	1.86697	75.89
51.8014	40.37	0.4723	1.76491	1.80
64.4706	439.54	0.1771	1.44533	19.65
66.1942	268.37	0.1574	1.41182	12.00
73.5300	378.46	0.1680	1.28697	16.92
75.8831	289.64	0.1200	1.25281	12.95
77.5126	411.30	0.1200	1.23049	18.39
84.4591	302.03	0.1920	1.14610	13.50
92.3072	19.69	0.9446	1.06896	0.88
99.0735	194.98	0.1920	1.01246	8.72

Table 4.1(g): Peak List for WC/Co (14 vol. % Co) Composite.

Pos. [°2Th.]	Height[cts]	FWHM [°2Th.]	Spacing[A]	Rel. Int.[%]
12.2982	709.95	0.1181	7.19721	49.24
12.4488	834.02	0.1572	7.11045	57.84
24.9588	155.55	0.1574	3.56769	10.79
31.5823	782.55	0.0984	2.83296	54.27
35.7199	1441.84	0.0787	2.51372	100.00
44.2853	81.89	0.3149	2.04539	5.68
47.2893	103.15	0.3936	1.92223	7.15
48.3677	1299.12	0.0720	1.88031	90.10
64.0929	267.68	0.0960	1.45173	18.56
65.8372	139.57	0.0720	1.41743	9.68
73.1825	304.35	0.0960	1.29223	21.11
75.5581	165.95	0.1440	1.25739	11.51
77.1788	317.72	0.0960	1.23498	22.04
77.4292	146.88	0.1440	1.23467	10.19
84.1366	258.12	0.0960	1.14967	17.90
98.8038	139.99	0.1920	1.01449	9.71
108.2134	109.68	0.2880	0.95086	7.61
109.8953	116.88	0.1920	0.9496	8.11
117.3986	229.50	0.2400	0.90152	15.92
117.8535	127.83	0.2400	0.91058	8.87

Concentration calculation:

The integrated intensity of a particular peak $I_A = I_P \times FWHM$

And the total integrated intensity of the detected materials $I_T = \sum I_A$

For WC/Co (6.5 volume percentage of Co)-

I_A for WC= 5631.84*0.1181=665.12

I_A for Co= 67.42*0.2755= 18.57

I_T= 665.12+18.57= 683.69

The concentration of WC in the sample in weight percent ages

$$= \frac{I_A}{I_T} \times 100=97.3\%$$

The concentration of WC in the sample in weight percentages

$$= \frac{I_A}{I_T} \times 100=2.7\%$$

Similarly, the concentration of WC and Co in the other samples was found in weight percent ages.

After analysis, the concentration of WC and Co in different sample is listed in table 4.2 .

Table 4.2: Concentration of WC and Co in different sample.

Sample no.	**Sample**	Constituent material	**Volume %**	**Weight %**
1	WC/Co	WC	86	81.5
		Co	14	18.5
2	WC/Co	WC	93.5	97.3
		Co	6.5	2.7
3	WC/Co	WC	92.5	95.05
		Co	7.5	4.95
4	WC/Co	WC	91.5	94.5
		Co	8.5	5.5
5	WC/Co	WC	89.5	90.1
		Co	10.5	9.9

Table 4.2 shows the experimentally determined concentration of Co in WC composite. Co was found to be in the range of (5 – 20) percent, the rest was found as WC. WC and Co showed two different phases. Figure (4.1) shows the X-ray diffraction pattern of standard WC materials. Figure (4.2) shows the X-ray diffraction pattern of standard Co materials and Figure (4.3-4.7) show the X-ray diffraction pattern of WC-Co composite with different vol. % of Co.

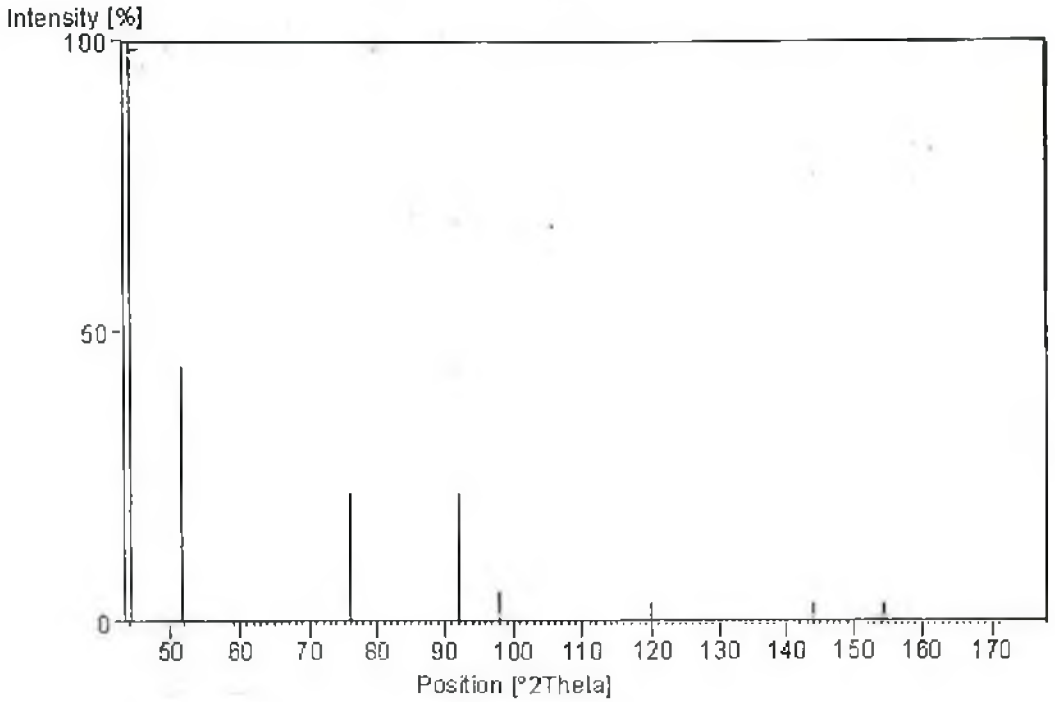

Figure (4.2): X-ray diffraction pattern of standard Co material.

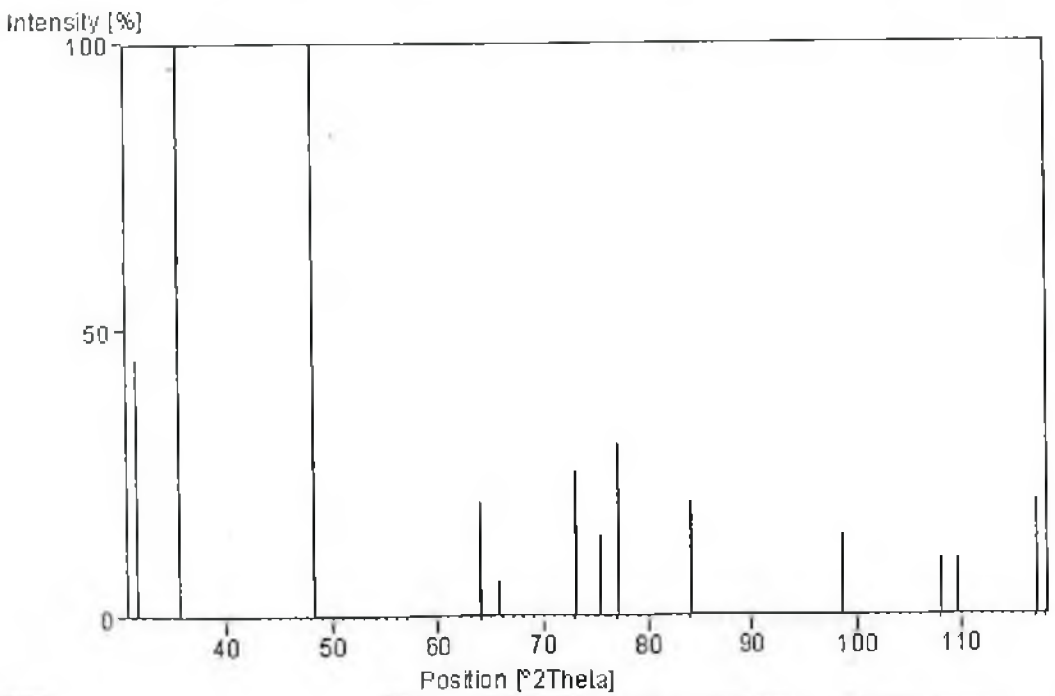

Figure (4.1): X-ray diffraction pattern of standard WC material.

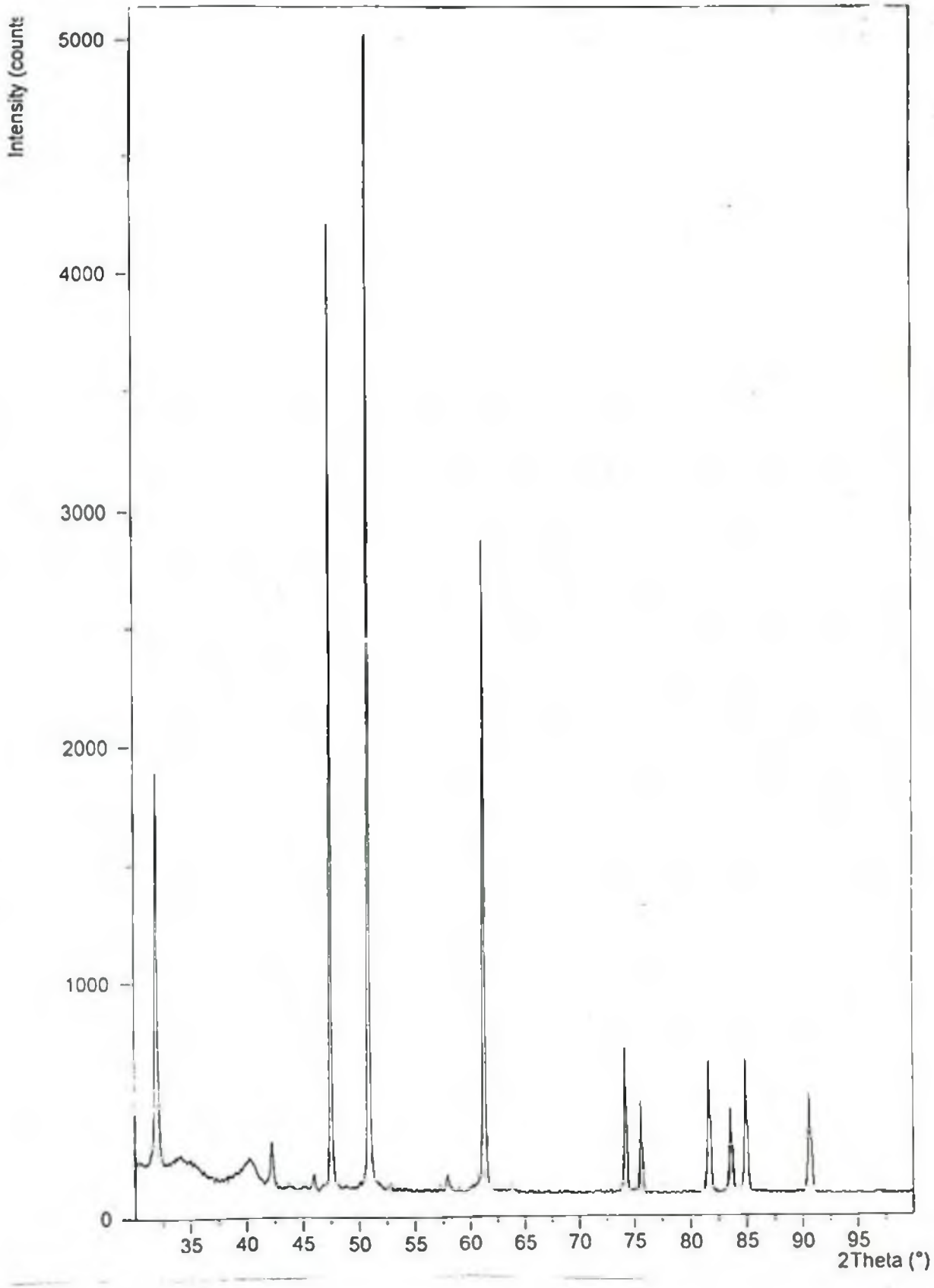

Figure (4.3): X-ray diffraction pattern of WC-Co composite with 6.5 volume percentage of Co.

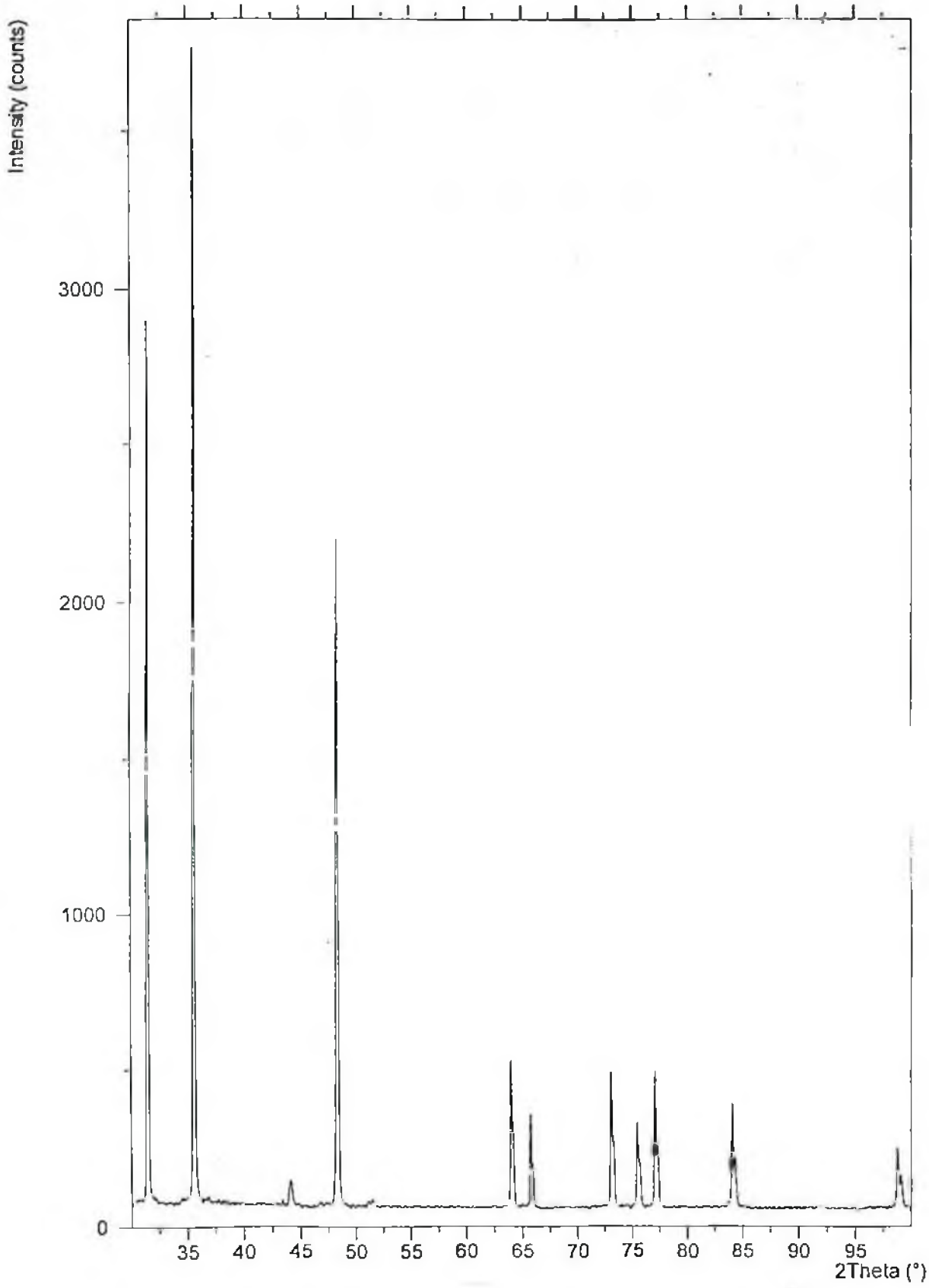

Figure (4.4): X-ray diffraction pattern of WC-Co composite with 7.5 volume percentage of Co.

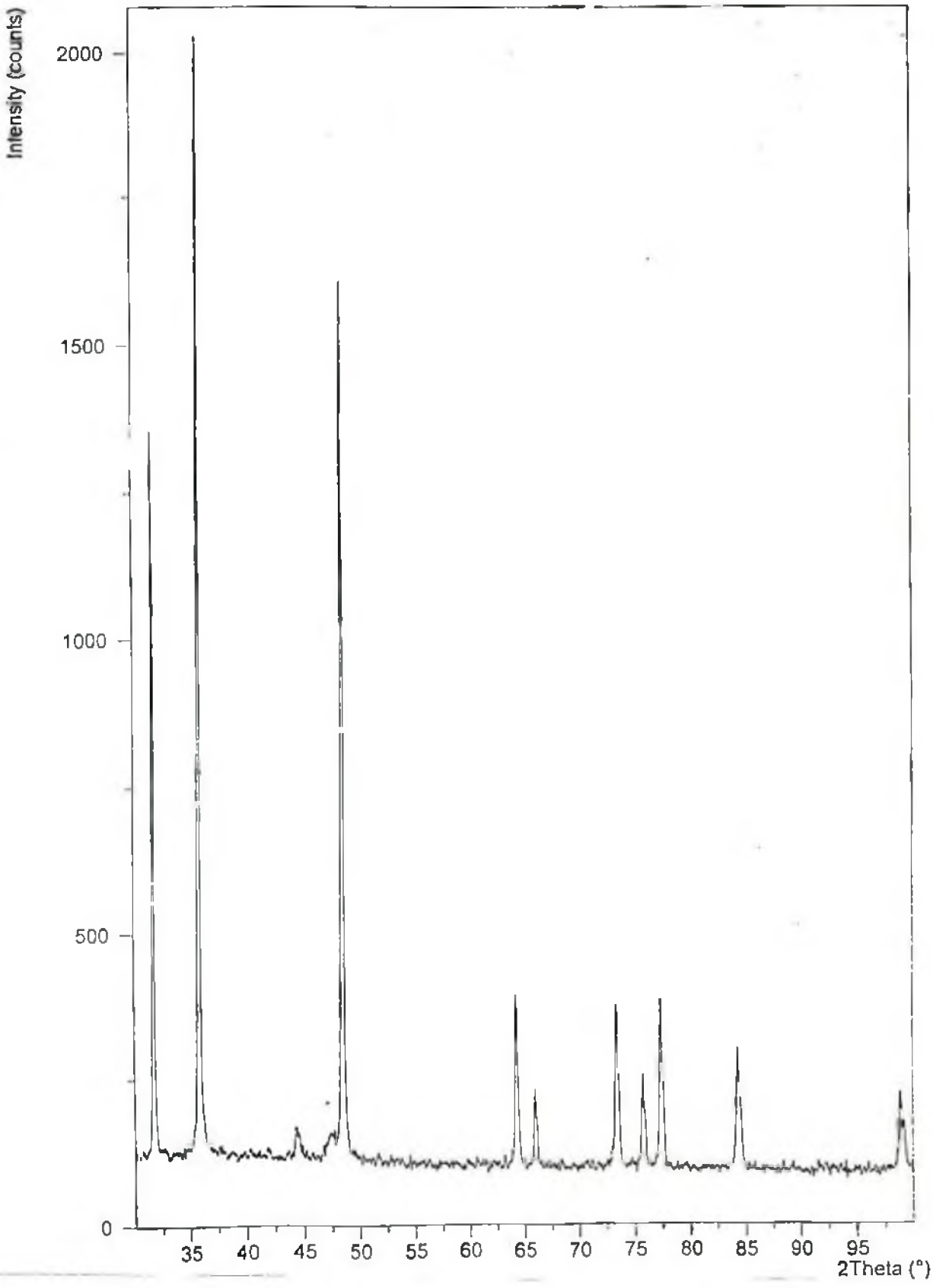

Figure (4.5): X-ray diffraction pattern of WC-Co composite with 8.5 volume percentage of Co.

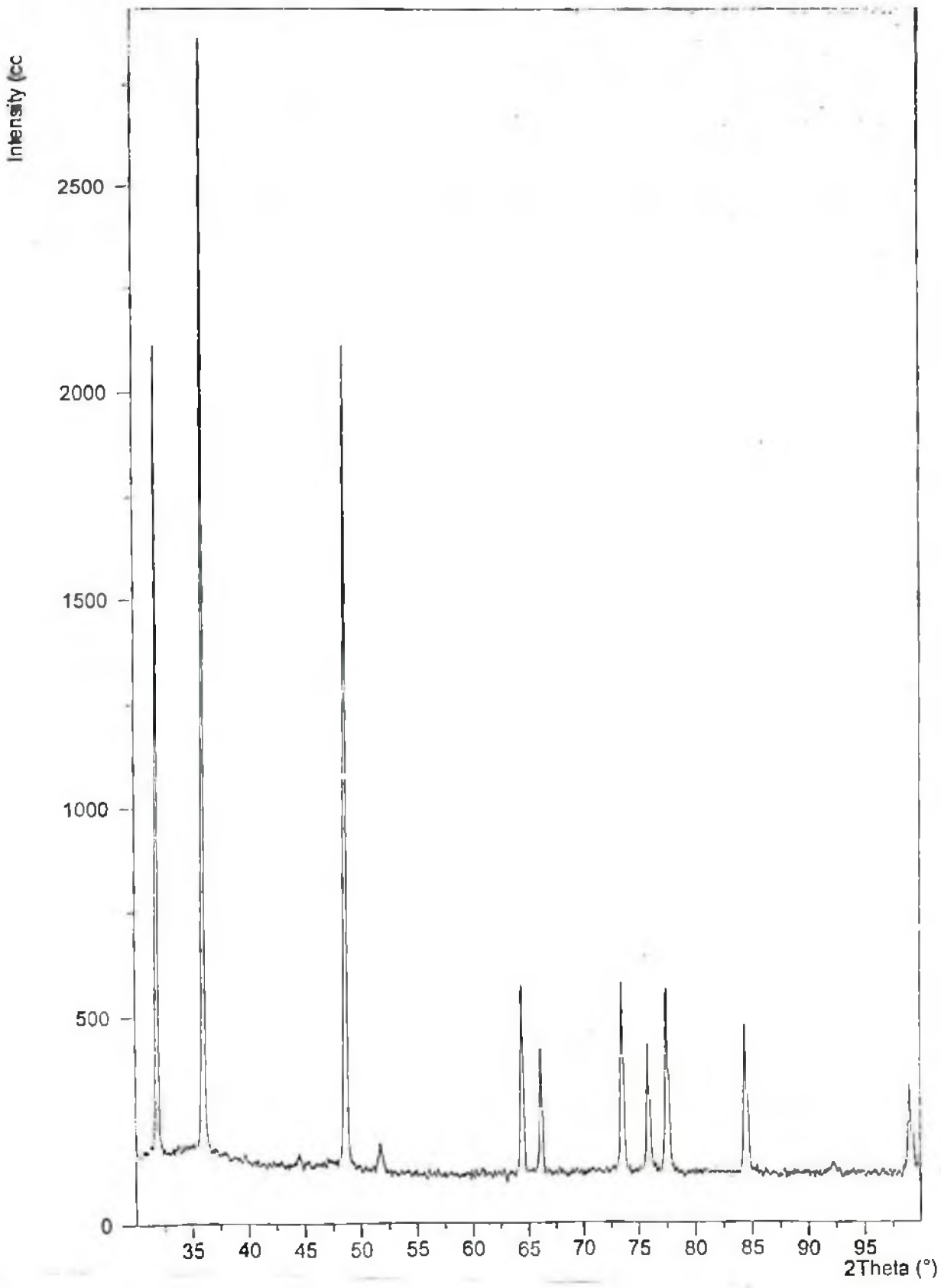

Figure (4.6): X-ray diffraction pattern of WC-Co composite with 10 volume percentage of Co.

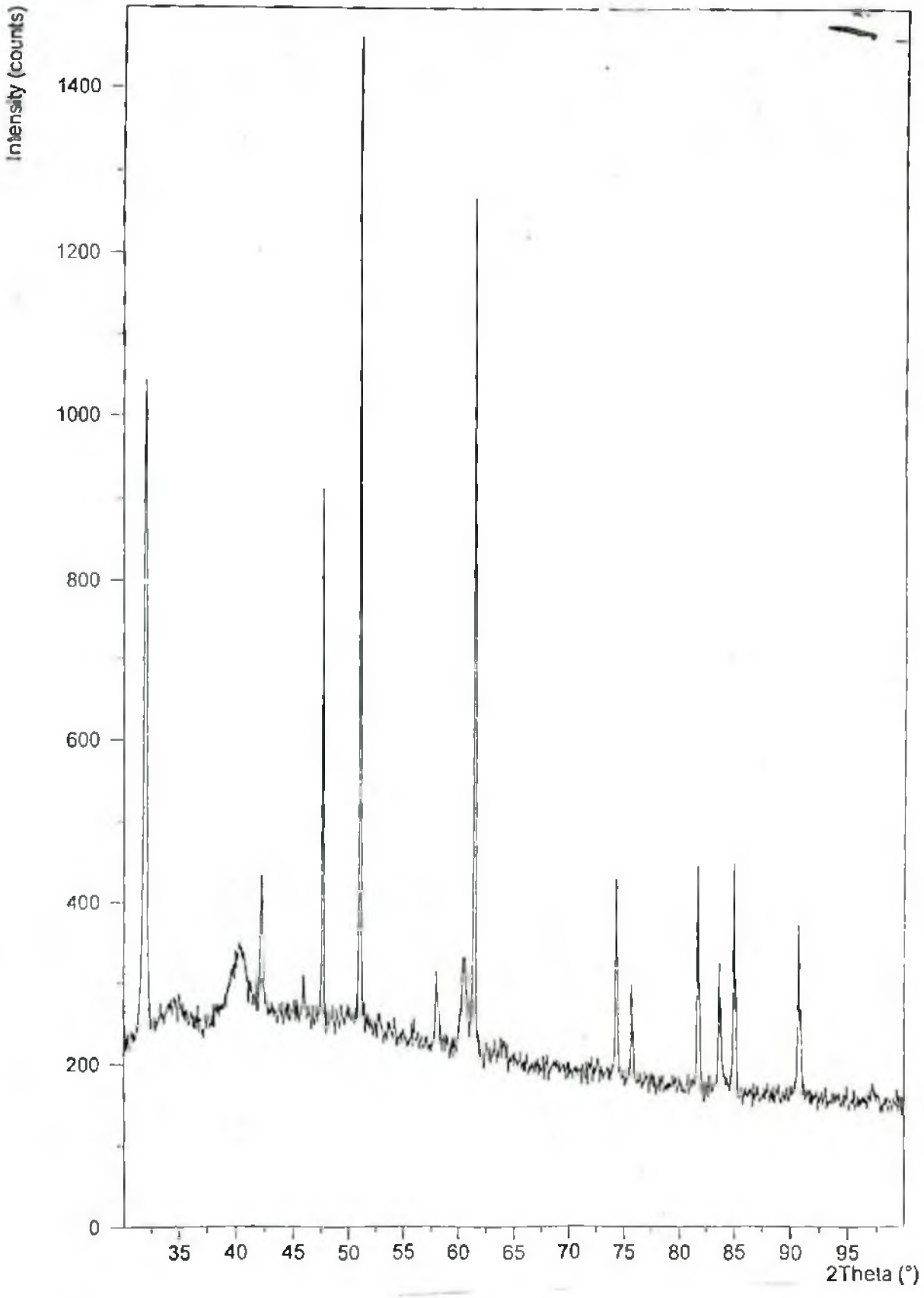

Figure (4.7): X-ray diffraction pattern of WC-Co composite with 14 volume percentage of Co.

4.2.2 Determination of some structural parameter of WC:

Reference Value for WC:

Crystallographic parameters-

Crystal system:	Hexagonal
Space group:	P-6m2
Space group number:	187
a (A):	2.9062
b (A):	2.9062
c (A):	2.8378
Alpha (α):	90.0000
Beta (β):	90.0000
Gamma (γ):	120.0000
Calculated density:	15.66
Volume of Cell:	20.76

Interpretation of the XRD data:

The XRD data consisting of θ_{hkl} and d_{hkl} values corresponding to the different following structural information of the sample-

- Identification of the plane spacing.
- Determination of the lattice parameter.
- Determination of Nelson-Riley (N.R.) function.
- Plot of a & c.
- Identification of interplanar angles and
- Determination of cell volume.

Comparing experimental value and standard value, we get the value of plane (h k l), then calculate the required structural features.

Identification of the plane spacing:

The sample WC was Hexagonal system. So the value of d, the distance between adjacent planes in the set (h k l), may be found from the following equation.

$$\frac{1}{d^2} = \frac{4}{3}\frac{(h^2+hk+k^2)}{a^2} + \frac{l^2}{c^2} \quad \ldots\ldots\ldots\ldots\ldots\ldots\ldots\ldots \quad (1)$$

But for calculating d-spacing we use Bragg's law which is –

$$2d\sin\theta = n\lambda$$

or $$d = \frac{n\lambda}{2\sin\theta}\ \theta \quad \ldots\ldots\ldots\ldots\ldots\ldots\ldots\ldots\ldots\ldots \quad (2)$$

where, n = 1, λ= 1.54178 A

Taking the data $2(\theta)$ from peak list we easily identified the plane spacing d which is shown in table (4.3).

Determination of lattice parameter:

A crystal lattice is a three-dimensional distribution (cubic, rhombic etc.) of atom in space. These are arranged so that they form a series of parallel planes separated from one another by a distance d which varies according to the nature of the material. For any crystal, planes exit in a number of different orientations-each with its own specific d-spacing.

The lattice parameter (a, b, c) of the sample crystal can be determined by the two index point like (h_1, k_1, l_1) and (h_2 k_2 l_2) by using the d-spacing value and with the help of equation (1).

Determination of Nelson-Riley (N. R.) Function:

The sum in the brackets $[\frac{\cos^2\theta}{\sin\theta}+\frac{\cos^2\theta}{\theta}]$ is termed as the Nelson-Riley (N. R.) Function. It is used primarily for data collected with Hull/Debye-Scherrer camera. For the samples N. R. function= $\frac{1}{2}[\frac{\cos^2\theta}{\sin\theta}+\frac{\cos^2\theta}{\theta}]$. Using above this formula the calculated value is tabulated in the table (4.3).

Table (4.3): Table for d-spacing, lattice parameter and N. R. function at different Miller indices.

No. of obs erva tion	Plane Index			Pos [°2Th]	θ°	d-spacing [A·]	Lattice parameter		N. R. function
	h	k	l				a = b [A°]	c[A°]	
1	0	0	1	31.5823	15.79115	2.83296	------	2.83296	1.73059
2	1	0	0	35.7199	17.85995	2.51372	2.902593	---	1.502301
3	1	0	1	48.3677	24.18385	1.88031	----------	2.82994	1.032878
4	1	1	0	64.0929	32.0464	1.45173	2.90346	-----	0.088225
5	0	0	2	65.8372	32.9186	1.41743	------- -	2.83486	0.659032
6	1	1	1	73.4825	36.74125	1.29223	---------	2.82921	0.545475
7	2	0	0	75.5581	37.77905	1.25739	2.903817	--------	0.518127
8	2	0	1	84.1366	42.0683	1.14967	----------	2.83205	0.41779
9	2	1	0	108.2134	54.1067	0.95086	2.904925	---------	0.215321
10	0	0	3	109.8953	54.94765	0.94096	-----	2.82288	0.204465

For the determination of lattice parameter a_o, plotting the lattice parameter value a versus N.R function as shown in fig (4.8), it is easy to get the value a_o which is (2.9047).

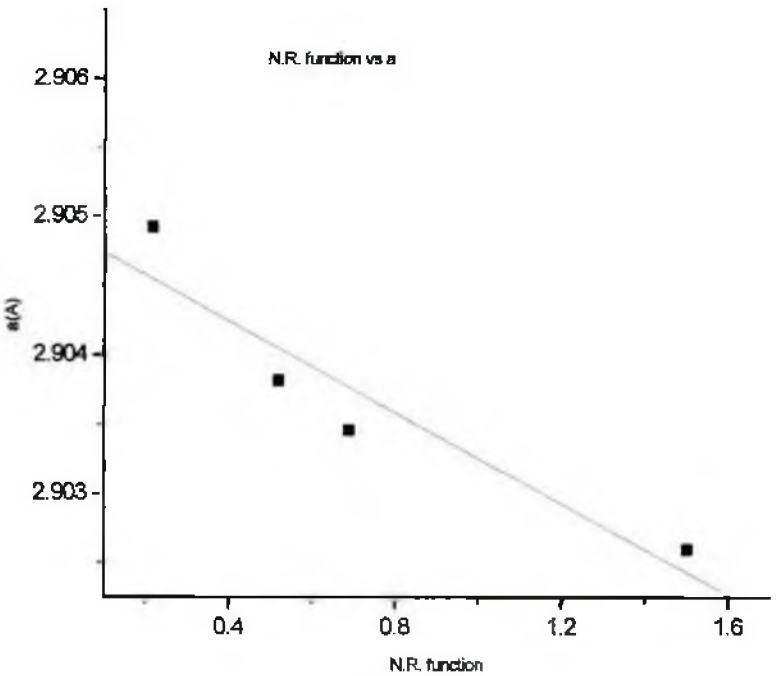

Fig (4.8): Lattice parameter value a versus N.R function.

Similarly for the determination of lattice parameter c_o, plotting the lattice parameter value c versus N.R function as shown in fig (4.9), we get the value c_o which is (2.8275).

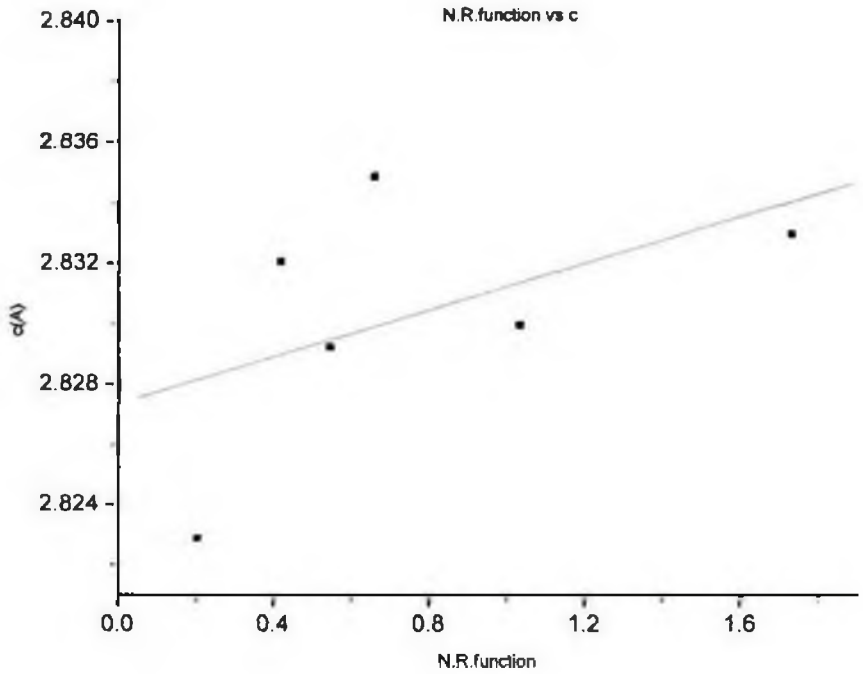

Fig (4.9): Lattice parameter value c versus N.R function.

Determination of the cell volume:

The volume of the unit cell of a hexagonal sample is $V= a^2c$.

Using above formula the calculated values are tabulated in table (4.4).

Comparing the calculated lattice parameter and cell volume of WC with the reference value are tabulated bellow –

Table (4.4): Table for Lattice parameter and Cell volume of WC crystal:

Lattice parameter				Cell volume	
Ref. value		Calculated value		Ref. value	Calculated value
a = b	c	a = b	c		
2.9062	2.8378	2.9047	2.8275	20	23.86956

From table (4.4) it is observed that the calculated values are good agreement with the reported values. But there is little difference between the calculated values and reference values; this is due to the defect in crystal structure when it is grown.

4.3 The electrical measurement findings:

4.3.1 I-V measurements:

The current-voltage characteristics of the samples were measured using a standard four-probe method within a temperature range of room temperature (300K) to 483K and magnetic field of 0 to 4 KG with an electromagnet.

(I) For H=0, Fig.(4.10) shows the current-voltage curves for WC/Co composites containing different volume percentage of Co at 300K, 333K, 363K, 393K, 423K, 453K and 483K temperature. It was observed that with increase in temperature the current-voltage curves became steeper.

(II) For H=1KG, Fig.(4.11) shows the current-voltage curves for WC/Co composites containing different volume percentage of Co at 300K, 333K, 363K, 393K, 423K, 453K and 483K temperature. With increase in temperature the current-voltage curves became steeper.

(III) For H=2KG, Fig.(4.12) shows the current-voltage curves at H=2KG for WC/Co composites containing different volume percentage of Co at 300K, 333K, 363K, 393K, 423K, 453K and 483K temperature. It was observed that with increase in temperature the current-voltage curves became steeper.

(IV) For H=3KG, Fig.(4.13) shows the current-voltage curves at H=3KG for WC/Co composites containing different volume percentage of Co at 300K, 333K, 363K, 393K, 423K, 453K and 483K temperature. With increase in temperature the current-voltage curves became steeper.

(V) For H=4KG, Fig.(4.14) shows the current-voltage curves at H=4KG for WC/Co composites containing different volume percentage of Co at 300K, 333K, 363K, 393K, 423K, 453K and 483K temperature. With increase in temperature the current-voltage curves became steeper.

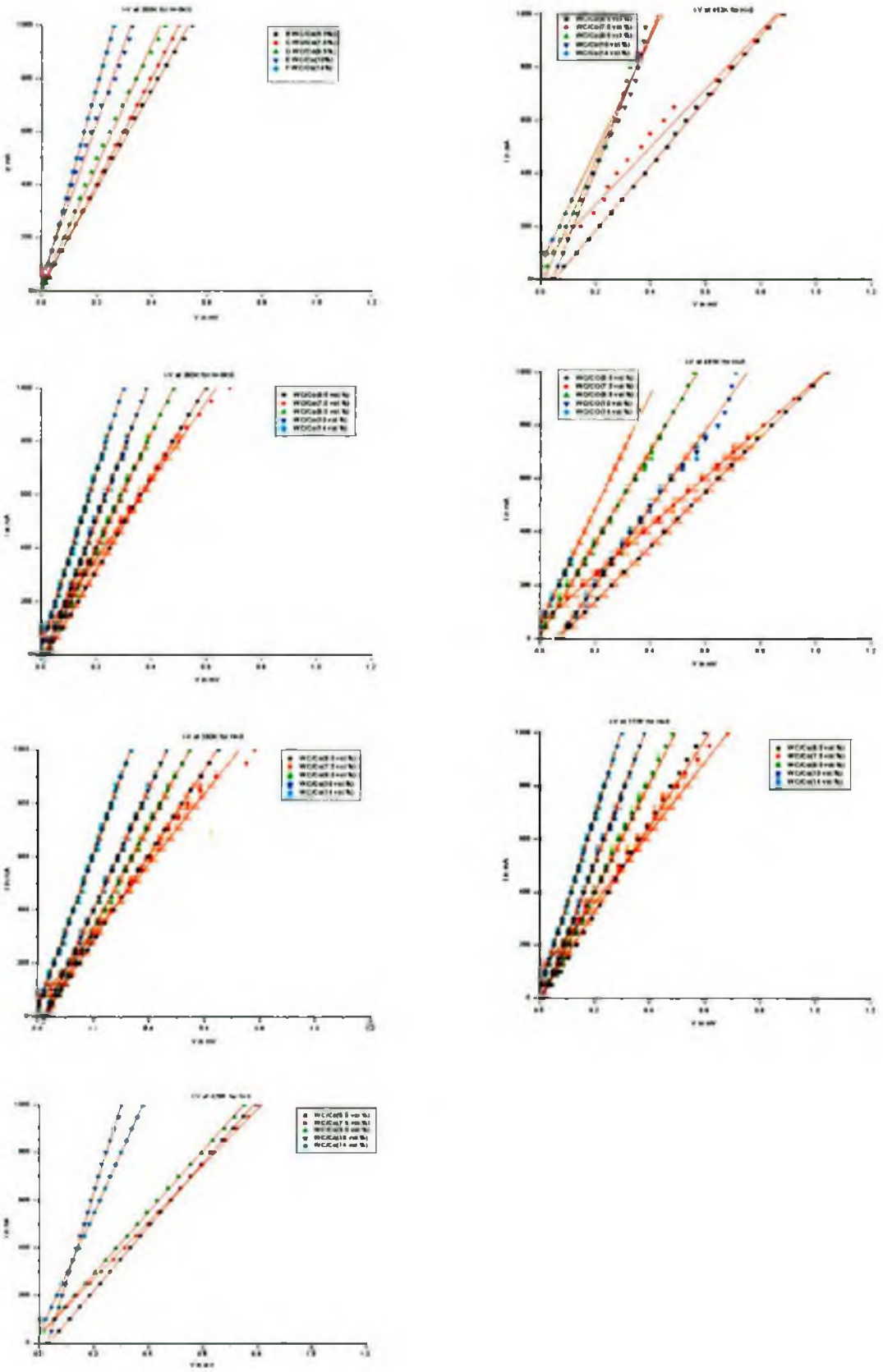

Fig.(4.10) The current-voltage curves at H=0KG for WC/Co composites containing different volume percentage of Co at different temperature.

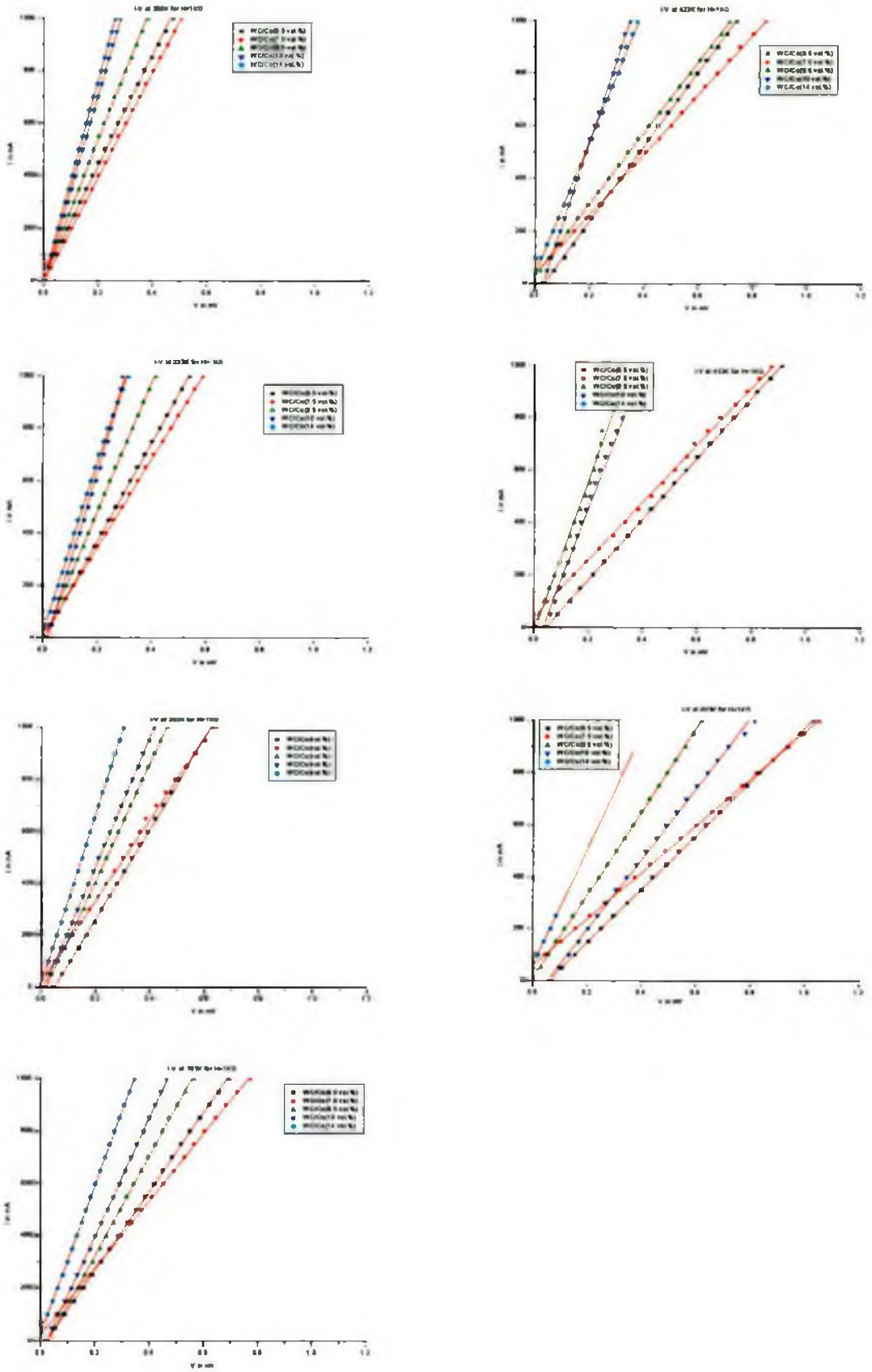

Fig.(4.11) The current-voltage curves at H=1KG for WC/Co composites containing different volume percentage of Co at different temperature.

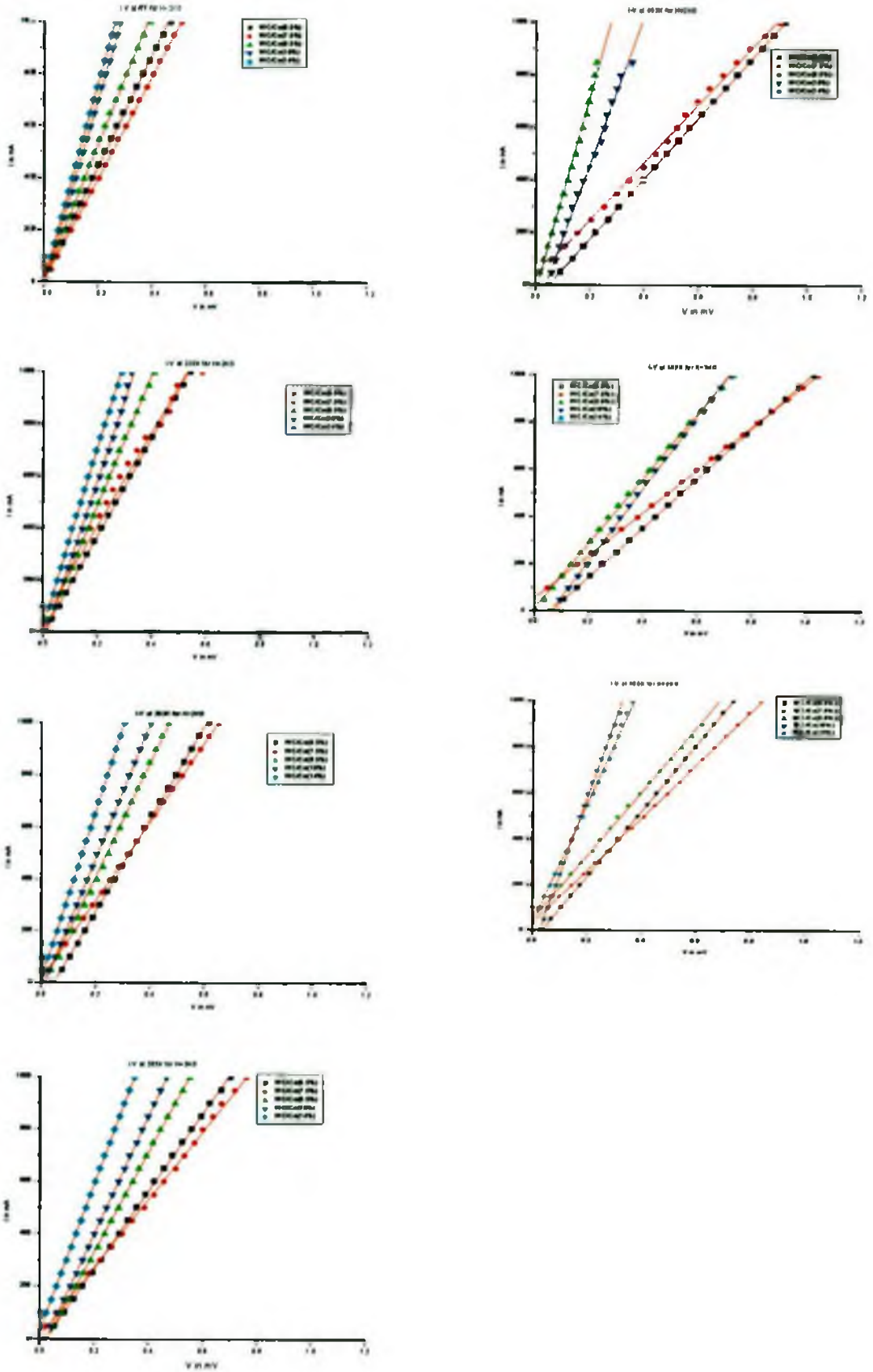

Fig.(4.12) The current-voltage curves at H=2KG for WC/Co composites containing different volume percentage of Co at different temperature.

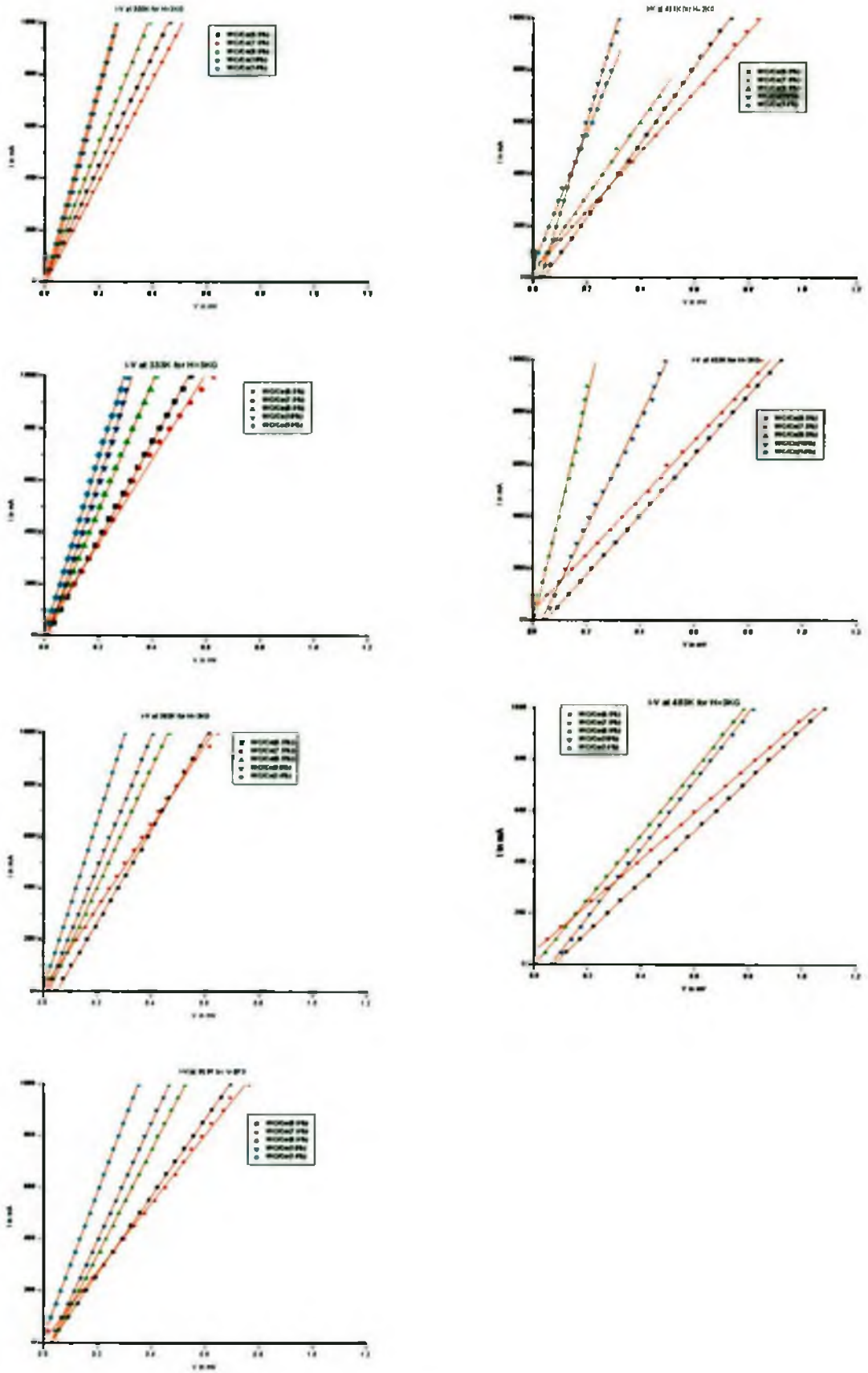

Fig.(4.13) The current-voltage curves at H=3KG for WC/Co composites containing different volume percentage of Co at different temperature.

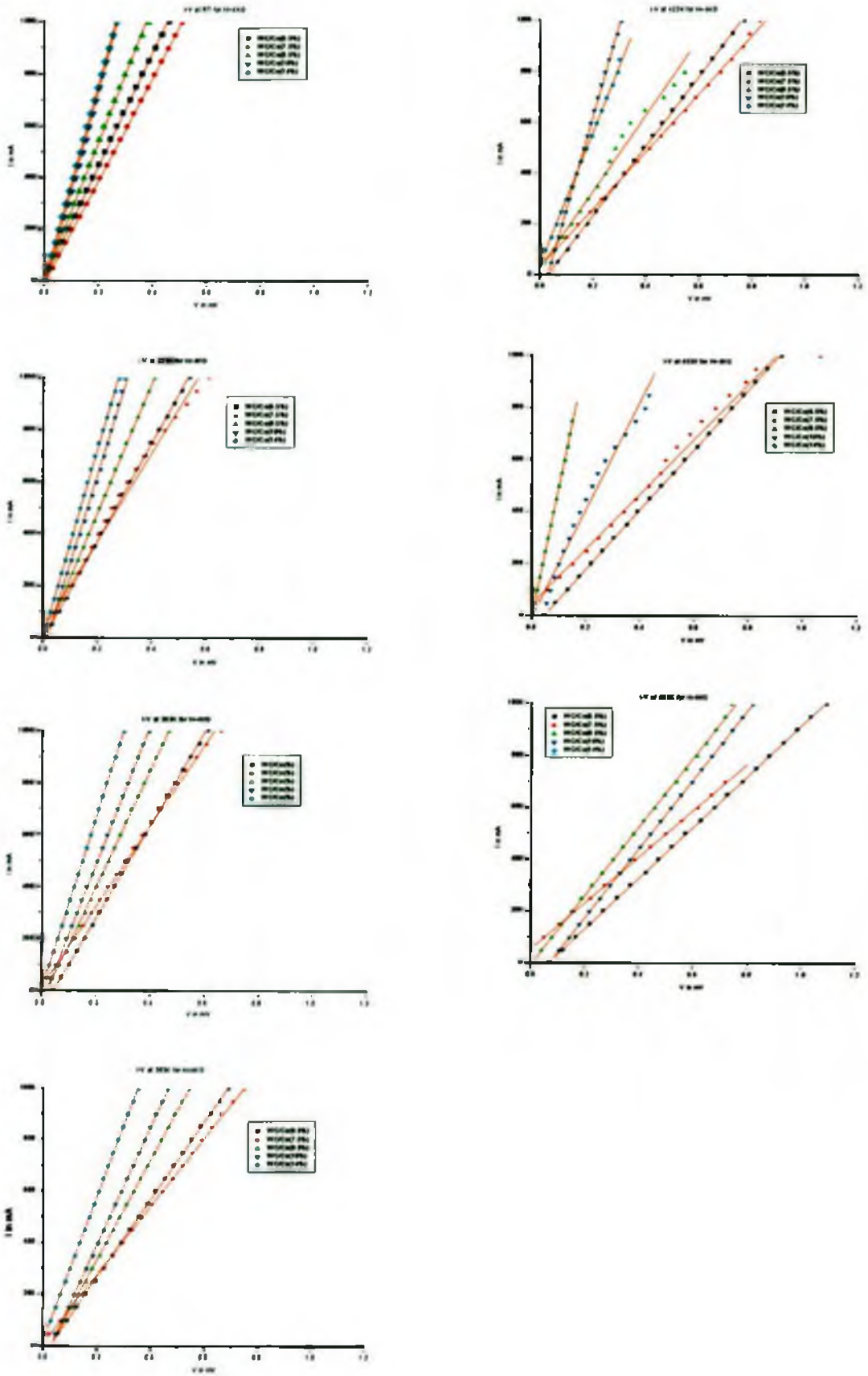

Fig.(4.14) The current-voltage curves at H=4KG for WC/Co composites containing different volume percentage of Co at different temperature.

Conductivity measurements:

Resistance was calculated from the gradient of the I-V curves. Then the resistivity ρ (ohm-centimeter) was found for a rectangular sample of known dimensions using the following relation

$$R = \rho L/A$$

Where L is the sample length, A is the cross section.

The conductivity σ is defined as the reciprocal (inverse) of electrical resistivity i.e.

$$\sigma = 1/\rho$$

4.3.2 Conductivity as a function of temperature:

(I) For H=0, fig (4.15) shows the conductivity vs. temperature graph for WC/Co composites containing different volume percentage of Co. It was observed that with increase in temperature, the conductivity of the samples was decreased. In case of 6.5 to 8.5 volume percentage of Co the conductivity is low but in case of 10 volume percentage of Co the conductivity is comparatively high and the conductivity in case of 10 &14 volume percentage of Co is of the same order.

(II) For H=1KG, fig.(4.16) shows the electrical conductivity as a function of temperature for WC/Co composites containing different volume percentage of Co inclusions. Here also the electrical conductivity decreases linearly with temperature as fig. (4.15), but the conductivity for each volume percentage of Co is increased. Also the gradient of the curve is increased.

(III) For H=2KG, fig.(4.17) shows the electrical conductivity as a function of temperature for WC/Co composites containing different volume percentage of Co inclusions. Here also the electrical conductivity decreases linearly with temperature as fig. (4.15), but the conductivity for each volume percentage of Co is increased. Also the gradient of the curve is increased.

(IV) For H=3KG, fig.(4.18) shows the electrical conductivity as a function of temperature for WC/Co composites containing different volume percentage of Co inclusions. Here also the electrical conductivity decreases linearly with temperature as fig. (4.15), but the conductivity for each volume percentage of Co is increased. Also the gradient of the curve is increased.

(V) For H=4KG, fig.(4.19) show the electrical conductivity as a function of temperature for WC/Co composites containing different vol. % of Co inclusions. Here the effect of magnetic field is also prominent. A significant difference has been observed between the conductivities for low volume percentage (6-8 volume percentage) and for high volume percentage of Co (10-14 volume percentage) when magnetic field increases from 0 to 4 KG. The conductivity curve for 10 and 14 volume percentages were observed to be overlapped.

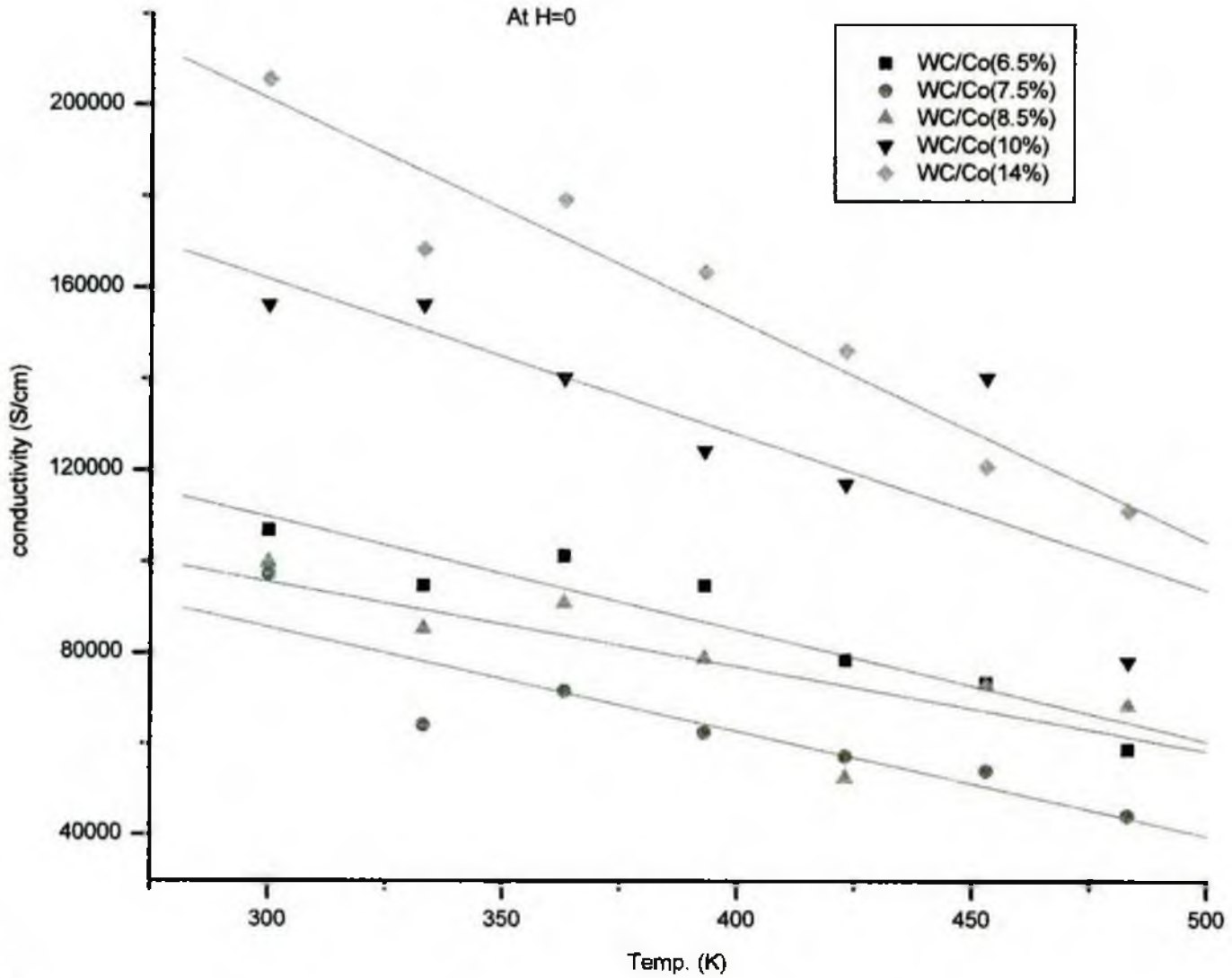

Fig. (4.15): Conductivity vs. temperature graph for WC/Co composites at H=0.

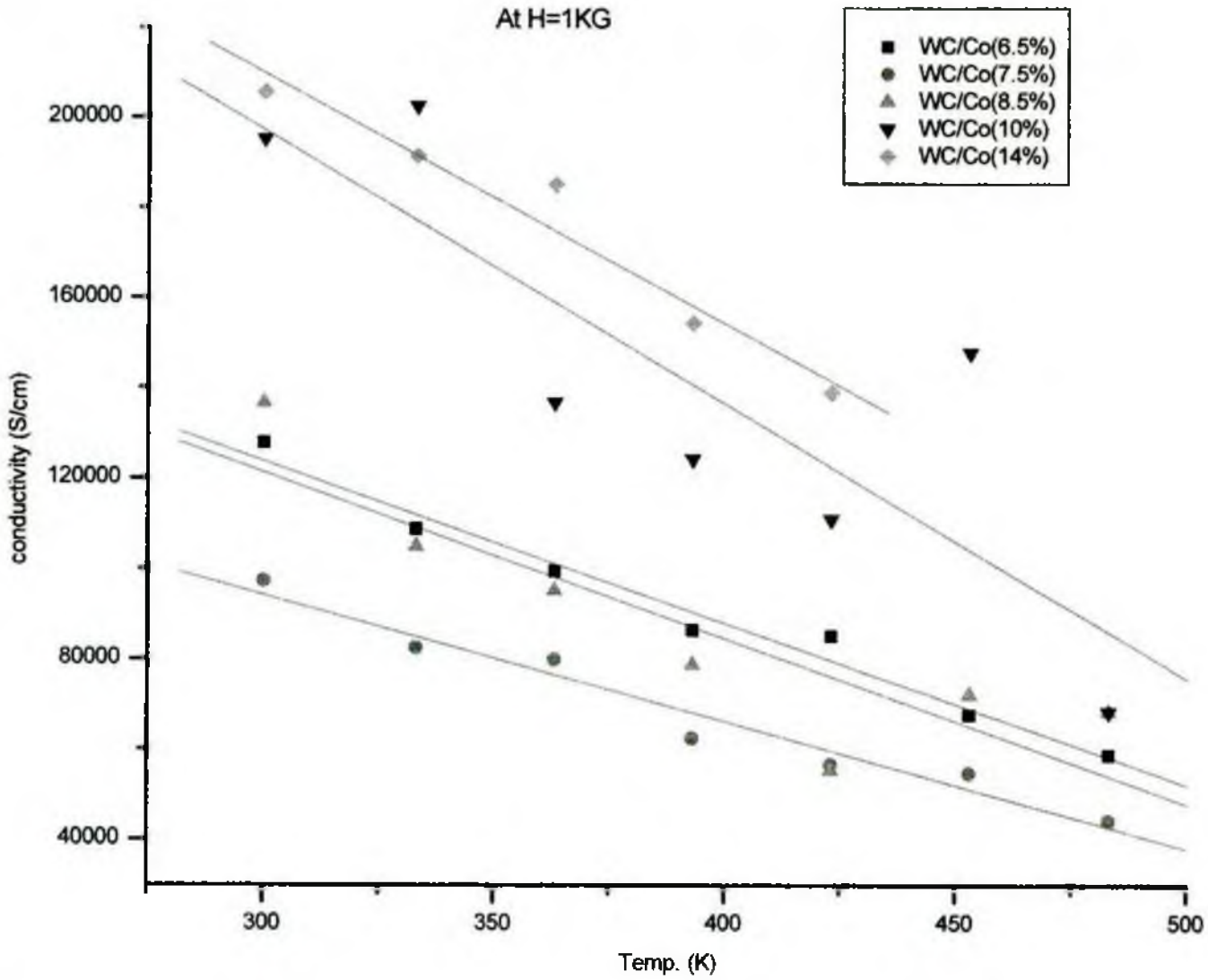

Fig. (4.16): Conductivity vs. temperature graph for WC/Co composites at H=1KG.

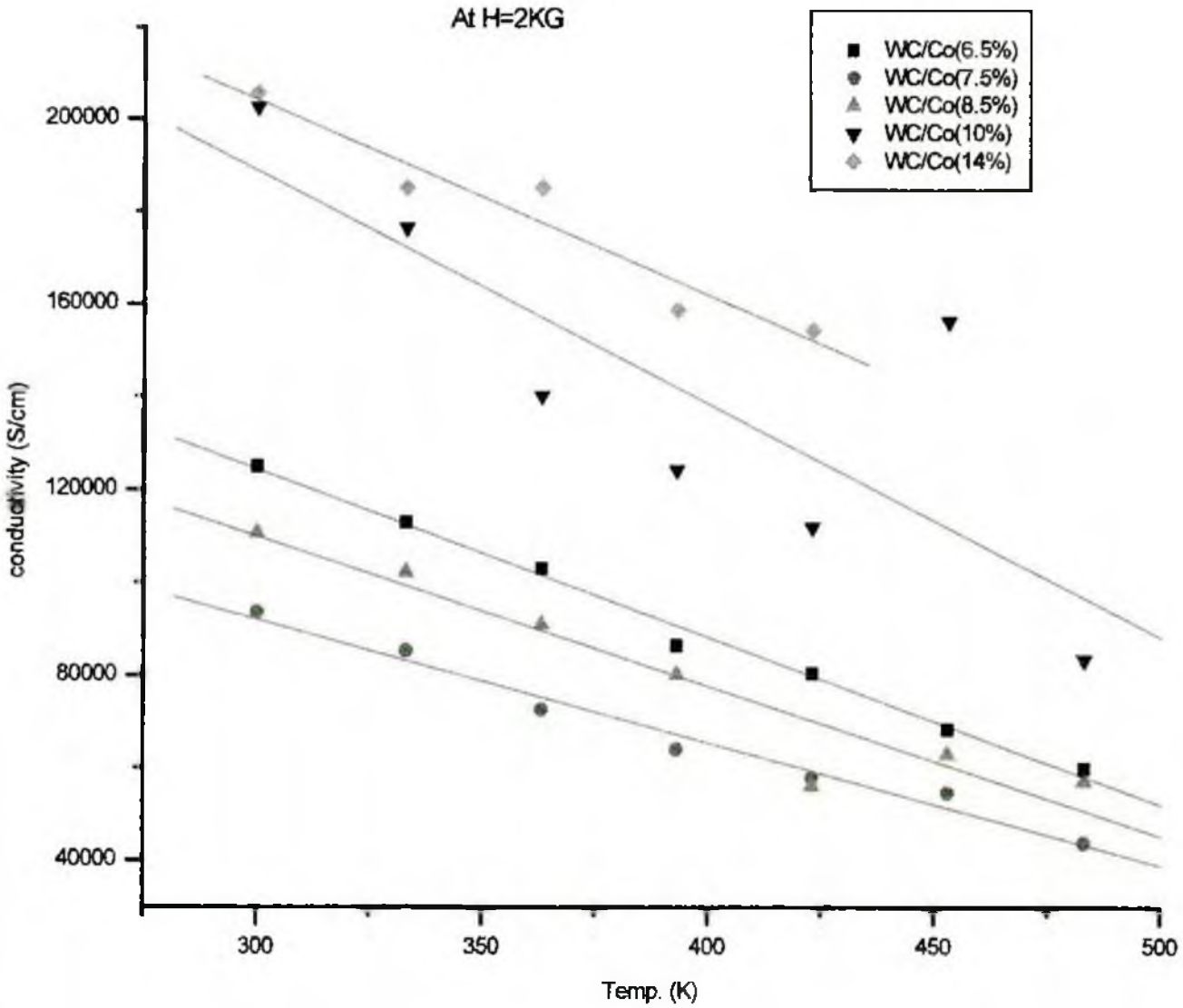

Fig. (4.17): Conductivity vs. temperature graph for WC/Co composites at H=2KG.

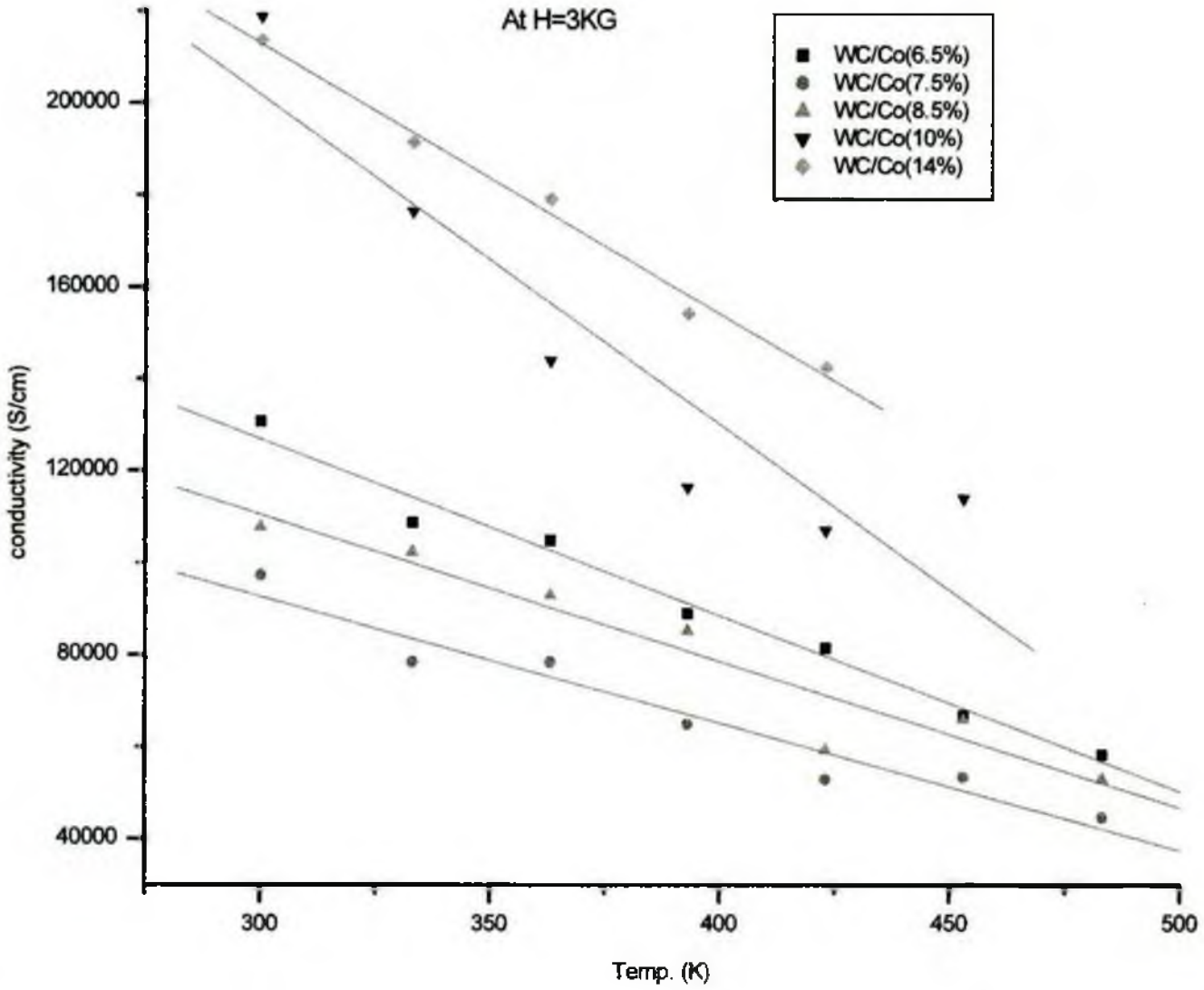

Fig. (4.18): Conductivity vs. temperature graph for WC/Co composites at H=3KG.

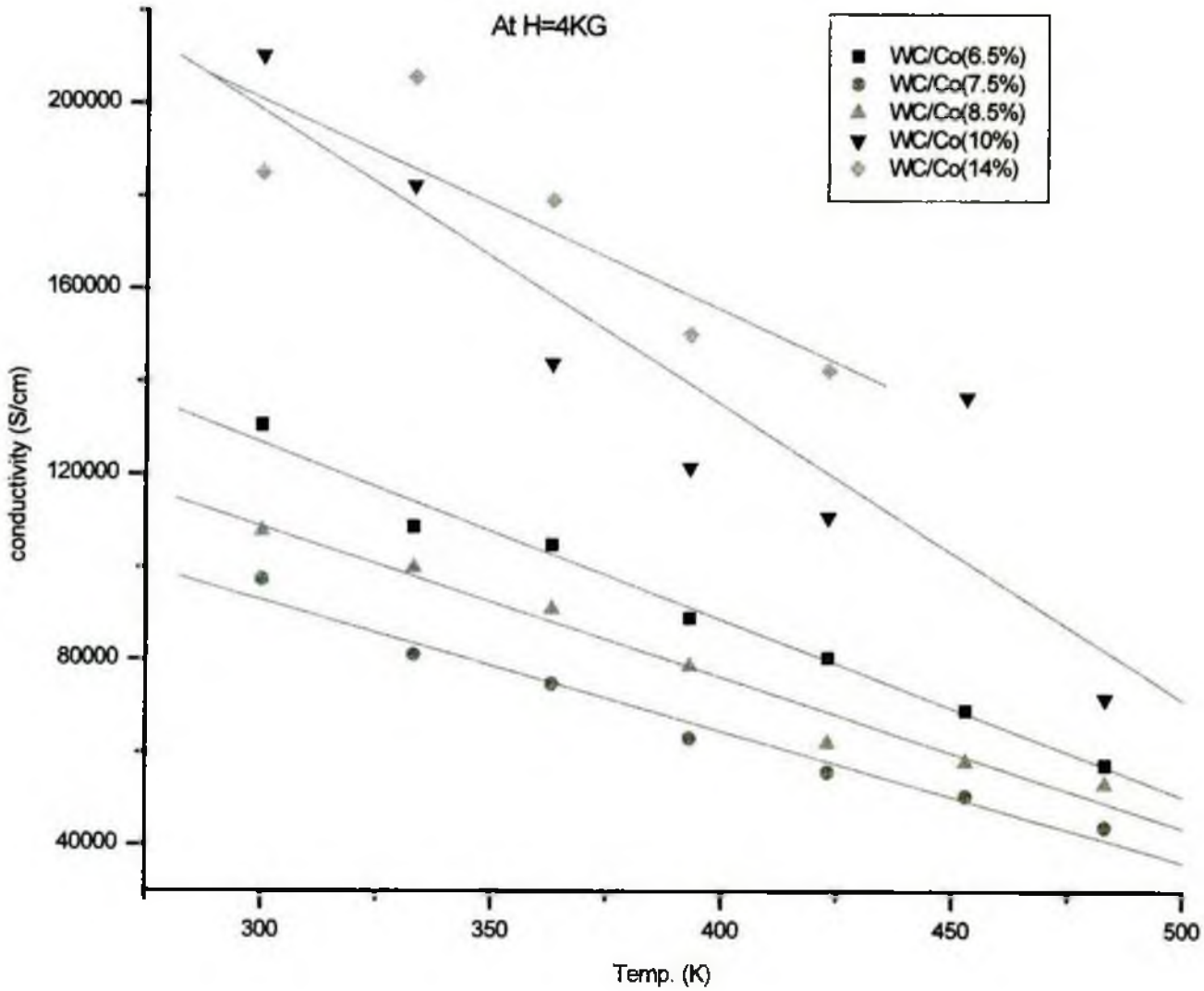

Fig. (4.19): Conductivity vs. temperature graph for WC/Co composites at H=4KG.

4.3.3 Conductivity as a function of Co concentration in a WC matrix:

(I) For H=0, fig.(4.20) shows the electrical conductivity as a function of Co concentration in a WC matrix .As can be seen from the figure there are three distinct region related to the electrical conductivity behavior. Region I shows that up to 8.5 volume % of Co the conductivity does not change abruptly. In region II i.e. at 10 volume % of Co, a sharp rise of the electrical conductivity occurs which is typical of a percolation process. In region III i.e. at 14 vol. % of Co, a small change in the electrical conductivity occurs.

(II) For H=1KG, fig.(4.21) shows the electrical conductivity as a function of Co concentration in a WC matrix for WC/Co composites containing different temperature. Here all the curve show similar behavior as fig.(4.20). Here the electrical conductivity for each vol.% of Co is increased compared to that of fig. (4.20). Also the electrical conductivity at low temperature (300K, 333K) was more than that at high temperature (363K-483K).

(III) For H=2KG, fig.(4.22)shows the electrical conductivity as a function of Co concentration in a WC matrix for WC/Co composites containing different temperature. Here all the curve show similar behavior as fig.(4.20). Here the electrical conductivity for each vol.% of Co is increased compared to that of fig. (4.20). Also the electrical conductivity at low temperature (300K, 333K) was more than that at high temperature (363K-483K).

(IV) For H=3KG, fig.(4.23)shows the electrical conductivity as a function of Co concentration in a WC matrix for WC/Co composites containing different temperature. Here all the curve show similar behavior as fig.(4.20). Here the electrical conductivity for each vol.% of Co is increased compared to that of fig.

(4.20). Also the electrical conductivity at low temperature (300K, 333K) was more than that at high temperature (363K-483K).

(V) For H=4KG, fig.(4.24)shows the electrical conductivity as a function of Co concentration in a WC matrix for WC/Co composites containing different temperature. Here all the curve show similar behavior as fig.(4.20). Here the electrical conductivity for each vol.% of Co is increased compared to that of fig. (4.20). Also the electrical conductivity at low temperature (300K, 333K) was more than that at high temperature (363K-483K).

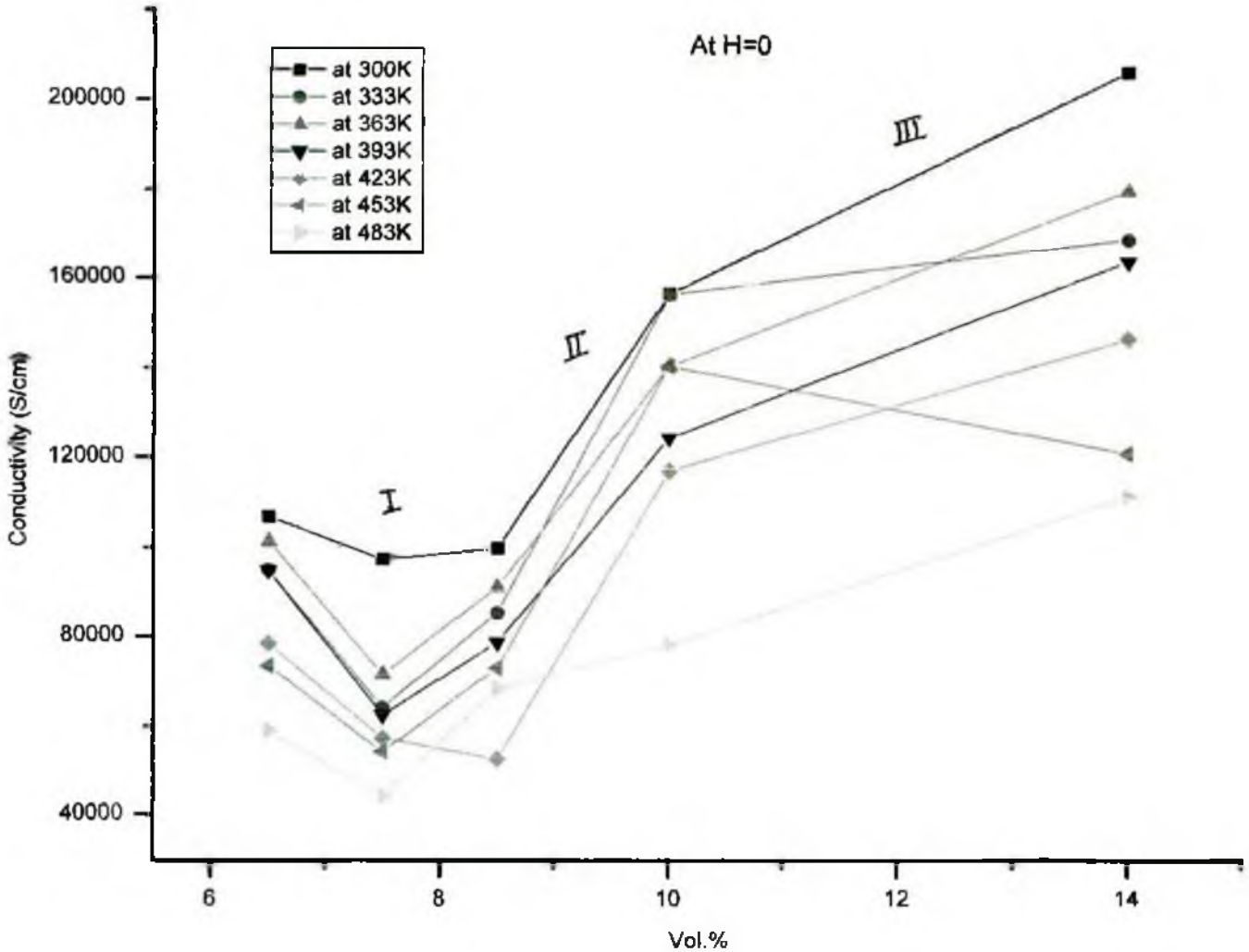

Fig.(4.20): Electrical conductivity as a function of Co concentration in WC matrix for WC/Co composites at H=0.

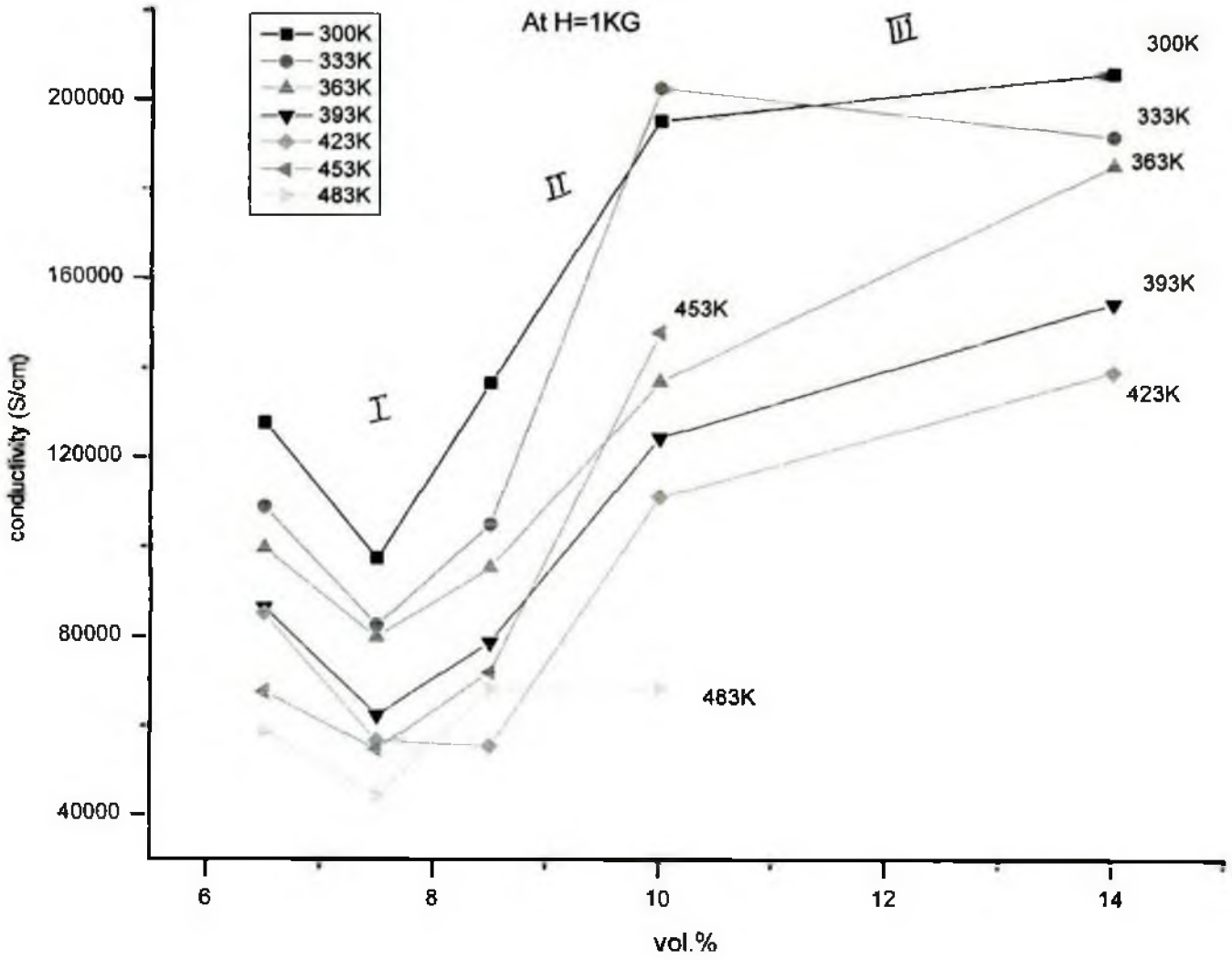

Fig.(4.21): Electrical conductivity as a function of Co concentration in WC matrix for WC/Co composites at H=1KG.

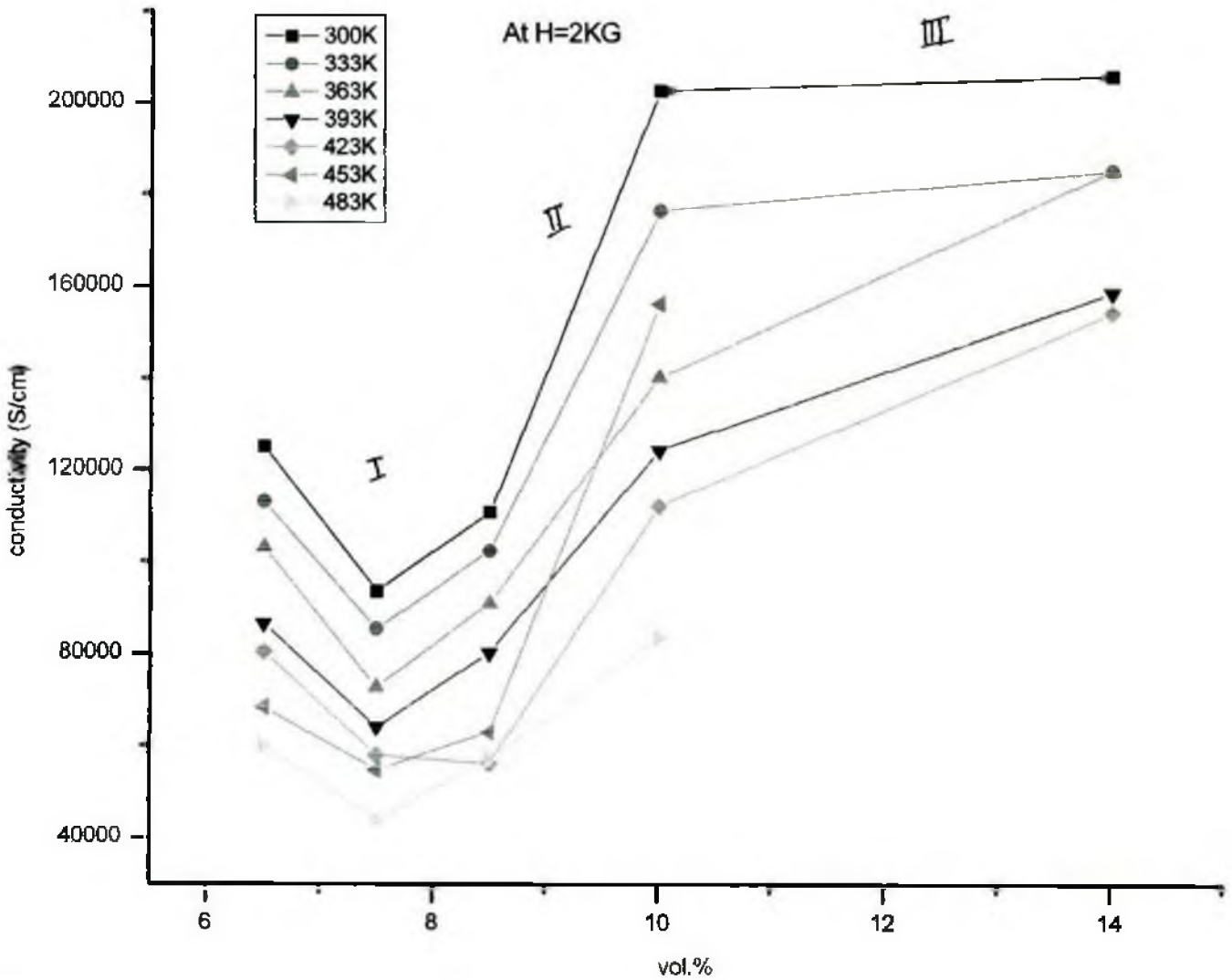

Fig.(4.22): Electrical conductivity as a function of Co concentration in WC matrix for WC/Co composites at H=2KG.

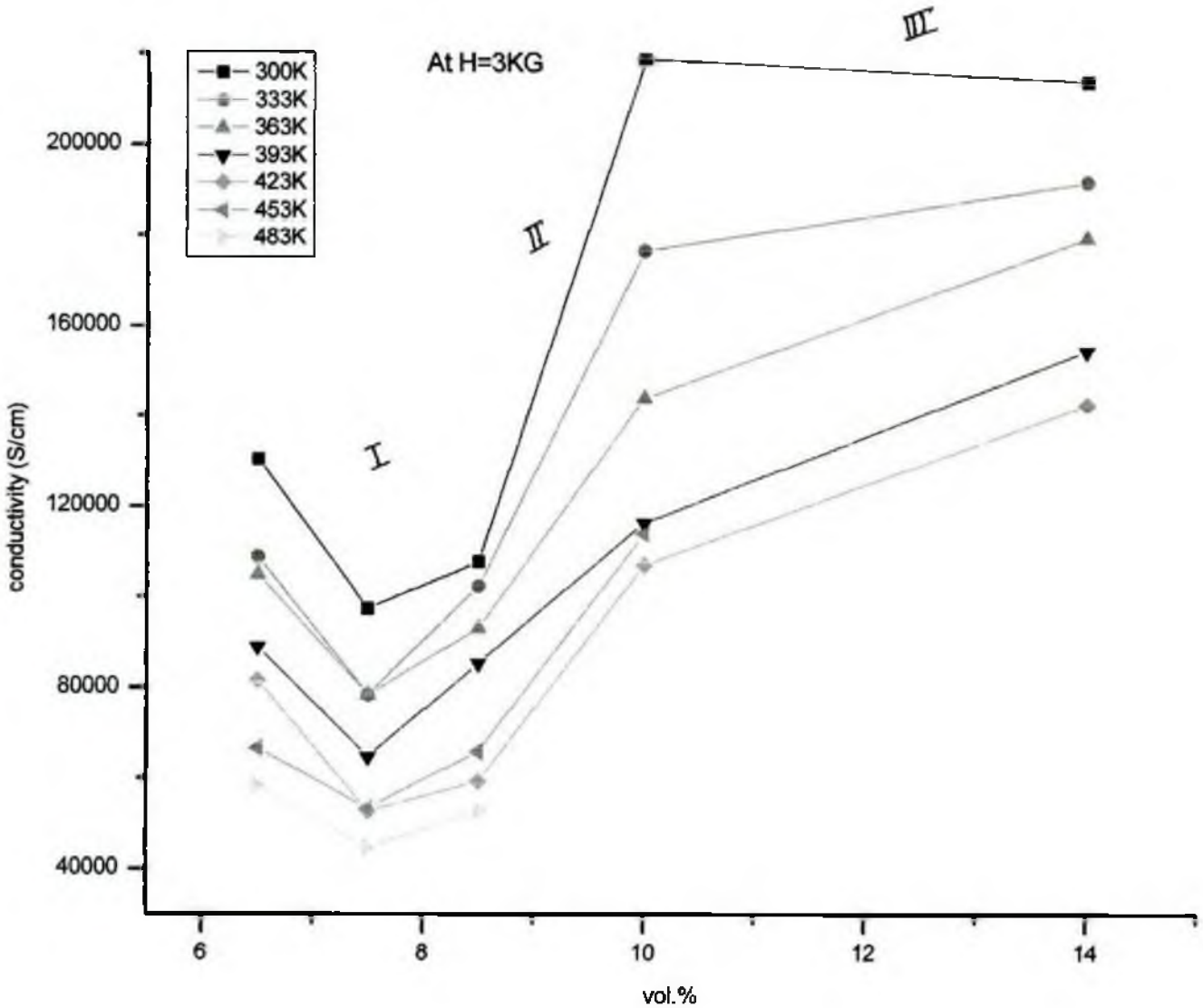

Fig.(4.23): Electrical conductivity as a function of Co concentration in WC matrix for WC/Co composites at H=3KG.

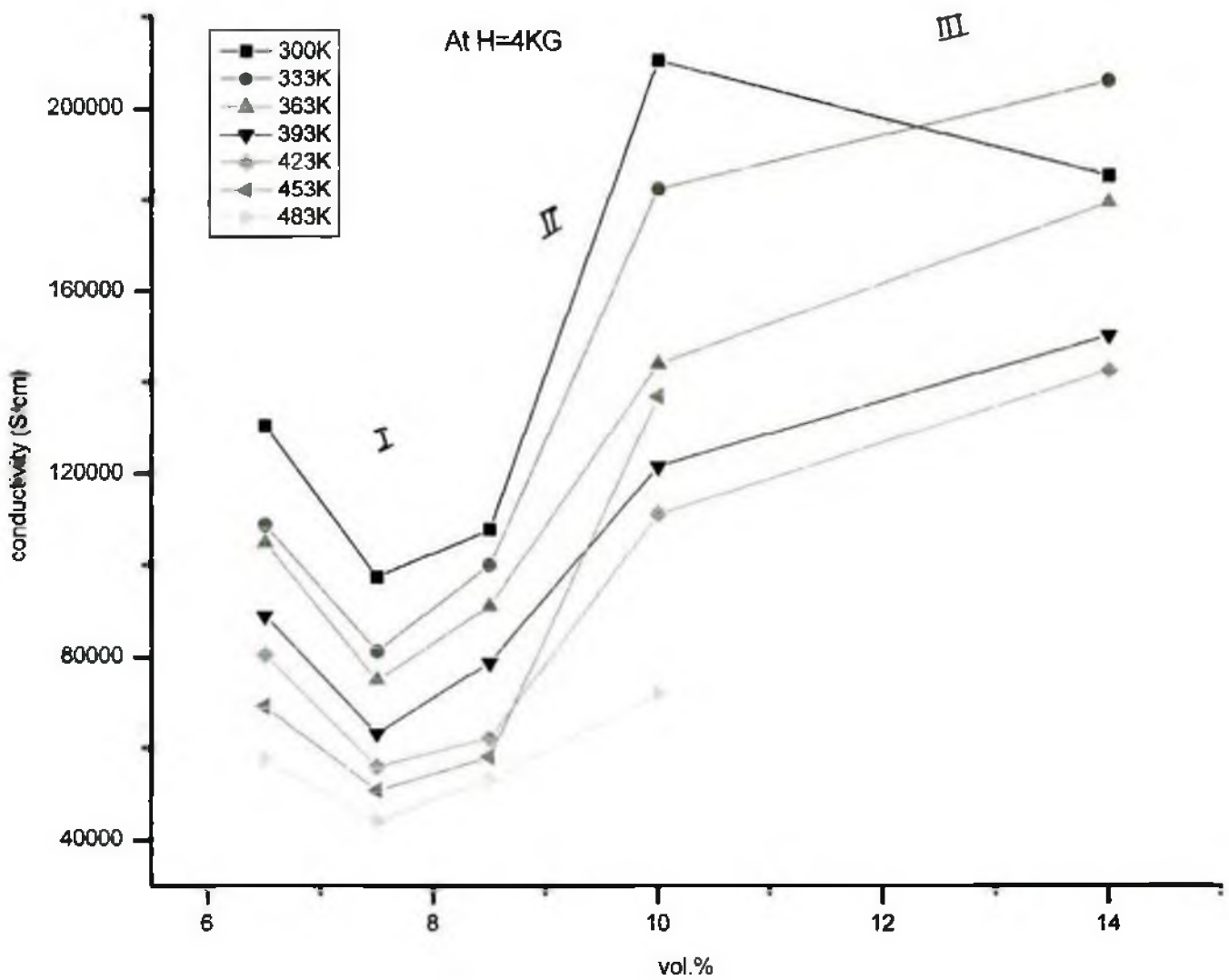

Fig.(4.24): Electrical conductivity as a function of Co concentration in WC matrix for WC/Co composites at H=4KG.

4.4 Magnetoresistance

The magnetoresistance MR is defined as,

$$MR\% = \frac{\rho(H) - \rho(H=0)}{\rho(H=0)} \times 100$$

4.4.1 Magnetoresistance as a function of applied field:

The MR as a function of magnetic field for all the samples were obtained at RT and high temperature are shown in Fig (4.25 -4.31). Typical MR curves obtained at 298K for the samples sintered at 1640° C. Room temperature MR was observed to be very low with a maximum value of 28.66631 % within the range 0 to 4 KG and was varied within -26.82966 to 28.66631 %.

(I) At room temperature (300K), fig.(4.25) shows the MR as a function of magnetic field for all the samples (WC/Co composites). Observed MR was almost constant with field. The curves show negative MR.

(II) At T=333K, fig.(4.26) shows the MR as a function of magnetic field for all the samples (WC/Co composites). Observed MR was almost constant with field. The curves show negative MR.

(III) At T=363K fig.(4.27) shows the MR as a function of magnetic field for all the samples (WC/Co composites). The curves show negative MR. The negative MR was decreased.

(IV) At T=393K, fig.(4.28) shows the MR as a function of magnetic field for all the samples (WC/Co composites). The decrease in negative MR was more than that of previous figure.

(V) At T=423K, fig.(4.29) shows the MR as a function of magnetic field for all the samples (WC/Co composites). The Magneto Resistances were very close to zero.

(VI) At T=453K, fig.(4.30) shows the MR as a function of magnetic field for all the samples (WC/Co composites).At this temperature positive MR was observed but the values of Magneto Resistances were very close to zero.

(VII) At T=483K, fig.(4.31) shows the MR as a function of magnetic field for all the samples (WC/Co composites). Positive MR was observed.

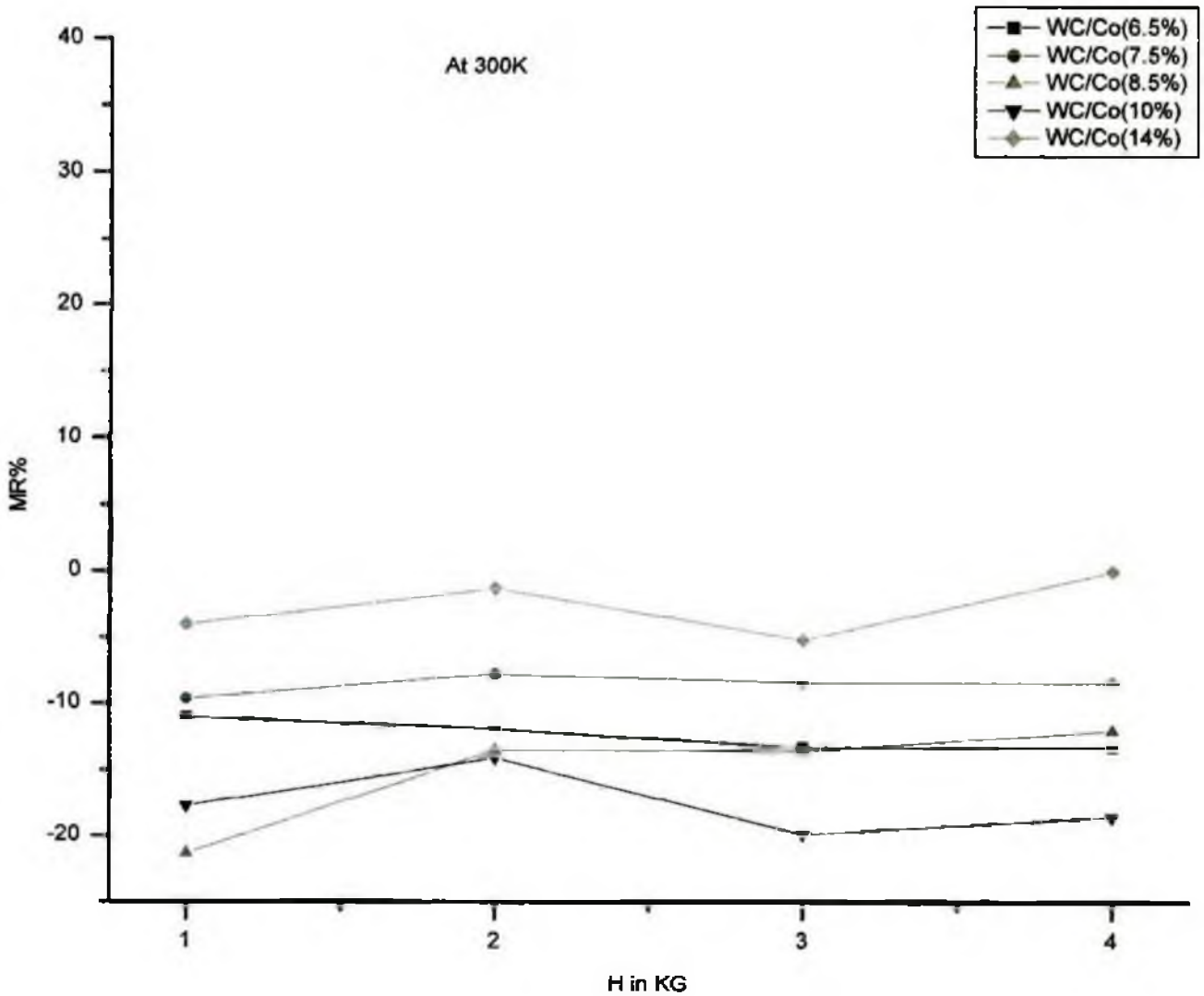

Fig.(4.25): MR as a function of magnetic field for WC/Co composites at T=300K.

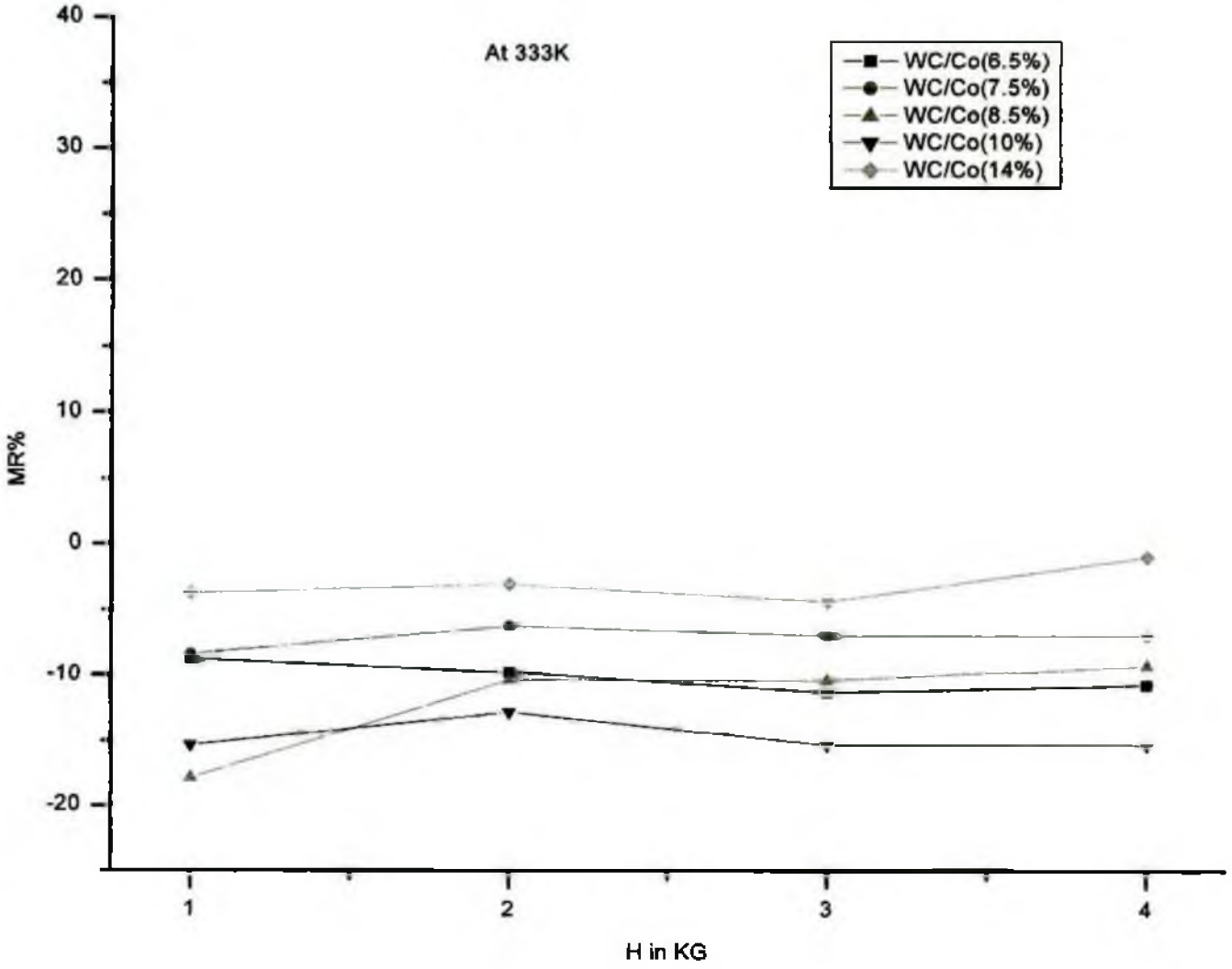

Fig.(4.26): MR as a function of magnetic field for WC/Co composites at T=333K

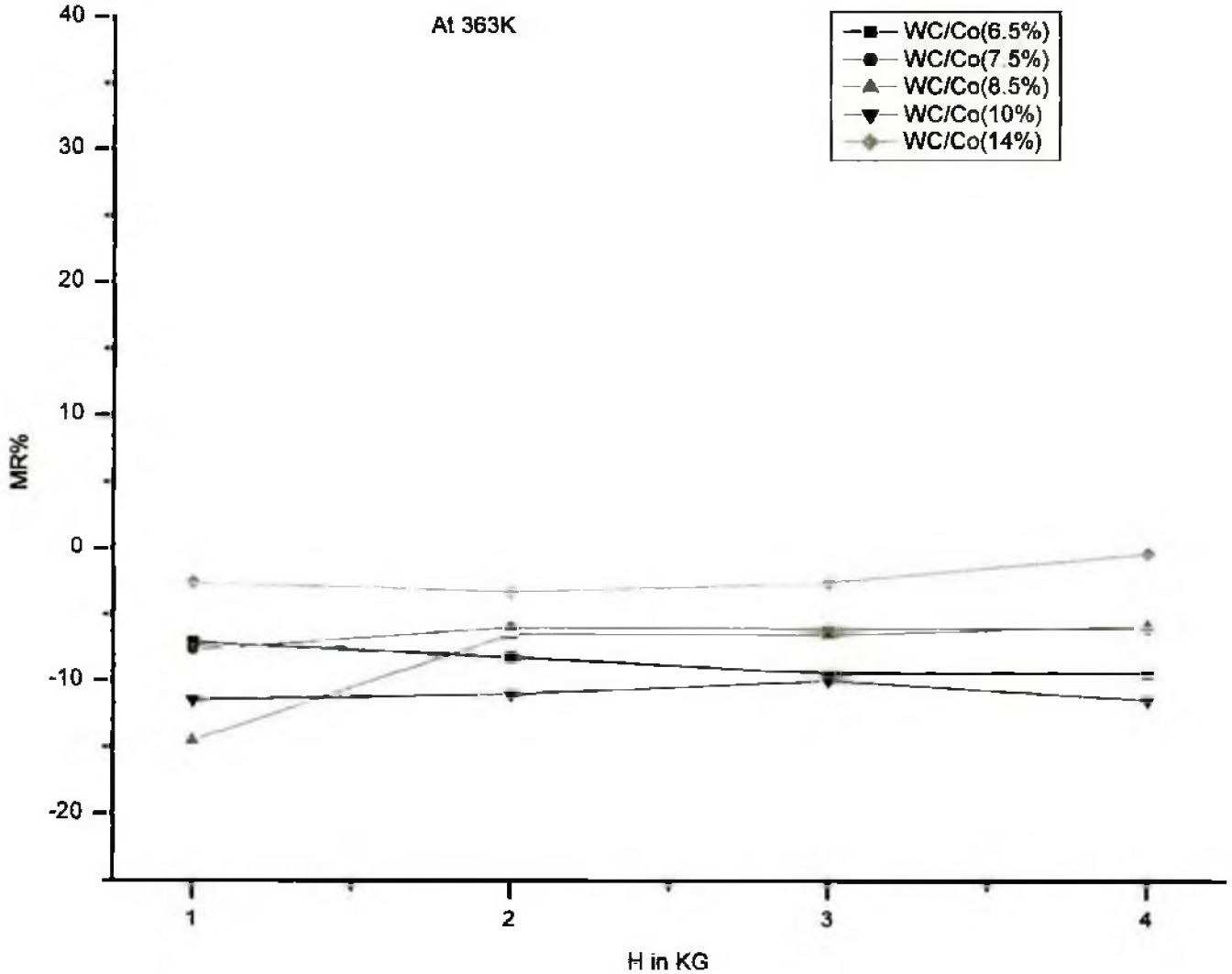

Fig.(4.27): MR as a function of magnetic field for WC/Co composites at T=363K.

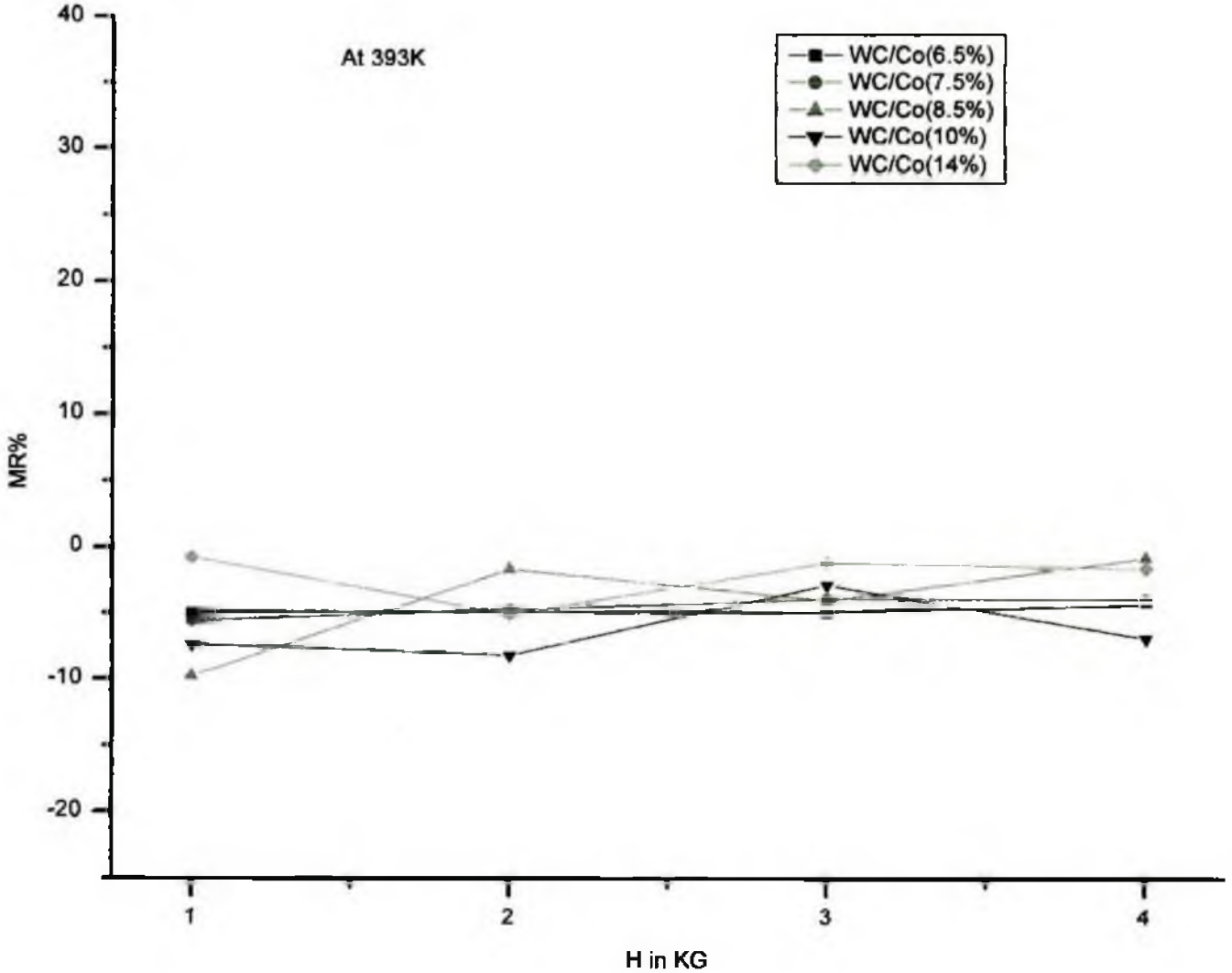

Fig.(4.28): MR as a function of magnetic field for WC/Co composites at T=393K.

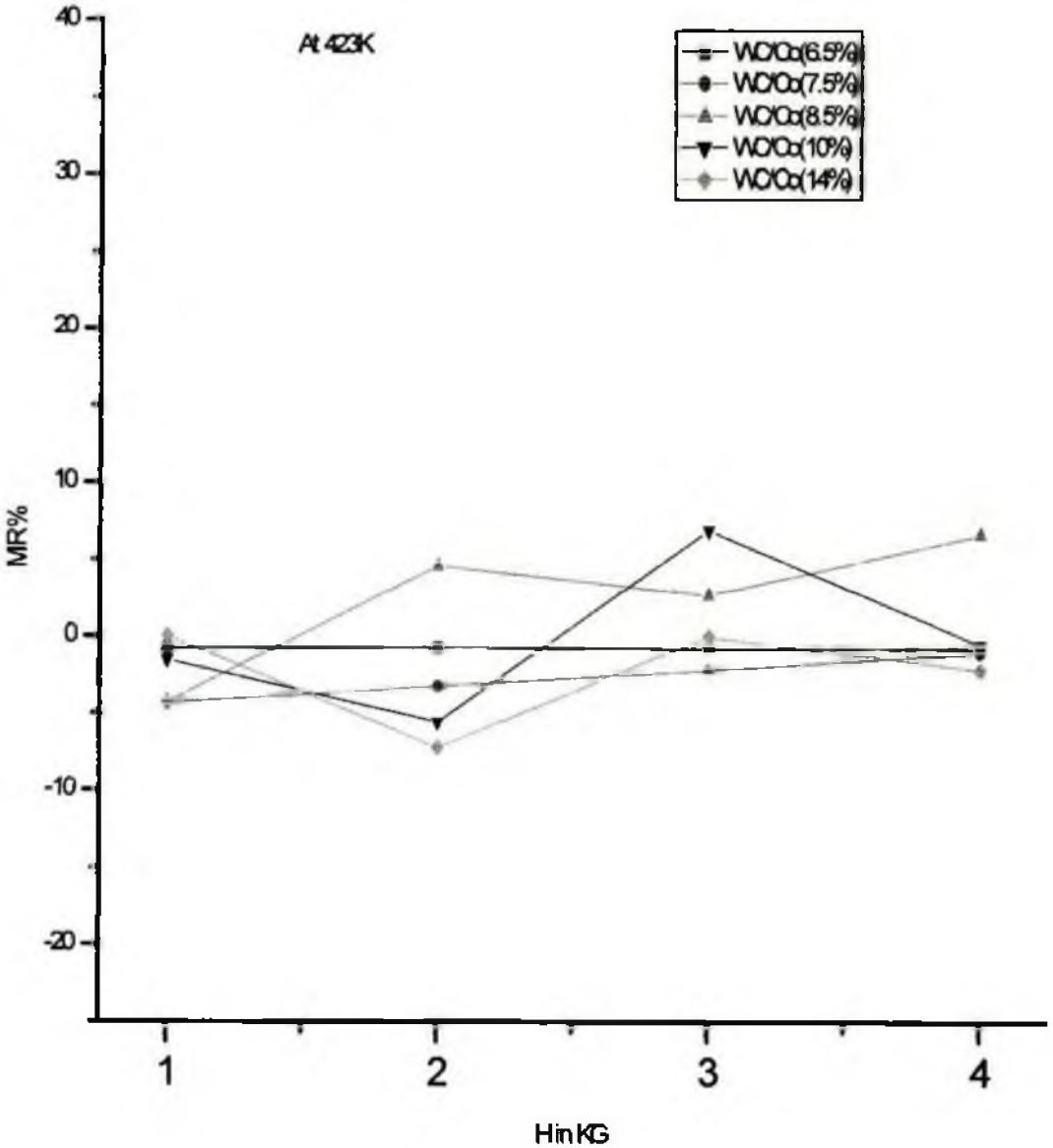

Fig.(4.29): MR as a function of magnetic field for WC/Co composites at T=423K.

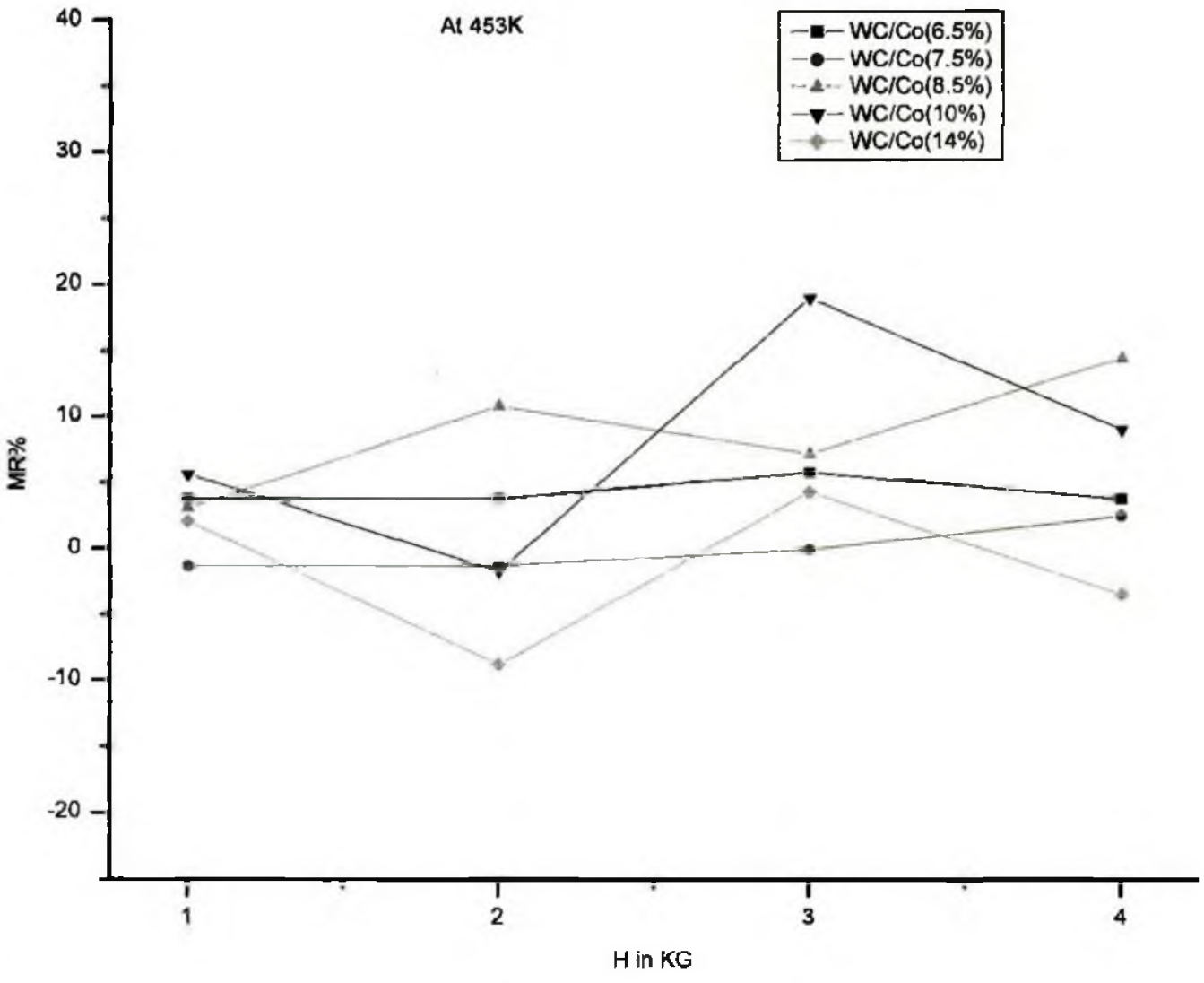

Fig.(4.30): MR as a function of magnetic field for WC/Co composites at T=453K.

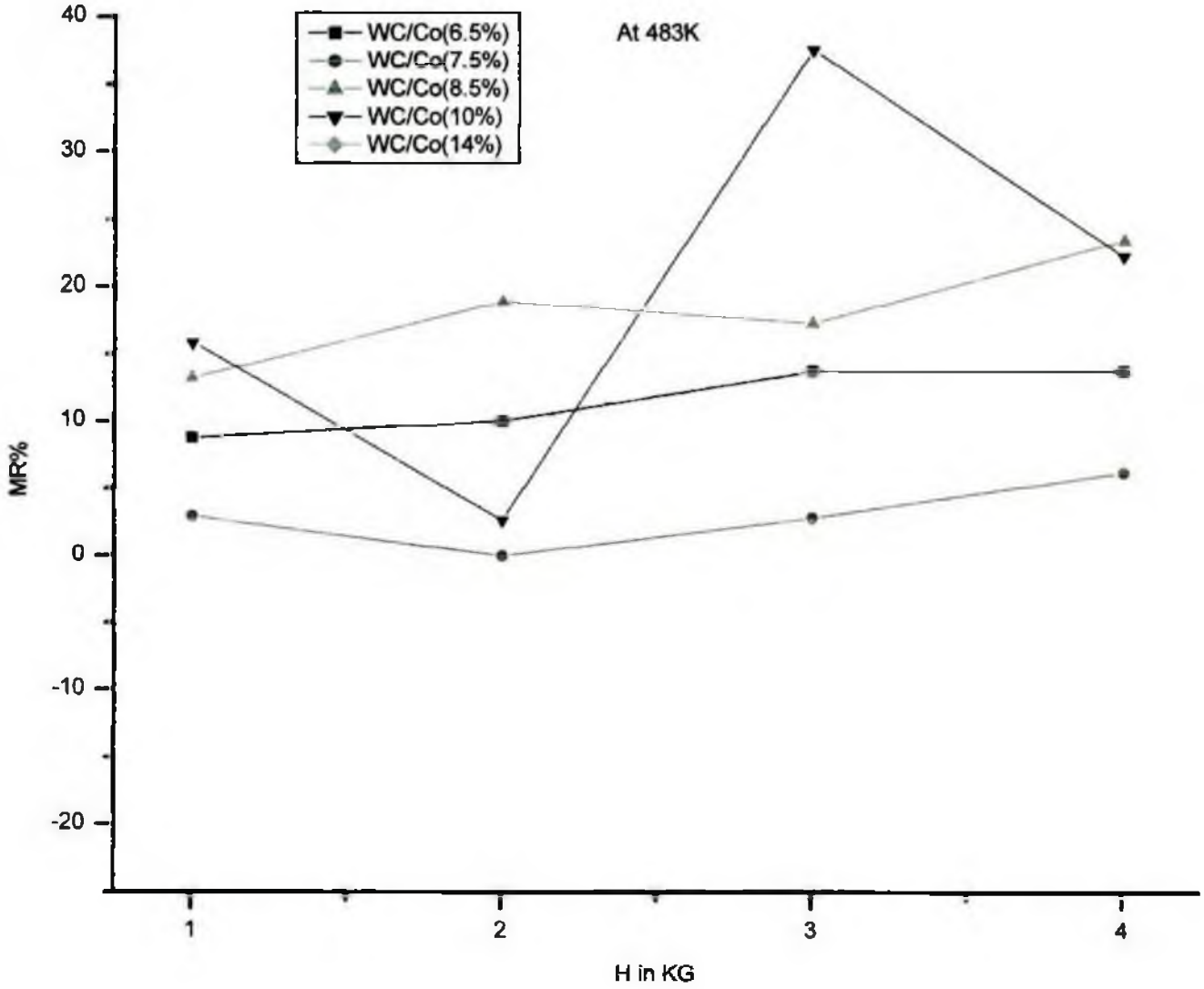

Fig.(4.31): MR as a function of magnetic field for WC/Co composites at T=483K.

4.4.2 Magnetoresistance as a function of temperature:

The MR as a function of temperature for all the samples were obtained at H = 0, 1, 2, 3, 4 KG are shown in Fig(4.32-4.35). Most of all shows low temperature MR, which varies within the range -26.82966 to 28.66631%. The sample shows maximum value of MR 28.66631%.

(I) For H=1KG, fig.(4.32) shows the MR as a function of temperature for all the samples (WC/Co composites). At 300K all the sample shows negative magneto resistance. With increase in temperature the value of negative magneto resistances starts to decrease and above 423K the negative magneto resistances of the entire sample turn into positive magneto resistance.

(II) For H=2KG, fig.(4.33) shows the MR as a function of temperature for all the samples (WC/Co composites). At 300K all the sample shows negative magneto resistance. With increase in temperature the value of negative magneto resistances starts to decrease and above 423K the negative magneto resistances of all the sample except the one containing 14 volume percentage of Co turn into positive magneto resistance.

(III) For H=3KG, fig.(4.34) shows the MR as a function of temperature for all the samples (WC/Co composites). At 300K all the sample shows negative magneto resistance. With increase in temperature the value of negative magneto resistances starts to decrease and above 423K the negative magneto resistances of the entire sample turn into positive magneto resistance.

(IV) For H=4KG, fig.(4.35) shows the MR as a function of temperature for all the samples (WC/Co composites). At 300K all the sample shows negative magneto resistance. With increase in temperature the value of negative magneto resistances starts to decrease and above 423K the negative magneto resistances of all the sample except the one containing 14 volume percentage of Co turn into positive magneto resistance.

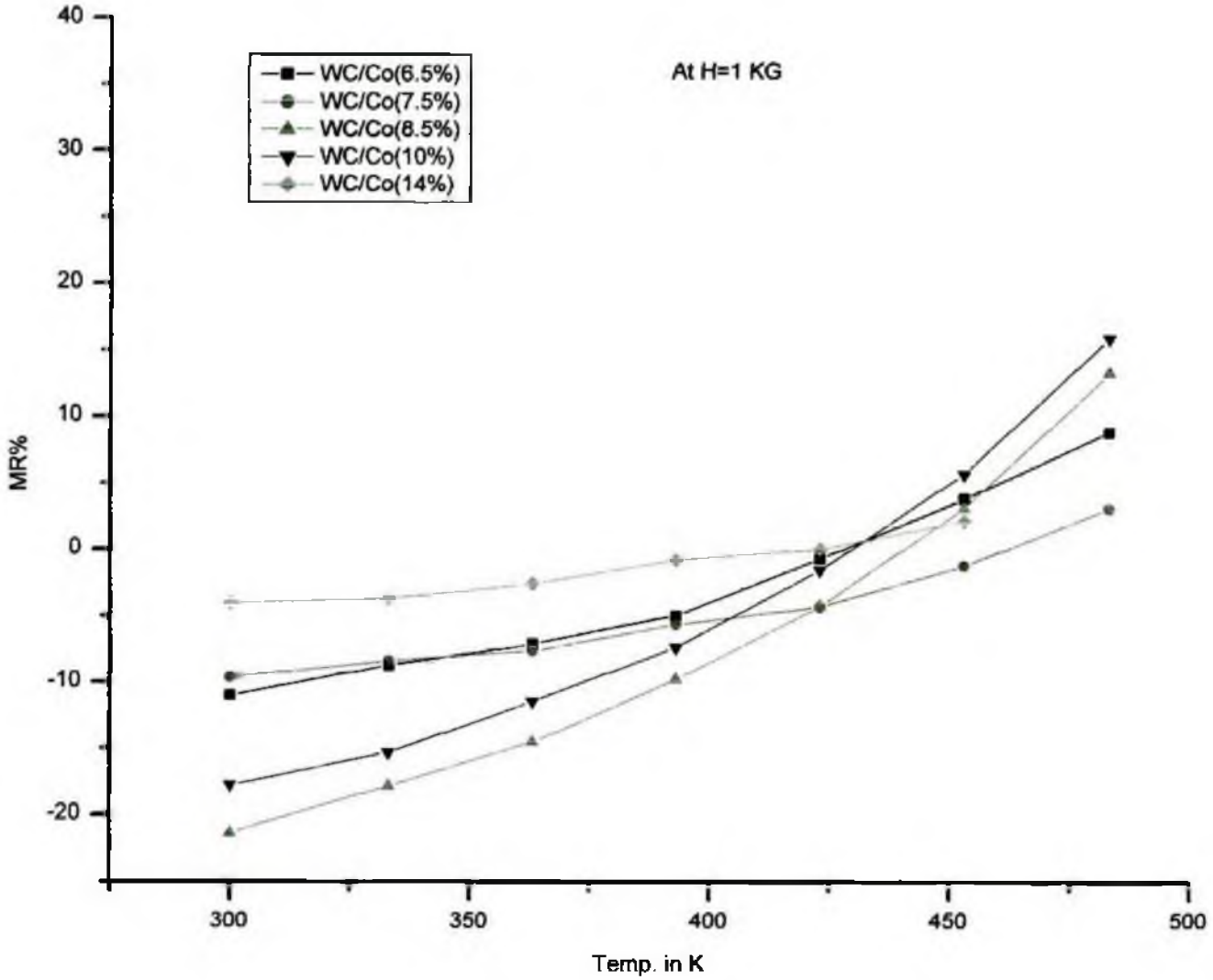

Fig.(4.32): MR as a function of temperature for WC/Co composites at H=1KG.

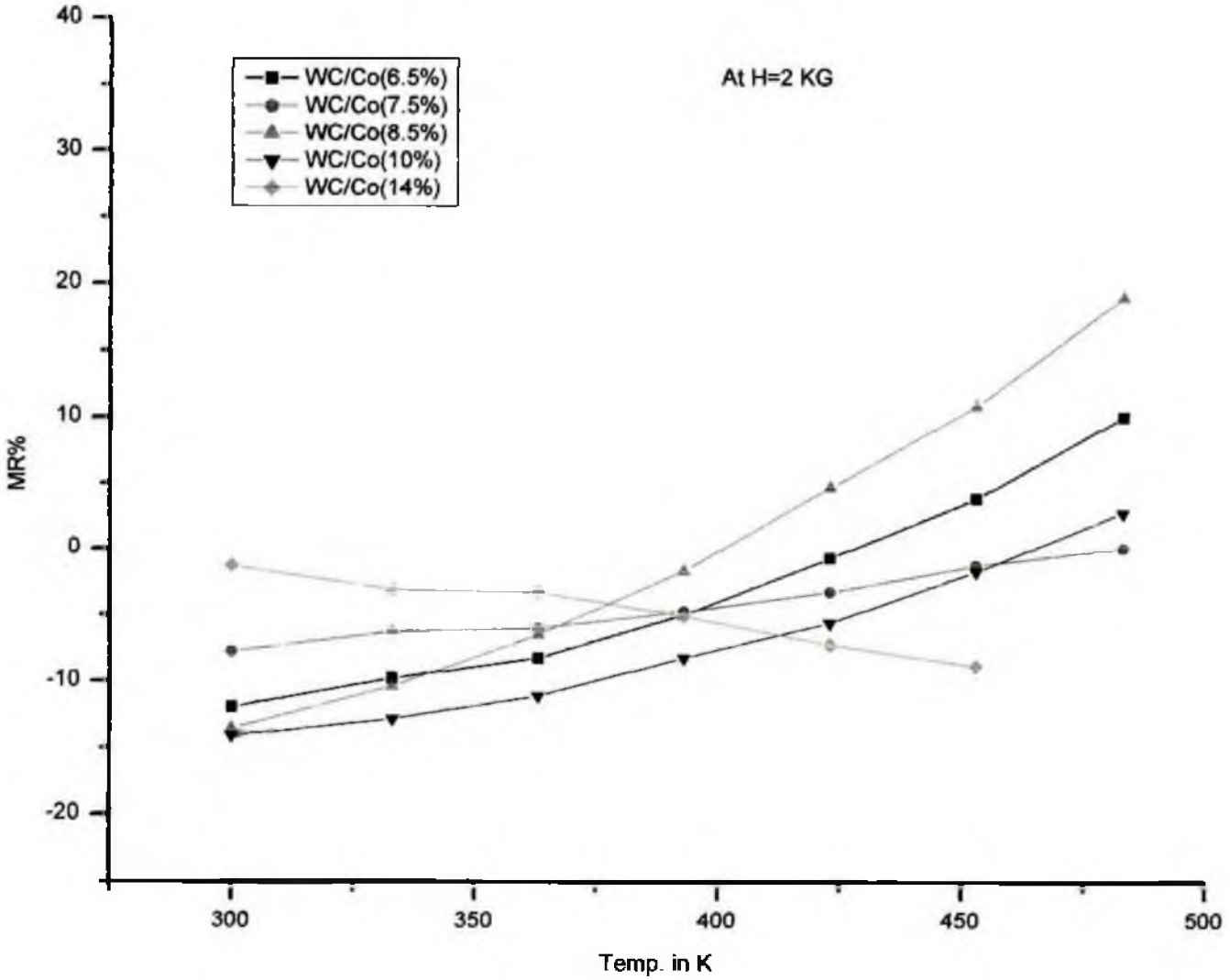

Fig.(4.33): MR as a function of temperature for WC/Co composites at H=2KG.

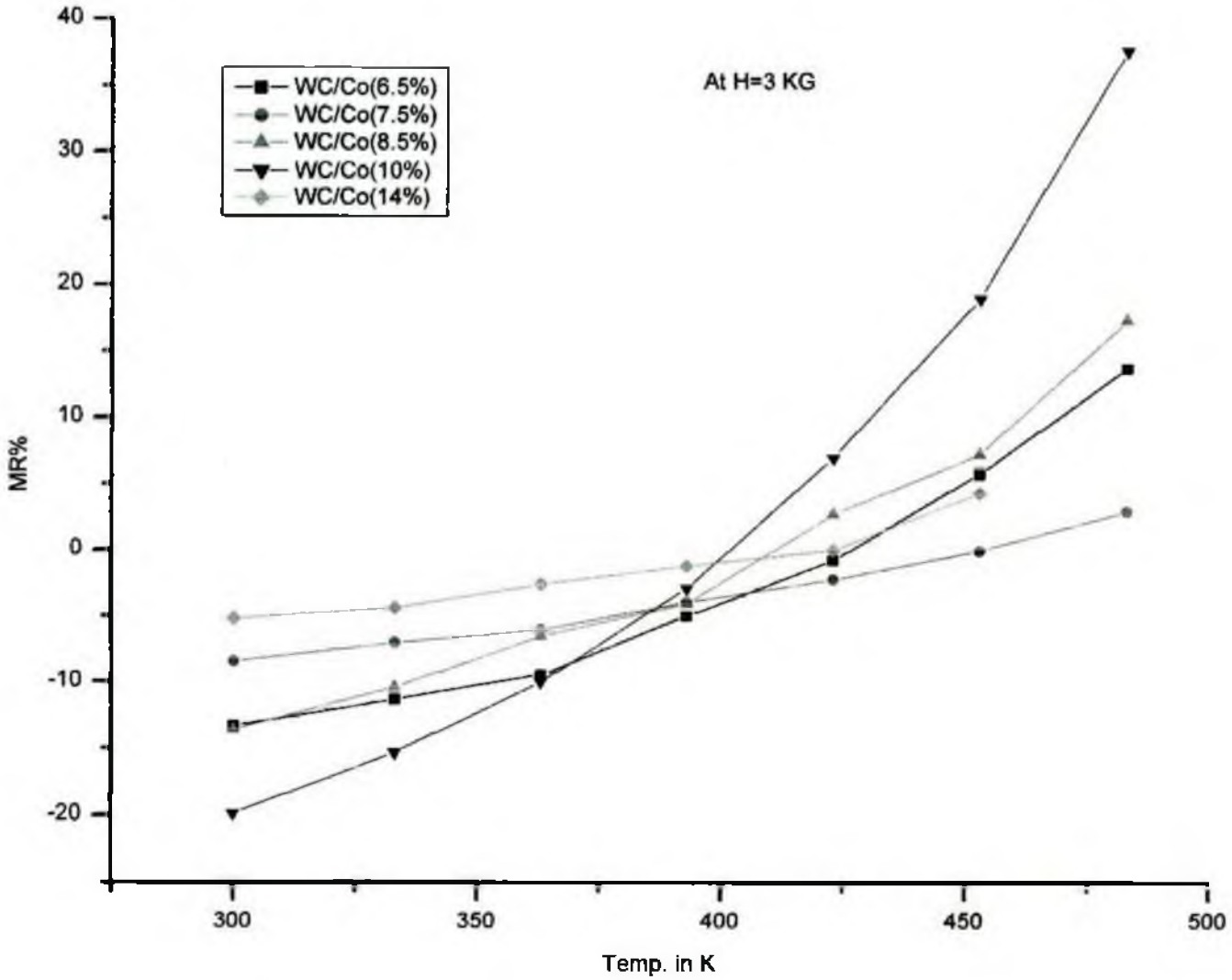

Fig.(4.34): MR as a function of temperature for WC/Co composites at H=3KG.

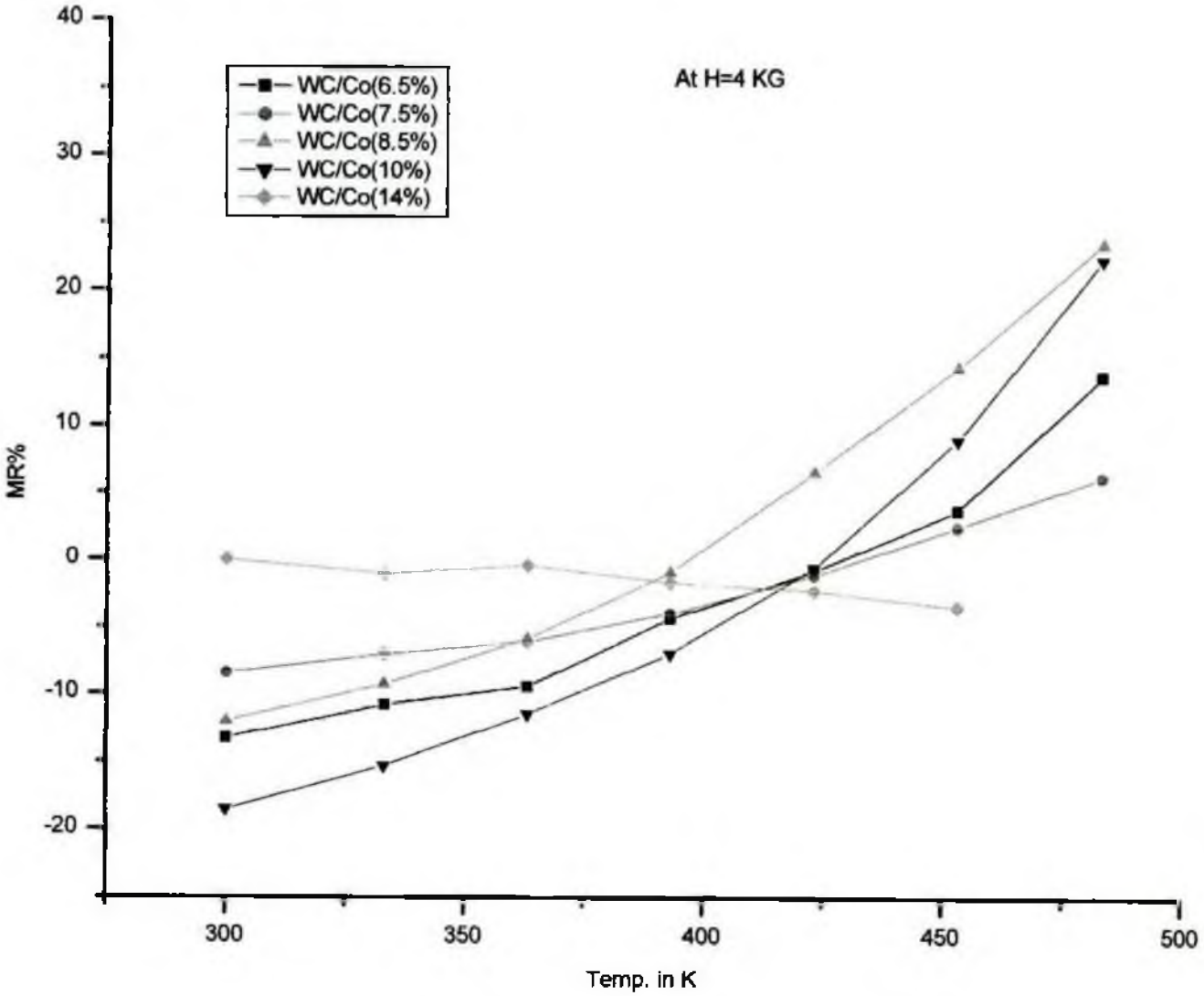

Fig.(4.35): MR as a function of temperature for WC/Co composites at H=4KG.

Reference:

1. Selected Powder Diffraction Data for Minerals, by Joint Committee on Powder Diffraction Standards, USA, First Edition, 1974.

CHAPTER FIVE

CHAPTER 5: DISCUSSIONS AND SUGGESTION FOR FURTHER WORK

5.1 Discussions

5.2 Suggestions for further work

5.1 Discussions

A systematic study has been performed on the structural, electrical and magnetoresistive properties of WC composite with increasing vol.% of Co. X-ray diffraction analysis was carried out on the samples to determine some structural parameter and weight percentages of WC and Co. Philip's X'Pert PRO X-ray diffractometer was used to get X-ray data for the samples. An experimental setup was established for the measurement of DC electrical and magnetic field dependent resistance and magnetoresistance. Sample probe was designed and wired properly. An electromagnet was calibrated. All the samples were sintered at 1640° C for measurements. The DC electrical resistivity of all the samples was measured by standard four-point probe method (a) as a function of temperature (ranging from room temperature 300K to 483 K with 30 K interval) keeping magnetic field constant and (b) as a function of magnetic field keeping the temperature constant.

(i) X-ray diffraction analyses shows that the samples are homogeneous and of hexagonal crystalline structure. From the X-ray curves it is observed that WC and Co atoms are positioned themselves in such a way so as to make separate phases – which is one of the important characteristics of composites. The weight percentage of cobalt in WC matrix was also determined by this measurement. Co was found to be in the range of (5 – 20) percent, the rest was found as WC. The lattice parameters (a, b, c) of the sample crystal were determined plotting the lattice parameter values versus Nelson-Riley (N.R.) function and the values were found to be a=b=2.9047 and c=2.8275 (fig4.8 and fig4.9). The volume of the unit cell of the hexagonal sample is V=23.86956. It is observed that the calculated values are in good agreement with the reported values (a=b=2.9062 and c=2.8378, V=20). But there is little difference between the calculated values and reference values; this may be due to the defect in the crystal structure when it is grown and due to the experimental errors.

(ii) The current-voltage curves for all the samples have been drawn (1) at different temperature (from RT to 483K), (2) at different magnetic field ranging from 0 to 4 KG (fig.4.10-4.14). All the curves show that current was found to be increased with increasing voltage. Also it has been observed that with increasing volume % of Co, the curves are shifted towards right thereby decreasing resistance.

(iii) Conductivity as a function of temperature curves for WC/Co composites containing different volume percentage of Co were plotted keeping magnetic field constant (fig.4.15-4.19). From the curves certain observations have been made: (1) Conduction for 10 volume percentage and 14 volume percentage of Co were comparatively higher than the conductivities for low volume percentages of Co. The effect of magnetic field is also prominent. A significant difference has been observed between the conductivities for low volume percentages (6-8 volume percentage) and for high volume percentage of Co (10-14 volume percentage) when magnetic field increases from 0 to 4 KG. Moreover, for H=4KG, the conductivity curves for 10 volume percentage and 14 volume percentage were observed to be overlapped. From which it can be inferred that the threshold percolation limit can be achieved at lower volume percentage of filler (Co) if magnetic field is increased, (2) with increasing temperature, the conductivity of the samples for all volume percentages of Co was found to be decreased showing that the electrical conduction is metallic type and probably it will occur through the metallic conduction paths [1].

The Landauer's percolation model expresses the electrical conductivity as a function of the variation of the volumetric fraction for each component. For composite materials built by components with different thermal expansion co-efficient, the percolation phenomenon can be induced by the temperature variation. A volumetric fractional change caused by different thermal expansion co-efficient can lead to the percolation region, mainly if there are some spaces available among metal particles to allow their expansion [3]. As the temperature is raised the metallic inclusion fraction

volume reaches the critical fraction and the metallic particles touch themselves forming conduction paths.

(iv) Electrical conductivity as a function of Co concentration in a WC matrix was taken for 300K, 333K, 363K, 393K, 423K, 453K and 483K keeping magnetic field constant (fig.4.20-4.24). The higher the volume percentage of Co, the higher is the conductivity with or without the applied magnetic field. So it is evident that the electrical conductivity of composites depends on the Co volume fraction. For all the temperature at constant magnetic field, it was found that there are three distinct region related to the electrical conductivity behavior. Region I shows that up to 8.5 volume % of Co the conductivity does not change abruptly. In region II i.e. at 10 volume % of Co, a sharp rise of the electrical conductivity occurs which is typical of a percolation process. In region III i.e. at 14 vol. % of Co, a small change in the electrical conductivity occurs. The critical volume fraction after which conductivity rises sharply is known as the percolation limit. Below this limit the composite conductivity is basically through the matrix phase. At a critical volume fraction, the particles or fibers are sufficiently close-packed to form an unbroken conducting pathway through the composites and the conductivity rises sharply [4].

It should however be noted that although the conductivity rises when Co particles are in contact, it does not necessarily follow that a fully connected network of Co is formed. McLachlan showed that at volume fraction just above the percolation limit, conducting particles would be arranged in such a way to form a large, but finite interconnected clusters which do not span the entire specimen [5].

(v) The MR as a function of magnetic field for all the samples were obtained at RT(300K) and high temperature(up to 483K) are shown in Fig (4.25 -4.31). Typical MR curves obtained at 298K for the samples sintered at 1640° C. At room temperature (300K) observed MR was negative and almost constant with the field. With increase in temperature the negative MR started decreasing and above 423K

positive MR was observed but the values of Magneto Resistances were very close to zero.

(vi) The MR as a function of temperature for all the samples were obtained at H = 0, 1, 2, 3, 4 KG (fig. 4.32-4.35). At 300K all the sample shows negative magneto resistance. With increase in temperature the value of negative magneto resistances starts to decrease and above 423K the negative magneto resistances of the entire sample turn into positive magneto resistance. This behavior of MR was explained by Hossain et al. [6] in the following grain boundary model.

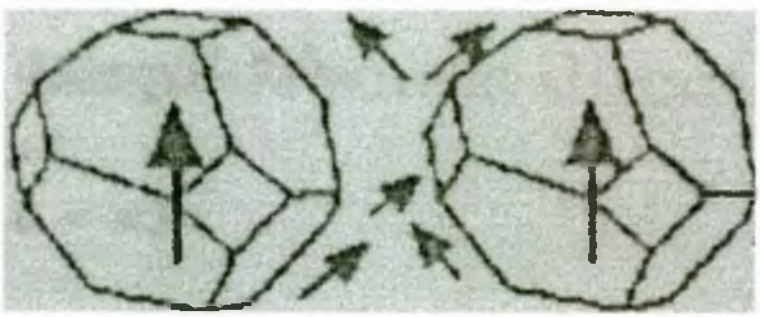

Fig.5.1(a)

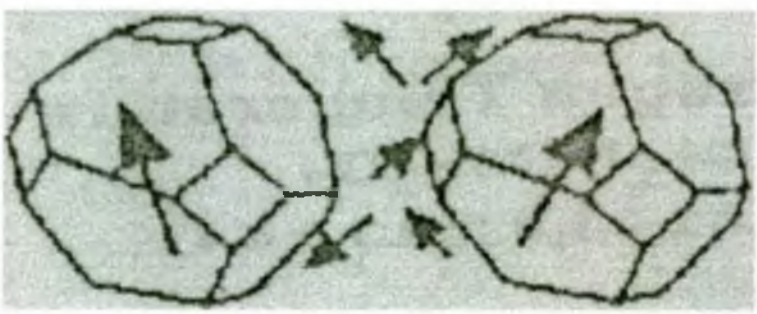

Fig.5.1(b)

The samples are in ferromagnetic domain or region, so at low temperature the magnetization of the grain of the material will be like in fig.5.1 (a), the domain

spins are comparatively aligned keeping MR low. But with increase in temperature the magnetization of each grain starts to disorder as shown in fig.5.1 (b). Also, the individual spin at the grain boundary region are randomly oriented. A carrier will suffer scattering from the unaligned magnetic, as well as disordered spin at the grain boundary region and thus an increase in MR is observed. Therefore it can be suggested that the increase of temperature affects the magnetoresistive properties of Co which reduce the conductivity of the composites.

5.2 Suggestions for further work

Here we have investigated the DC electrical and magnetic field dependant resistive properties of WC composite with increasing fraction of Co. Because, Tungsten carbide-cobalt (WC/Co) is widely used for cutting tools and wear resistance surface with wide range of applications. For these applications, the mechanical properties were given of special interest over the past century. But electrical properties of composite materials are also relevant and should be investigated more extensively which could lead to a wide range of applications.

From this point of view, we have focused our attention to the electrical analysis of WC/Co. However, the work that we performed was not so sufficient to make a comprehensive study of the system due to the lack of specimens and equipments. Therefore, in future, the following points may be investigated.

a) Study of electrical and magnetoresistive properties at low temperature.
b) Study of microstructure using SEM/TEM.
c) Permeability measurements.
d) Variation of resistivity with temperature (from room temperature to high temperature) by impedance spectroscopy.
e) Variation of resistivity with low temperature (at liquid nitrogen temperature).

References:

1. J.R. Martinelli, F.F. Sene, "Electrical resistivity of ceramic-metal compositematerials: application in crucibles for induction furnaces". Ceramics International 26 (2600) 325-335.
2. Afruja Akter Nasreen, 'Study of the Magnetoresistive properties of $La_2Ba\ Mn_2O_7$ system', M. Phil thesis, p85.
3. Martin,C., Mathieu,P. and Cales,B., Electrical discharge machinable ceramic composites, Mater. Sci. Eng., 1989, A109, 351-356.
4. Nicola Harfield. "Conductivity calculation for a two phase composite with spheroidal inclusions". Phy.D : Appl. Phys.. 32(1999) I 104 - I 1 13.
5. Mcl.achlan. D.S.. et al. Electrical resistivity of composites. *J. Amer Cenim. Soc.*. 1990. 73(8). 2187.
6. A.K.M.A. Hossain, L.F. Cohen, F. Damay, A. Berenov, J.L. Macmanus-Driscoll. N.M. Alford, N.D. Mathur, M. Blamire and J. E. Evetts, "influence of grain size on magnetoresistance properties of bulk $La_{0.67}Ca_{0.33}MnO_{3-6}$." J. Mag. & Mag. Mat. 192, 263 (1999).